Final Technical Report

Recipient Organization:	3M Company
Project Title:	Degradation of Poly- and Perfluoroalkyl Substances (PFAS) in Water via High Power, Energy-Efficient Electron Beam Accelerator
Date of Report:	October 26, 2023/Revised May 6, 2024
Award Number:	Award No. DE-EE0009132
Total Project Costs:	Total $ 848,927
DOE Share:	DOE Share $ 679,141
Recipient Cost Share:	Cost Share $ 169,786
Project Manager:	Cleston Lange, clange@mmm.com
Project Partner(s):	Charles Cooper, ccooper@fnal.gov

ACKNOWLEDGMENT

This material is based upon work supported by the Department of Energy (DOE), Office of Energy Efficiency and Renewable Energy (EERE), under the FY19 Advanced Manufacturing Office Multi-Topic FOA: DE-FOA-0001980, Topic 2.2: Lower Thermal Budget (LTB) Processes for Industrial Efficiency and Productivity: Thermal Process Intensification; AOI 2: Electromagnetic Energy for Advanced Manufacturing Applications and performed under award number DE-EE0009132.

We would like to acknowledge others who contributed to this work from Fermilab, Slavica Grdanovska, Yichen Ji, Nikolay Solyak and Vyacheslav Yakovlev, and from 3M, Eric Olsen, David Johnson, Steve Kays and Brian Mader. Additionally, contracted laboratory work through Pace Analytical at the 3M EHS laboratory was provided by Jack Norman.

DISCLAIMER

ABBREVIATIONS AND ACRONYMS

3M	3M Company
AFFF	Aqueous film forming foam
Ar	Argon
CW	Continuous wave
DO	Dissolved oxygen
DOE	United States Department of Energy
EB	High-energy electron beam
ECF	Electrochemical fluorination process
EERE	DOE Office of Energy Efficiency and Renewable Energy
EHS Lab	3M Global Environment, Health, and Safety Laboratory
EMS	Electromagnetic shield
EU	European Union
FBSA	Perfluorobutanesulfonamide
FNAL	Fermi National Accelerator Laboratory (Fermilab)
GAC	Granular activated carbon water treatment
HCl	Hydrochloric acid
HPLC	High performance liquid chromatography
HWR	Half wave resonator
IE	Ion exchange water treatment
kGy	kiloGray
LC-MS/MS	Liquid chromatography tandem mass spectrometry
LC-QTOF	Liquid chromatography-quadrapole time-of-flight mass spectrometry
MCL	Minimum contaminant level
N2	Nitrogen
NaOH	Sodium hydroxide
PFAS	Poly- and perfluoroalkyl substances
PFBA	Perfluorobutanoate
PFBS	Perfluorobutane sulfonate
PFCA	Perfluoroalkyl carboxylic acid
PFDA	Perfluorodecanoate
PFDS	Perfluorodecane sulfonate
PFDoA	Perfluorododecanoate
PFHxA	Perfluorohexanoate
PFHpA	Perfluoroheptanoate
PFHxS	Perfluorohexane sulfonate
PFHpS	Perfluoroheptane sulfonate
PFNA	Perfluorononanoate
PFNS	Perfluorononane sulfonate
PFOA	Perfluorooctanoate
PFPA	Perfluoropropanoate
PFPeA	Perfluoropentanoate
PFES	Perfluoroethane sulfonate
PFPS	Perfluoropropane sulfonate
PFPeS	Perfluoropentane sulfonate

ABBREVIATIONS AND ACRONYMS

PFOS	Perfluorooctane sulfonate
PFOSA-NO	Perfluorooctane sulfonamide amine oxide
PFSA	Perfluoroalkyl sulfonic acid
ppb	Part-per-billion (typically units of μg/L)
ppm	Part-per-million (typically units of mg/L)
ppt	Part-per-trillion (typically units of ng/L)
RF	Radio frequency
RO	Reverse osmosis water treatment
RT	Room temperature (non-superconducting cryogenic)
SOPO	Summary of Project Objectives
SRF	Superconducting radio frequency
SSA	Sold state amplifier (RF power supply)
TFA	Trifluoroacetate
TFMS	Trifluoromethane sulfonate
2233TFPA	2,2,3,3-Tetrafluoropropanoate
2333TFPA	2,3,3,3-Tetrafluoropropanoate
TFSI	(Bis)-trifluoromethane sulfonyl imide
USEPA	United States Environmental Protection Agency

TABLE OF CONTENTS

TABLE OF FIGURES

TABLE OF TABLES

EXECUTIVE SUMMARY

Objectives: The goal of the 2-year workplan was to see if electron beam (EB) could be used to break down a sub-set of the larger chemical family of per and polyfluoroalkylated substances (PFAS) in an energy efficient and economical manner when compared to conventional water treatment technologies.

Technical Approach. Year one (Y1) work focused on sample EB treatment work in the Fermi National Accelerator Laboratory's (FNALs) Accelerator Applications Demonstration and Development (A2D2) EB accelerator. While there are reportedly thousands of types of PFAS, for the point of most of the work herein, a small subset was examined, typically perfluorooctane sulfonate (PFOS) and perfluorooctanoate (PFOA). PFOA and PFOS are two of the most well studied PFAS and are studied for baseline evaluations and are considered most useful. The work from Y1 provided information about the optimal operating parameters and additives to use when treating PFOS and PFOA via EB. The data were then used to see where in a water treatment system an EB accelerator would be best suited to treat PFAS. A conventional water treatment technology, GAC, was then compared to e-beam treatment technology with respect to energy and costs for treatment. In year two (Y2), several conventional e-beam accelerator designs, and FNAL's developmental compact SRF accelerator design, were evaluated for their suitability in PFAS treatment, from an energy efficiency and cost standpoint.

Results. Several EB parameters were evaluated and optimized for the removal of PFOA and PFOS from water at normal pressure and temperature, measured as total PFAS removal. Under the optimized test conditions both PFOA showed complete destruction to inorganic fluoride, and PFOS to inorganic fluoride and sulfate, with mass balance. The effect on PFAS removal relative to solution pH, total EB dose, EB dose rate, dissolved oxygen concentration (DO), temperature, and initial PFAS concentration were evaluated. In general, PFOA was easier to destroy than PFOS. Degradation products, typically observed under less-than-optimal EB conditions, provided insight to degradation mechanisms. Products were identified to rule out possible deleterious biproduct formation. The water radiolysis radical reaction kinetics with PFOS and PFOA were not dependent on the initial concentration over 5-orders of magnitude from 2 μg/L to 20 mg/L. This is thought to be because there was an overabundance of the reactive water radiolysis radicals relative to PFAS molecules and largely attributed to aqueous electrons. The reaction rates appeared to be diffusion limited. Testing at higher concentrations (100-200 mg/L) showed a decrease in removal efficiency, suggesting alternative kinetics, possibly second order rates, at higher concentrations. In all, we successfully defined a set of optimal EB parameters to treat PFOA and PFOS at concentrations of 20 mg/L in water with destruction efficiencies near 100%. We further tested the optimized EB parameters with other types of PFAS, including shorter and longer fluorocarbon chain homologs of PFOA and PFOS, and PFAS with alternative functional groups such as sulfonamides. Based on our results EB can be optimized as an effective destructive technology for removing PFAS from water. The conditions optimized for PFOA and PFOS were less effective with ultra-short fluorocarbon compounds like TFMS, PFES, PFPS and PFBS, and likely require re-optimization of parameters to them. In all, it was determined that from a cost and energy efficiency standpoint, EB would be best applied to waste streams with relatively high concentrations of PFOS and PFOA and is not as cost effective as GAC treatment for removing low concentrations of PFAS from water. Higher concentrations of PFAS can be found in the wastewater of conventional treatment processes such as RO and IE and therefore EB may be used to supplement such treatment technologies. Some real-world IE regeneration wash water and RO reject water containing higher concentrations of PFAS and obtained from pilot scale industrial wastewater treatment system at a fluorochemical manufacturing facility, showed that EB could

remove PFAS from such types of wastewaters. The IE regenerant wash water appeared to be the most efficient of the two types of wastewaters tested. However, some further optimization of the EB parameters for the specific PFAS types present in those wastewaters may be required. Also, the effects of co-present TOC and mineral salts should be considered during such optimization efforts.

From the experimental Y1 results it was seen that the aqueous electron drives degradation of the PFAS. In a hypothetical water treatment skid using EB for PFAS destruction the parameters of the system should be optimized to promote aqueous electron production. Before EB treatment, the PFAS should be preconcentrated when possible, the pH should be raised to pH 10 or higher to enhance aqueous electron production, and the water should be nitrogen purged to remove dissolved oxygen to minimize aqueous electron scavenging. An excel spreadsheet was created that calculates optimal conditions based on inlet PFAS concentration and desired outlet concentration, by optimizing the accelerator power, dose rate, water treatment rate, pH and dissolved oxygen levels to reach the desired endpoint. Given this information on accelerator operating conditions five different EB accelerator systems were compared. One EB system was a continuous-wave, linear superconducting accelerator being designed at Fermilab. Three other EB systems (IMPELA at 5% and 25% duty factor and the ILU-14) were normal conducting pulsed linear accelerators. The fifth system was an IBA Rhodotron which is a normal conducting, circular, continuous-wave accelerator. The accelerator efficiency (% of the incoming power that is used in water treatment) was the dominating factor in accelerator choice. The radio frequency (RF) power supply and the accelerator design (superconducting versus warm technology) drive the accelerator efficiency. The IBA Rhodotron was seen to be the most energy efficient commercially available technology with a wall-plug (total) power efficiency of 43% at 400 kW. The Fermilab design, with a prototype for a different application currently being fabricated, was the most energy efficient at 55% when driven by a Klystron RF power supply and as high as 77% when powered by a magnetron. As the Fermilab design was the most energy efficient by approximately 10-30%, further design work was done on the accelerator and beam delivery system specific to the destruction of PFAS in water. The Fermilab design is unique from industrial accelerators in that is superconducting. Superconducting technology allows for the acceleration of electrons without losses. The accelerator must be cooled to below the point where it is superconducting and is operated around 4 degrees Kelvin. The bulk of the design work for the accelerator is on making the accelerator as energy efficient as possible so that it does not require liquid helium and can be cooled with conduction cooling via cryocoolers.

Final design work resulted in an EB accelerator that would operate at minimally 200 kW and 10 MeV. Prototype construction would cost $7.8 million dollars when driven by a Klystron power supply. A second version of the same accelerator would cost $5.5 million dollars when driven by a magnetron that is still under development. The commercially available 300 kW IBA Rhodotron cost was estimated at approximately $9 million. While it is hard to directly compare, an operational GAC system used by 3M for groundwater treatment capital cost (2022 dollars) was estimated to cost $3.3 million. While the capital expense of the EB accelerator systems was higher than GAC, the accelerator EB treatment would result in destruction of the PFAS and not just sequestration of PFAS to form a new waste stream that requires further treatment or disposal. The operating cost to destroy the PFAS via 400 kw EB system was less than $1000/kg of PFAS destroyed when treating at a 20 mg/L PFAS concentration, compared to GAC with operating costs that calculated at $27,530 per kg of PFAS sequestered when treating 100 μg/L PFOA and PFOS combined concentration.

DOE Impact. This effort brings together 3M, subject matter experts in PFAS fate testing and analytical measurement, and FNAL, experts in EB accelerator design, construction, and operation. The present funding allowed for proof-of-principle studies on the efficiency of PFAS degradation via EB and cost analysis versus current costs, energy requirements associated with a GAC treatment facility. The positive results will potentially lead to further funding for field demonstration of FNAL's novel e-beam accelerator and ultimately

commercialization of the technology. 3M believes this work is imperative to advance tools needed to effectively treat water that contain PFAS at levels higher than regulatory action levels. FNAL's capability in EB technology may provide such a breakthrough when combined with 3M's knowledge and capability for the analysis of PFAS and 3M's experience with the scaling and operation of PFAS treatment technologies. This work is also relevant to other parallel research activities funded in part by DOE for characterizing PFAS present at AFFF impacted sites with the intent of remediation of such sites and funded via co-sponsored DOE/EPA/DOD Strategic Environmental Research and Development Program (SERDP).

BACKGROUND

Water is essential to sustainable development and properly managing water resources is an important component of growth, social and economic development, poverty reduction and equity, and sustainable environmental services [1]. Nearly 80% of the world's population is exposed to high levels of threat to water security due to watershed disturbance, disruptive water resource development, biotic factors, and pollution [2]. Water reclamation through treatment has the potential to significantly increase water productivity, but there are limitations to conventional water treatment technologies [3].

A. General Information on PFAS

Per- and polyfluoroalkylated substances (PFAS) are a large, complex family of specialty chemicals used for more than 70 years in various commercial, industrial, and military applications, ranging from stain and water repellency treatment to surfactants in AFFF for extinguishing petroleum-based fires [4]. PFAS typically contain a fluorocarbon tail bonded to a polar functional head group. The polar functionality can be a variety of chemical groups with cationic, anionic, or amphoteric properties. The poly- or perfluoroalkyl tail is highly inert to degradation due the strong carbon-fluorine bond energy (~116 kcal/mol), one of the strongest bonds in chemistry. The structure of one PFAS of interest in the present study, perfluorooctane sulfonate (PFOS), is shown below in **Figure 1**.

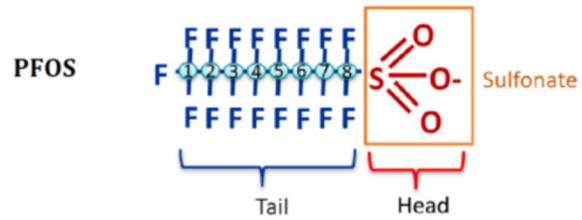

Figure 1 Chemical structure of PFOS

While stability has been a desired property of PFAS for their functionality, it is also an attribute that contributes to their presence in the environment, biota, and humans. Because of historical manufacture, imports from foreign manufacture, use, and disposal practices, PFAS can be found in a variety of wastewater, groundwater, and surface waters. PFAS hot spots have been identified near PFAS manufacturing locations, industrial sites, at military bases and airfields, and near commercial airports where AFFF was used [5,6]. The most studied PFAS to date are PFOA and PFOS stemming largely from their broad legacy use and large-scale production. 3M was a primary producer of PFOS and PFOA in the U.S. but voluntarily phased out production of PFOS and PFOA related chemistries in the early 2000s [7]. Other manufacturers following suit by 2015 under

agreement with the USEPA [8]. Today, both PFOA and PFOS are generally prohibited from manufacture and use in developed countries such as the U.S., Japan, Canada, Australia, and European Union (EU). PFAS manufacturing in many countries subsequently switched to replacement chemistries such as shorter fluorocarbon chain PFAS or PFAS with oxygen atoms integrated into the fluorocarbon chain. Some replacement chemistries such as shorter fluorocarbon chain homologs are still recognized as persistent, and can be found in the environment, but are considered less bioaccumulative [9]. PFAS have also been detected in the water supplies of some U.S. residents at levels exceeding MCLs in effect at the time [10].

Various traditional water treatment technologies have been utilized to address PFAS remediation to varying degrees of success[11]. One commonly used water treatment technology employs large granular activated carbon (GAC) beds to remove PFAS and has been shown to be a cost-effective and efficient method for removal of PFOA, PFOS and some other PFAS. Ion exchange (IE) and reverse osmosis (RO) are also considered effective removal methods for PFAS, but considered more expensive to implement and maintain[12,13]. A significant downside to all three of these technologies is that they are sequestration technologies and generate a concentrated PFAS waste that must be further treated or disposed of.

Sequestration technologies can be effective at removing PFOA and PFOS from water [14,15] but can be less efficient at removing lower molecular weight, short chain PFAS and can result in shorter breakthrough times that lead to costly high frequency replacement of the adsorbent [16,17]. Another complicating issue for treatment is that some proposed state and federal minimum contaminant levels (MCLs) may require removing PFAS from drinking water to extremely low levels that may be beyond the capabilities of some current water treatment technologies. Although alternative treatment technologies can be cost effective at treating concentrated PFAS streams, they are significantly less energy and cost effective than GAC when treating high volumes of water containing low concentrations of PFAS, but this does not mean they are incapable of such treatment and may require further evaluation to improve upon their cost and energy requirements.

Alternative water treatment methods have shown some promise as a means of destructively removing PFAS from water and have been reviewed[18], however, they may create undesirable chemical by-products, resulting in increased costs for removal. Such methods include incineration, advanced oxidation with hydroxyl radicals ($OH^{\bullet}$), or reductive processes that generate aqueous electrons (e^-_{aq}) or hydrogen radicals ($H^{\bullet}$) [19,20,21,22,23,24,25,26,27]. While high-temperature incineration can be effective for PFAS contaminated solids, it does not offer a practical solution to water treatment. When implemented as a stand along technology, the oxidative and reductive processes do not perform well and can act upon different PFAS classes with different mechanisms and slow rates.

Electrons are effective at breaking down a wide range of contaminants in industrial and municipal water [28,29,30] and may be an effective solution to remove PFAS from water. Electron beam treatment of water offers distinct advantages over conventional treatment techniques that may make it a preferred treatment method for PFAS. For example, e-beam technology can completely break down contaminants instead of just concentrating contaminants into another form like GAC, IE and RO treatment technologies. EB technology relies on the use of accelerators to induce water radiolysis and simultaneously forming an oxidative ($OH^{\bullet}$) and reductive (e^-_{aq}) environment which can be very effective at degrading many water-borne contaminants of concern [31] to elemental composition with no harmful byproducts. It has been suggested that a synergistic role of e^-_{aq} and $OH^{\bullet}$ may be required for complete mineralization of PFAS, as demonstrated for perfluorooctanoic acid (PFOA) in water exposed to gamma-irradiation [32]. Furthermore, EB is not adversely affected by the size or charge of the chemical species as some conventional water treatment technologies are.

B. General Information on Electron Beam Processes

Destroying contaminants in water to create a cleaner water stream has been demonstrated to be effective utilizing EB technology. Electron beams can effectively destroy a wide range of contaminants including but not limited to solvents, halogenated solvents, polyaromatic hydrocarbons, biocides, pharmaceuticals, and personal care products [33,34,35,36,37,38,39,40]. Electrons entering the water solution drive a process called water radiolysis which creates radicals that are effective at breaking down the wide range of contaminants previously listed. While most of the destruction of these contaminants in aqueous solution is achieved through reactions driven by radicals created from water radiolysis, direct electron interaction plays a role as well. Electron beam technology has not been used widely at industrial scales for wastewater treatment, primarily limited to processes that either do not have conventional water treatment technology solutions or for chemistries that are especially vulnerable to attack by the water radiolysis radicals.

While there are many different types of accelerators, the two that are most relevant for water treatment application are the linear accelerator (LINAC) and the Rhodotron. Numerous accelerator technologies have been demonstrated to fulfill the beam prerequisites of PFAS treatment. The analytical objective of this study is to pinpoint an accelerator system that optimizes accelerator efficiency. The study chiefly explores two integral components of the accelerator system: the RF power source and the accelerating device. The RF power source's function involves transforming wall-plug power to RF power, which is converted into beam power by the accelerating device. For this study, 6 different accelerators were examined (Section 5). Two conventional, high frequency, warm LINACs were examined operating at two different duty factors. The third conventional LINAC studied was at a low frequency compared to the other two. The final 2 LINACs studied were superconducting operating a different frequency. The superconducting technology, while often used in high energy physics has not seen much if any industrial application. Superconducting LINACs allow for higher dose rates, more energy efficient operation, and for continuous wave electron deposition (compared to pulsed for warm LINACs). The sixth and final accelerator examined was a Rhodotron which offers high power (high dose rate) and continuous wave electron deposition.

An electron beam LINAC with major subsystems is listed below in the left side of **Figure 2**. Incoming power is conditioned and sent in pulses to an injector which introduces electrons into the accelerating cavity. The injection system, which can range from a gridded field emission cathode to even another accelerator, controls the pulse form of the incoming electrons and gives the electrons some initial acceleration. Leaving the injection system, the electrons enter high vacuum ($1x10^{-7}$ mbar or lower). After the injector the electrons are accelerated under high vacuum in the acceleration cavity to the designed energy that is typically in the range of 1-10 MeV. Radio frequency power that is at the same resonance frequency of the accelerating cavity coupled with the pulse structure of the injector facilitates the electron acceleration. After acceleration the electrons are focused in a nearly cylindrical shape that is then further focused and scanned using magnets to create a uniform electron beam field which then exits the system through a thin window, typically constructed from titanium or beryllium, of the scanning horn and to the target. Linear accelerators can be designed to operate at 10 MeV of beam energy (or higher) but are typically limited in beam power because of the heat generated in the accelerating structure. This beam power issue can be overcome using superconducting LINACs, but normal conducting accelerators are almost exclusively used in industry. Although LINACs can easily be made to produce beam energy above 10MeV, this is typically the design operational limit to avoid activation in high Z materials of either the accelerator or the target.

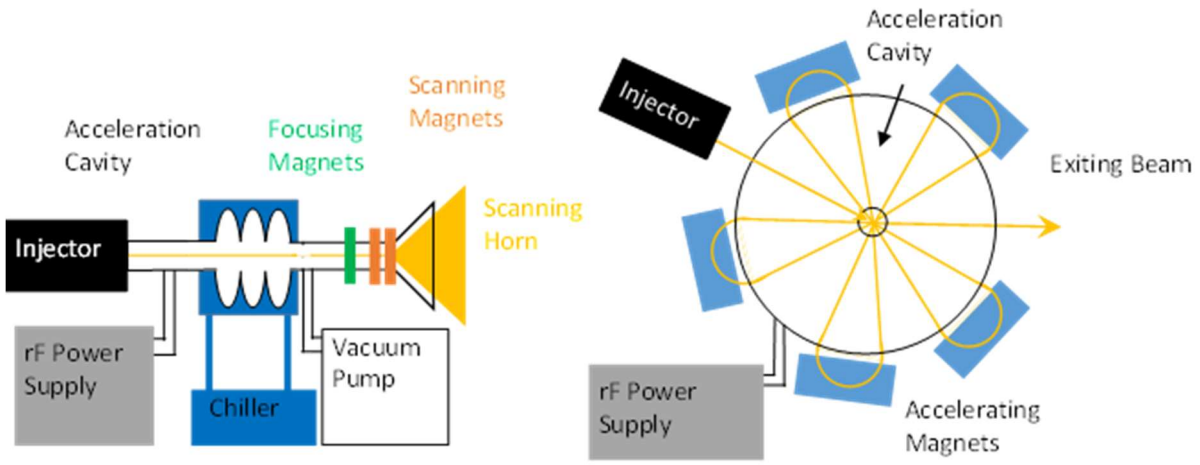

Figure 2. Electron beam system with major subsystems: LINAC (left), Rhodotron (right)

The Rhodotron shown on the right side of **Figure 2**, has most of the same systems as the LINAC but the acceleration of electrons is achieved by multiple passes through accelerating magnet fields. The Rhodotron is one of the most common accelerators for high power applications. One of the key advantages of commercial Rhodotron is that high power systems can be obtained that can allow for higher treatment rates. The Rhodotron was based on a design concept first proposed in1989 by J. Pottier of the French Atomic Agency. In December 1991, the Belgian particle accelerator manufacturer, Ion Beam Applications (IBA) entered into an exclusive agreement with the CEA to develop and industrialize the Rhodotron[41]. Today these are manufactured and sold by IBA Industrial Solutions under many models but three of the best known are the TT100, TT200 and TT300 that are typically specified with guaranteed beam powers of 35, 80 and 150 kW, respectively [42].

Electron beam accelerators take electrons from a resting state and accelerate them to close to the speed of light. The operating parameters of the accelerator that are most relevant in general and specifically important for PFAS degradation in water are dose, beam energy, beam power and dose rate. Perhaps the most relevant quantity is the dose, which is amount of energy deposited per unit mass, typically measured in units of gray (Gy = J/kg). The dose required to achieve the desired goal is important as is specifies the amount of power needed, which dominates the operating cost of running the accelerator. Previous studies on treating *E. coli* in municipal wastewater[43] and dyes in textile wastewater[44] via electron demonstrate the need to optimize dose and minimize operating costs.

For the application of treatment of PFAS in water we can assume the EB energy will be in the range of 1 – 10 MeV. The beam energy affects the penetration depth of the electron in the water and the number of interactions a single electron will have before it comes to rest. A 10 MeV beam energy is a practical limit for water treatment to avoid activating the water stream or system components and generating radionuclides. The left plot in Figure 1.2 shows the effect of EB energy on the penetration depth in water. At the surface of the water approximately 80% of the maximum dose is deposited. As you go deeper into the sample the % of maximum dose deposited increases to 100% before then decreasing again. If the EB is increased the shape of the curve gets flatter as the maximum penetration depth increases. As the percent of maximum dose deposited changes with depth it is important to design the interaction area of the water and EB to minimize the variation in dose delivered and maximize the amount of beam that is utilized (right plot in **Figure 3**).

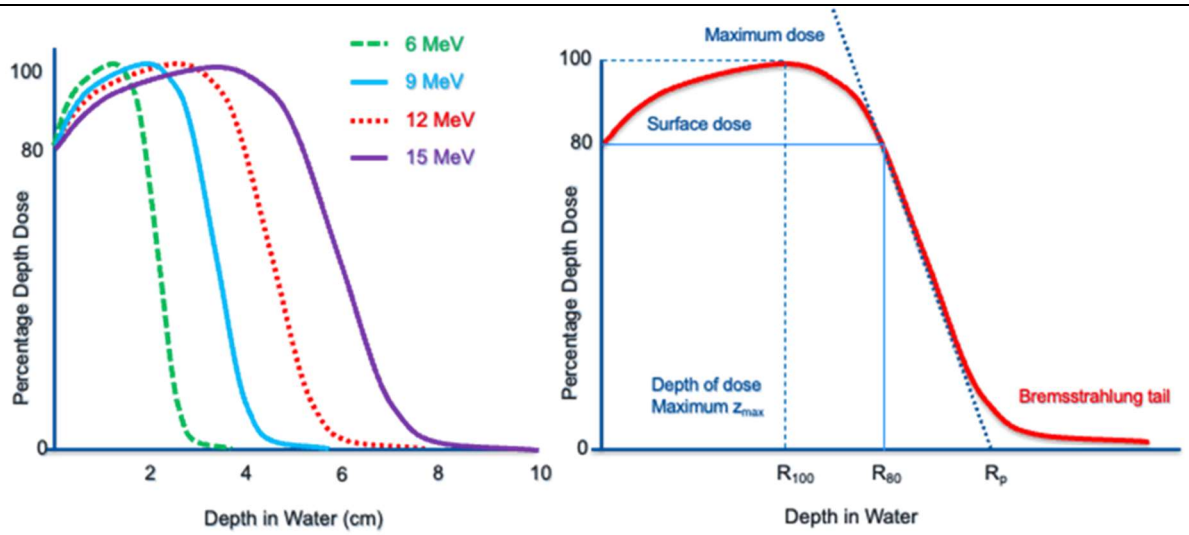

Figure 3. Effect of different EB energies on penetration depth in water (left); Typical EB percentage depth-dose curve, illustrating surface and maximum dose (right)

The beam power is an important metric as it determines the mass flow rate of water that can be treated. There are commercially available e-beam accelerators ranging in power from a few kilowatts (kW) to 100s of kW. As the beam power increases the capital costs increase and higher mass flow rates can be treated. Coupled with the beam power is the dose rate. The dose rate is the amount of ionizing radiation delivered per unit time, typically measured in kGy/sec. When discussing dose rate, the average dose rate is usually used but it is also important to understand the instantaneous dose rate or pulse form. For example, a pulsed copper LINAC could deliver the dose as 100s of microsecond electron pulses per second while a pulsed superconducting LINAC, or other continuous wave device, could deliver 100s of thousands of nanosecond long pulses. Understanding the dose rate is important as it can affect the ratios of the active species created during e-beam driven water radiolysis and thus effect the kinetics and breakdown efficiency of PFAS.

C. Information on Water Radiolysis

Water radiolysis is the mechanism by which the EB creates reactive chemical species that can facilitate the destruction of PFAS. The radiation chemistry of water has been thoroughly studied due to its significance in many fields like biology, environmental remediation, radiochemistry, and nuclear technology. Water radiolysis is the decomposition of water molecules due to ionizing radiation. Out of all radiation-chemical reactions that have been studied in aqueous solution, the most difficult and perplexing is the dissociation of pure water. When exposed to radiation, water undertakes a breakdown sequence into hydrogen peroxide, hydrogen radicals, and various oxygen compounds, such as ozone, which once converted back into oxygen releases large amount of energy[45]. The description below provides a summary of the radiolysis of water that is by no means comprehensive. Detailed description of the phenomenon can be found in "*The Radiation Chemistry of Water*"[46] and "*Primary Products of the Radiolysis of Water and Their Reactivity*"[47].

Normally, water radiolysis consists of three phases that occur in different time scales. The first or *physical stage* involves ionization and excitation and is reached in about 1 femtosecond [48]. Following ionization, the electrons transfer energy to the water molecules yielding an ion pair consisting of a water cation (H_2O^+) and an electron (e^-). During the *physico-chemical stage* (10^{-15} – 10^{-12} s), various reactions occur. The product H_2O^+ reacts with another water molecule to form the hydronium ion (H_3O^+) and the hydroxyl radical ($OH^\bullet$). The

hydroxyl radical and hydrogen peroxide (H_2O_2) are powerful oxidizing species, while the atomic hydrogen radical ($H^{\bullet}$) and aqueous electron (e^-_{aq}) are strong reducing species [47,48,49]. Throughout the last stage, the chemical stage (10^{-12} – 10^{-6} s), the radicals diffuse into solution[50] where they can react with each other or other surrounding molecules.

The time scale of events and radicals formed can be seen in **Figure 4**. The aqueous electron has a very short half-life of only a few tens of microseconds [50]. This time is dependent on the presence of impurities in the solution. The most problematic is molecular oxygen (O_2), due to it being challenging to remove from solution as well as it being a very efficient radical scavenger of aqueous electrons. This also applies to H_2O_2 and H_3O^+, which are also produced during the process of water radiolysis. Also, the concentration of e^-_{aq} affects its lifetime; the higher the concentration, the shorter their lifetime, because the recombination reactions become more prevalent [51]. This critically effects the energy efficiency of the EB breakdown of PFAS at different dose rates.

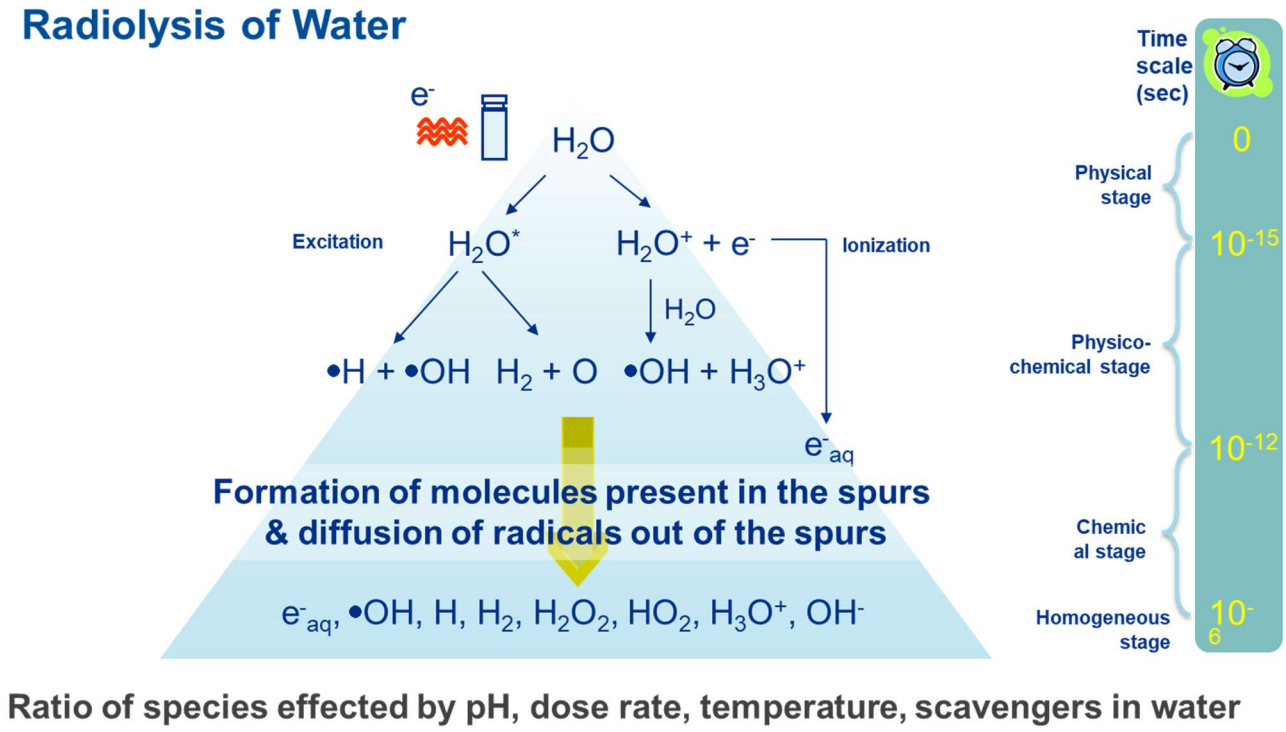

Figure 4. Time scale of events: water undergoes radiolysis to form ionization and excitation products. [52]

The highly reactive $H^{\bullet}$ and $OH^{\bullet}$ can react in several combinations to form stable products like H_2O, H_2 and H_2O_2. The hydroxyl radical is one of the most powerful oxidizing short-lived species. For instance, $OH^{\bullet}$ can oxidize inorganic ions that exist in higher valence states and can oxidize organic carbon species. Whether this will be seen as oxidation will always be dependent on the other radicals present in the aqueous system and their behavior under certain conditions. The types of reactions of $OH^{\bullet}$ with stable species or free radicals vary. The most common mechanism of $OH^{\bullet}$ induced oxidation for both inorganic anions and cations is electron transfer. Concerning most organic molecules, hydrogen atom abstraction and $OH^{\bullet}$ addition are the reactions that frequently occur.

Radical product yields are largely dependent on factors including the type of radiation, vapor pressure of the system, and linear energy transfer. These dissociated radicals are highly reactive and can affect the local environment by changing redox conditions. As e_{aq}^- is thought to be the dominant radical initiating PFAS

degradation via e-beam it requires closer study. Several destructive technologies utilize the reduction potential of aqueous electrons for PFAS degradation and defluorination. Auxiliary chemicals such as sulfite, iodine, and indole[53,54] can be combined with UV irradiation to generate e_{aq}^-. Destruction by direct current (DC) plasma also employs e_{aq}^- for breaking down PFAS in aqueous matrices[55]. Electron beam technology eliminates the use of auxiliary chemicals by utilizing the sample matrix itself to generate e_{aq}^- at a higher yield per unit energy. Moreover, as e-beam technology produces a beam of high energy electrons that interact with the sample, the spent adsorbents from pre-concentration step can then either directly be irradiated, under optimal conditions to bypass the elution and regeneration steps.

The mechanisms of PFAS degradation by e_{aq}^- depend on PFAS structure, chain length and functional group. The complications in understanding PFAS degradation mechanisms can be illustrated by the variation in the degradation byproducts reported by previous studies. This is more challenging for e-beam technology as this technique produces reactive species other than e_{aq}^-, such as H^+ and $OH^\bullet$, that can react with the degradation byproducts, complicating the accurate estimation of the degradation mechanism. Although e_{aq}^- is thought to initiate the degradation process, the other radicals could certainly participate in full degradation.

D. Previous Work on Electron Beam Destruction of Municipal Biosolids

Electron beam technology has been demonstrated for treating water and specifically municipal wastewater and associated biosolids. In May of 2018 Fermilab hosted a workshop on use of EB to treat water and biosolids. In that workshop some previous work in the field was discussed as illustrated in **Figure 5** [56]. Using the accelerator shown 99.9% of sludge bacteria from a Miami, Florida water municipality were killed via EB at a cost of 1.5 to 2 cents/gal in 1995. Destruction of dye in textile manufacturing water via e-beam has also been demonstrated in multiple countries. In 2012 e-beam was used to decrease total organic carbon by 30-40% and improve the clarity of the water from opaque to clear[57]. In that work 180 gpm of textile wastewater was treated at an operating cost of 0.11 cents/gal and installed cost of $4M US 2005 dollars.

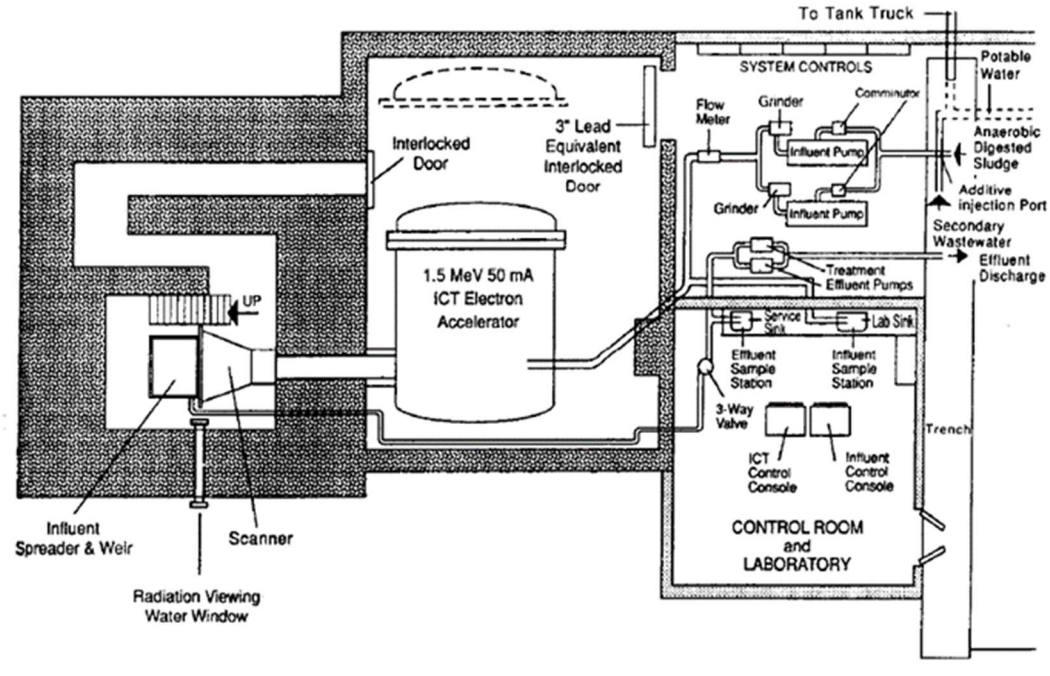

Figure 5. Electron beam accelerator used to treat municipal wastewater in Florida.

At the workshop held at Fermilab the following properties of EB treatment of water were recognized:

- Increases dewaterability.
- Removal of toxic chemicals not removed in conventional domestic water treatment: Pharmaceuticals, Agricultural runoff, Fuel additives (MTBE), PCBs, PFAS
- Reduction in pathogens
- No toxic residuals (no secondary waste generation)

At the same time the following limitations to the adoption of the technology were noted:

- Lack of Knowledge of Process – No book chapter on e-beam treatment of water
- Energy Intensive (High Operating Cost)
- Low Throughput

The Metropolitan Water Reclamation District (MWRD) of Chicago and FNAL have collaborated for over 5 years to prove that EB technology could be used in municipal wastewater treatment and to overcome some of the limitations associated with adopting EB technology. In recent years a growing number of utilities responsible for clean water have been moving from strict wastewater treatment to water resource management, some formally renaming themselves as water resource recovery facilities (WRRFs). Energy efficiency in equipment, processes, and operations is a fundamental part of this transition, and energy savings in facility retrofits can reach 50 percent.

In addition to energy efficiency improvements, wastewater contains about five times more energy than is needed for its treatment, creating an opportunity for new, innovative technologies and approaches for recovering that energy content. This summary identifies where in the water reclamation process e-beam is a good fit. Potential fits for e-beam in the flow chart of the reclamation process are shown as A through E in **Figure 6**. For the sake of this work, the primary application would be the treatment of biosolids to remove PFAS so that biosolids can be land applied (as fertilizers) without the risk of PFAS contamination.

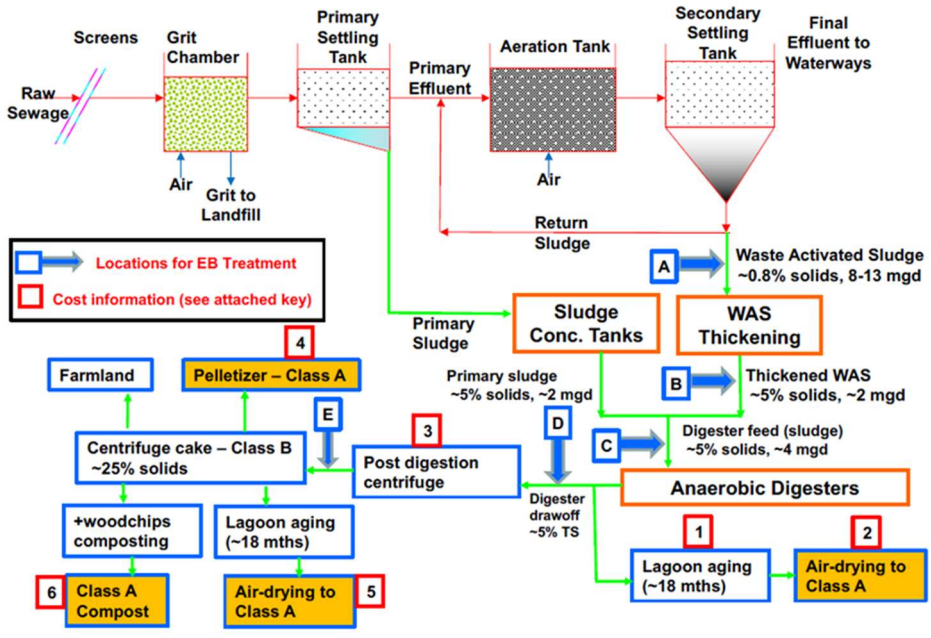

Figure 6. Process flow diagram of MWRD of Chicago municipal water treatment system from raw incoming sewage to biosolids treatment. Letters A-E represent potential application areas of electron beam technology.

For the destruction of PFAS in biosolids, two likely spots for e-beam application are (C) and (E) in **Figure 6**. At (C), just prior to anaerobic digestion, the EB breaks down the mixture allowing for a more complete conversion of the incoming carbon to energy, recovering some of the cost of the e-beam operation. At (E) the EB would have to treat the smallest mass flow rate so the total operational cost would be cheapest. At all application areas shown fecal coliform is killed to well below the required levels and some of the bad associated smell is remediated.

Although PFAS in biosolids is receiving a lot more attention recently, due to early results in the study we chose not to focus on using EB to destroy PFAS in biosolids. The main reason we chose to study other systems is that the concentration of PFAS in biosolids was so small that we determined it was not a good area to demonstrate the technology. More concentrated PFAS streams are more suitable for EB destruction as detailed in the following sections because of operating costs.

E. About the Recipient

3M is a more than 120-year-old company headquartered in St. Paul, MN and founded on the power of material science. In 2022, 3M had more than 90,000 employees at 200 sites worldwide, with manufacturing & converting operations in 29 countries, laboratory & application engineering in 47 countries, sales & marketing operations in 66 countries, and $1.9 billion in R&D spend. Every 5 years 3M establishes sustainability goals set on reducing its carbon footprint, greenhouse gas emissions, use of virgin fossil-based plastics, and increasing its use of renewable resources and energy. In line with EERE's goals, in 2022 3M achieved 51.9% of its electricity usage from renewable energy across its global operations and from 2020 to 2022 had a reduction in greenhouse gas (GHG) emission by 37.8% and a 13.1% improved energy efficiency[58].

3M has produced PFAS materials since the 1940s, primarily at its U.S. facilities in Decatur, AL, Cordova, IL and Cottage Grove, MN, and at European facilities near Antwerp, Belgium and Gendorf, Germany. 3M was the first manufacturer to announce its exit from production of C8-based PFAS like PFOA and PFOS [7] and in December 2022, 3M announced a full cease to its PFAS production by the end of 2025 [59]. This stewardship effort includes evaluating and implementing current water reclamation technology and exploring new technologies for removal of PFAS from soil and water. 3M has collaborated in several efforts to develop, test, implement and monitor drinking water and wastewater treatment technologies such as GAC, IE and RO. GAC, IE and RO are currently used by 3M at full scale for removal of PFAS from wastewaters and groundwater at its facilities, treating over 5 million gallons of water per day in such systems. The 3M Global Environment, Health, and Safety (EHS) Laboratory at 3M has also been instrumental in the development of sensitive analytical methods for PFAS measurement and providing analytical support for testing lab-scale and pilot scale PFAS treatment systems. The 3M EHS Laboratory also has a history of collaborations with academic and industrial leaders for testing and development of alternative PFAS removal technologies such as sonolytic treatment, advanced oxidation processes (i.e. hydroxyl radical) and reductive methods (i.e. aqueous electron) [60,61,62,63,22,23,24,64]. The unique EB accelerator capabilities at FNAL were coupled with 3M's expertise in PFAS analysis and knowledge of application of industrial-scale PFAS water treatment systems providing for a unique opportunity to evaluate this potential PFAS water treatment technology.

Electron beam accelerators are not widely used in the water treatment industry because conventional accelerators typically cannot handle large throughputs, require a large physical footprint, and have a cost-prohibitive energy requirement. A novel EB accelerator under development at the Department of Energy's Fermi National Accelerator Laboratory (FNAL), among other accelerator technologies, may address all three of these issues and unlock high throughput applications, like water treatment, for e-beam technology. FNAL, whose primary discovery tool is the particle accelerator, has over 50 years of experience in the design, building and operation of accelerators. Although the novel e-beam accelerator is not built yet, proof of principal work was done in FNAL's Accelerator Applications Demonstration and Development (A2D2) accelerator.

Summary of Project Objectives (SOPO)

The end goal of this project aimed at optimizing the conditions of the radiation-induced degradation of PFAS via EB accelerators to achieve the highest reduction efficiency while identifying an EB technology that can energy efficiently and cost-effectively mitigate the problem. We also planned to conduct an economic analysis on implementing EB technology into current process flows. This study will provide the data necessary for 3M to choose the best balance of increased efficacy and reduced total process energy requirements. Our research efforts will also focus on the examination of potential environmental and health impacts of EB treatment of PFAS. We shall also consider novel EB technologies to make the proposed treatment attractive for future development and commercialization.

To complete this project, two main research thrusts worked in concert to identify the cheapest, most effective way to destroy PFAS using a combination of an EB accelerator and additives that boost the performance of the EB process. The first thrust largely involved testing of laboratory prepared samples that contained PFAS of interest. The irradiation experiments included various concentrations of the PFAS of interest in water, spanning a large range in total doses, dose rates, dissolved oxygen concentrations, temperatures, and chemical additives. Extensive post-treatment characterization of PFAS was performed using 3M's advanced analytical capabilities. This enabled both confirmation of the parent and product species and screening for unforeseen species together with understanding the treatment performance. The chemical compounds and their products were characterized and quantified chromatographically using gas, liquid, and ion chromatographic methods, largely with mass spectrometric detection.

The EB treatment outlined in Y1 was conducted largely using the Accelerator Applications Development and Demonstration (A2D2) accelerator EB at FNAL's Illinois Accelerator Research Center (IARC), with some work performed in a commercial Dynamitron EB system at E-beam Services, Inc. (Lebanon, Ohio). Y1 work was focused on determining how much power is required to effectively decompose PFOA and PFOS with verification of complete mineralization to inorganics constituents, and with detection and identification for intermediate products to rule out potential hazardous biproducts. Additionally, other PFAS types were also evaluated, and expanding upon the original set goals of evaluating PFOS and PFOA. The work from Y1 provided necessary information about the optimal operating parameters and additives to use when treating PFOS and PFOA by e-

beam. The power requirements largely dictated the operating costs for EB accelerators, but costs of additives were also considered. The information gained was then used to see where in a water treatment system an EB accelerator would be cost and energy efficient to treat PFAS by comparing to a conventional PFAS water treatment system (i.e., GAC).

The Y2 work focused on the assessment of currently available commercial EB technologies that could potentially be suitable for PFAS treatment, as well as evaluation of new SRF accelerator technologies being developed at FNAL. The EB requirements determined experimentally during Y1 were used to conduct an economic and energy analysis of treating PFAS with different EB accelerator designs. Conventional EB accelerators and FNAL's compact SRF accelerator design were evaluated for their suitability, from an energy efficiency and cost standpoint. Furthermore, the energy requirements and greenhouse gas emissions associated with conventional water treatment technologies like GAC were compared to EB treatment technologies for water treatment.

A kickoff meeting was held October 26, 2020, prior to conducting Q0 preliminary work. The primary proposed 2-years work designated Q1-Q8 were accomplished in 2.5 years with a 6-month no-cost extension to the original 2-year planned project that largely stemmed from setbacks due to the COVID pandemic, as shown in **Figure 7**.

The major tasks and expected deliverables from the Summary of Project Objectives (SOPO) are listed below:

Y1: Task 1 – Health/Environmental Assessment

Partially degraded intermediates might be created during electron beam treatment. This has not yet been studied in laboratory samples. While many studies have been published on the environmental concerns of PFASs, less data is available on the byproduct substances. Since the e-beam can mineralize the test species, the form of fluorine will need to be tracked to make sure it is a fluoride ion in solution and is not toxic hydrofluoric acid (HF) gas that would require additional scrubbing to remove. Other byproducts in the form of short chain perfluoroalkyl carboxylic acids, perfluoroalkyl sulfonates and volatile fluorocarbons could be found in solution or the emitted gases, all of which will be determined analytically by 3M. This task will involve e-beam treatment of PFASs at two concentrations of the contaminant of interest, medium concentration level (20 ppb) and high concentration level (20 ppm), various total doses (0, 200, 500 and 1000 kGy) and with two degradation promoting additives (NaOH and HNO_3). For all samples we will use the maximum dose rate (1.2 kGy/sec) to minimize the treatment time. For all samples we will perform a nitrogen purge prior to irradiation to assist in the total breakdown of PFASs. Due to the high total electron beam dose, the samples will heat during treatment. The sample temperature will be kept below 70°C. This will either be achieved via active cooling or pulsed start-stop treatment to allow for cooldown periods.

Deliverable: Experimental results will provide confirmation of the anticipated breakdown species of PFASs in water, screen for unexpected species and examine if there are any health and environmental concerns associated with them. This will provide a more complete understanding of PFAS byproducts toxicity and help us identify if any byproducts are directly related to electron beam treatment. As a first step of the study, this will allow us to potentially adjust the treatment parameters to mitigate production of hazardous species (if any) or conclude that e-beam is not a viable treatment option for PFAS treatment. **GO/NO-GO Step.**

Y1: Task 2 – Optimal E-beam Dose and Additive Concentration

Description: Typically, water radiolysis leads to complete mineralization of contaminants without the need for additional chemicals in solution. This is mostly due to the generation of several charged species upon irradiation (hydroxyl radical and aqueous electron being predominant) that interact with the contaminants. The degradation process includes a few stages: free radical formation, diffusion of radicals, and reaction between radiolytic products and the contaminants. Limited number of studies show that PFASs, specifically PFOA and PFOS, can be decomposed via water radiolysis at 10 kGy to 2 MGy total dose.

Primarily, we will evaluate four e-beam doses (50, 100, 200 and 500 kGy) and three contaminant concentrations (20 ppt, 20 ppb and 20 ppm) covering the range from environmentally relevant levels to highly concentrated levels of PFASs. All the samples that receive an e-beam dose will be treated with 9 MeV electrons. Electron beam dose delivery is characterized by relatively high surface dose and a maximum dose occurring at certain depth in the medium dependent on the density of the material. Beyond the max, the dose drops off rapidly and levels off at low dose. To ensure homogenous dose delivery throughout the sample, the sample height will be controlled so that the dose received at the top surface of the liquid is equal to the dose received at the bottom of the sample. For water this is about 3 cm thick, and the dose received at the top and bottom of the sample will be 80% of the dose seen at the maximum of the sample. The total absorbed dose will be measured and verified by radiochromic film dosimetry that is NIST traceable. The data from each run will be collected in Fermi's internal data management system called "travelers" and be ported to Excel for data analysis and presentation. The data that will be collected includes, beam power, beam energy, total treatment time, ambient temperature, sample temperature, sample volume/mass and dose received.

Deliverable: The overall results of Task 2 will determine the total dose needed to treat various levels of PFAS in water. The results will also indicate if the contaminants can be cost effectively decomposed via e-beam alone or chemical additives would be required to increase the reaction rate and therefore reduce the overall power consumption. **GO/NO-GO step**

Subtask 2.1: Dose Rate

Description: Dose rate at FNAL's A2D2 accelerator can be varied from 0.2 to 1.2 kGy/sec, but it is expected that most treatment will be performed at the highest dose rate in order to minimize the treatment time. Dose rate effects are often related to high dose rates which are typically delivered by e-beam accelerators versus other sources of ionizing radiation. Hence, e-beam treatment is usually identified as radiation processing at high dose rates. The water radiolysis process based on high energy electrons has been described as more economical and effective for large scale applications as compared to other methods applied for the removal of emerging contaminants. High dose rates affect radiolysis yields by increasing the radical interaction probability. Small number of experiments will focus on determining if there are any dose rate effects associated with the treatment. We will investigate the chemistry effects at three dose rates – 0.2 kGy/sec (low), 0.6 kGy/sec (medium) and 1.2 kGy/sec (high).

Deliverable: The overall results of Task 2 will determine the total dose needed to treat various levels of PFAS in water. The results will also indicate if the contaminants can be cost effectively decomposed via e-beam alone or chemical additives would be required to increase the reaction rate and therefore reduce the overall power consumption. **GO/NO-GO Step**

Subtask 2.2: Effect of Dissolved Oxygen

Preliminary studies show that EB treatment is more effective in reduced dissolved oxygen conditions, and a likely scenario for groundwater. Purging with nitrogen appears to be both quick and effective procedure to remove dissolved oxygen from water. To study the effect of dissolved oxygen, its concentration will be controlled by purging oxygen-saturated water samples with high purity nitrogen gas. This set of experiments will focus on determining the optimum duration of purging. The expected number of samples to be evaluated in this testing period is 16. We will purge the samples with nitrogen for various times (1, 5, 10 and 30 minutes). In this work we will have to determine flow rate of the gas of choice that is appropriate for the samples volume. Dissolved oxygen levels can be determined using a dissolved oxygen meter. In addition, we will explore if other gases or gas mixtures, for example Argon and/or hydrogen, change the chemistry related to the degradation of PFASs.

Deliverable: Determining how long the gas needs to be purged through the samples will allow us to calculate associated costs for scaling up the procedure. It will also tell the scale of effect of the dissolved oxygen on PFAS breakdown.

Subtask 2.3: Chemical Additives NaOH & HNO_3

Description: Although the electron beam process can decompose the contaminants of concern without any chemical additives, preliminary work demonstrates the need of small amounts of nitric acid **Error! Bookmark not defined.**. Chemical additives can speed up the degradation reaction, making the overall process more economically feasible. Similarly, preliminary experimental results show complete defluorination of PFOA in N_2-saturated alkaline solution. Recent unpublished results, obtained in a collaboration between FNAL and the Army Corps of Engineers Engineering Research and Developmental Center, demonstrated the ability of e-beam to destroy over 99% of 20 ppb perfluorooctanesulfonate (PFOS) with high concentration of additives (HNO_3, NaOH). The scope of that work was extremely limited, but it was found that the amount of power required to breakdown the PFOS was roughly 10 times that needed to breakdown PFOA. Subtask 2.3 will focus on optimizing the treatment parameters. This will include assessing various levels of chemical additives in combination with individual contaminant or a mixed field sample. The selection of the additives is based on preliminary observations made by FNAL showing enhanced degradation of PFOS in the presence of HNO_3 and NaOH (unpublished data). In this round all samples are to be treated with the dose rate found in Subtask 2.1 and the inert gas purge found in Subtask 2.2. At a high level we look at bounding e-beam doses from 0 to 500 kGy. The table below lists the general parameters and ranges that will be assessed. If all combinations were to be tested there would be on the order of 400 experiments. To reduce this number a simplified design of experiments technique will be used to eliminate unneeded experiments. It is known for example that PFOS is harder to remove from solution than PFOA using e-beams. A bulk of the work need only be done on PFOS samples and the end results applied to PFOA contaminated samples.

Deliverable: The outcome of Subtask 2.3 will be a set of optimal operating parameters needed to treat a given water sample using e-beam technology. Plots of removal efficiency versus additive concentration will be made for multiple additives at various electron beam doses, ranging from 50 to 500 kGy.

Subtask 2.4: Other Potential Chemical Additives

Description: Within the scope of the proposed work, additional literature review will be done to see if there are other chemical additives that can be examined to potentially enhance the effect of breaking down PFASs via electron beam. It is anticipated that additional information gained from the experimental results in subtask 2.3 will yield information that helps to better define the chemistry and help in additive selection. We are anticipating investigating 160 samples in this testing period.

Deliverable: The outcome of Subtask 2.4 will generate PFAS removal efficiency curves versus additive concentration at various electron beam doses, ranging from 50 to 500 kGy.

Y1: Task 3 – Process Flow Specification

Description: 3M will evaluate at least one conventional water treatment technology used in treatment of PFASs. Although not limited to GAC, it seems the likely candidate. 3M will do a detailed analysis of the technology to find the total life cycle energy demands and costs associated with the use of each conventional water treatment technology examined. Based on the results from the year 1 sample work, 3M will determine where in the water treatment system e-beam technology would be the best fit. It will enumerate monetary costs, energy usage, and as necessary other factors such as logistics and regulatory constraints. This will be the metric to be used for evaluating the accelerator-based methods.

Deliverable: Total lifetime energy requirements and treatment costs for at least one conventional water treatment technology. If GAC is examined for example, energy costs considered associated with manufacturing, transportation, use, regeneration, and disposal will be included to compare with e-beam treatment.

Y2: Task 1 – Evaluation of Up to Three E-beam Technologies for PFAS Treatment

Description: Based on the dose and power requirements from Year 1 and recommendations from 3M as to where the e-beam technology could be integrated into a water treatment system, develop a general set of specifications for each of the e-beam technologies that purport to provide the optimal performance for treating PFASs. The e-beam designs that will be reviewed include FNAL's compact SRF design, a commercially available normal conducting (NC) RF accelerator - the IBA Rhodotron, and a high-intensity, low duty factor, pulsed NC accelerator. Specifications produced will include beam energy; beam current; peak power, pulse length, and duty factor for pulsed accelerators. These specifications can then be used to determine dose and throughput capabilities of each technology. This will place well-defined limits on each technology and will also inform a "first cut" of any technology that will not be able to meet the dose and power requirements.

Deliverable: A set of specifications for each technology will be evaluated and at least one chosen to do more detailed energy and cost analysis in the next task.

Y2: Task 2 – Technical Evaluation and Cost Analysis of E-beam Technologies

Description: After a descoping of e-beam technologies to a smaller list that is most appropriate for PFAS treatment in the previous task, a more thorough examination of the remaining technologies will be done. This task will develop the information that will feed a cost/risk/benefit matrix of the subject technologies. Simple conceptual designs of complete accelerator systems for at least one of the three technologies will be developed. Each design will then be examined to determine: 1) the capability of each technology in terms of beam power, the product throughput that such beam power can support, scalability of the technology, and reliability; 2) the technical readiness of each technology; 3) the amount of research and development yet required to bring each technology to application readiness; 4) an estimate of the cost of that research and development; 5) evaluation of any regulatory factors that might be unique to any individual technology. This task will also conduct a thorough, well-bounded, economic analysis of the actual implementation of each of the technologies. The study will look at how each of the electron beam technologies may be inserted into the total process flow and the process steps that may be eliminated, replaced, or complemented. The study will provide the data necessary for 3M to choose the best balance of increased efficacy and reduced total process energy requirements.

Deliverable: A data set to be used for the final report.

Y2: Task 3 – Review Panel & Recommendations

Description: This task will include a FNAL in-house (and/or an outside SME if needed) review to vet the analyses conducted in the previous tasks to ensure technical accuracy. If the review exposes any deficiencies, the teams of Tasks 2 and 3 will gather the suitable information to respond to recommendations of the review panel, or if beyond the scope of the remaining resources, the teams will provide a clear response and explanation of the deficiencies discovered.

Deliverable: A brief report of either concurrence or recommendations to fill gaps or deficiencies.

Y2: Task 4 – Final Report

Description: This task will summarize the work of the previous tasks and describe the technology options that was explored and the total cost of operating a facility for PFAS treatment.

Deliverable: A white paper report that describes PFAS treatment needs via e-beam accelerators, and a cost/risk/benefit matrix to achieve them.

Budge Period	Budget Period 1 (BP1)					Budget Period 2 (BP2)			
Year	2020	2021				2022			
Months	Oct-Dec	Jan-Mar	Apr-Jun	Jul-Sept	Oct-Dec	Jan-Mar	Apr-Jun	Jul-Sept	Oct-Dec
Quarter	Q0	Q1	Q2	Q3	Q4	Q5	Q6	Q7	Q8
BP1-Startup Activities									
BP1-Task 1 (Health/Env. Assessment)									
Subtask 1.1 (MWRD Stewardship-stakeholder input)									
BP1-Task 2 (Optimization of E-beam dose and Additives)									
Subtask 2.1 (Dose rate)									
Subtask 2.2 (Effect of DO)									
Subtask 2.3 (Chemical additives acid-base)									
Subtask 2.4 Other Additives									
Subtask 2. 5 Preliminary Techno-Economic Assessment									
BP1-Task 3 (Process Flow Specifcation)									
BP1-Task 4 (Project Management)									
BP2-Task 1 (Evaluate Appropriate E-beam Technologies for PFAS)									
BP2-Task 2 (Tech Evaluation and Cost Analysi sof E-beam tech)									
BP2-Task 3 (Review Panel & Recommendation)									
BP2-Task 4 (Final Report)									
BP2-Task 5 (Project Management)									

Figure 7. Original timelines for the project. (A 6-month no-cost extension added to the project covering Jan-July 2023 is not shown).

Activities Performed and Results Achieved

Pre-Study Tasks and Results

A fundamental initial task was to evaluate sample containers and identify one that was best suited for EB treatment and would accommodate the intended sample analysis procedures. We exposed several candidate containers to a total dose of 1 MGy, including a variety of headspace vials, volatile organics analysis (VOA) vials, autosampler vials, jars, centrifuge tubes and bottles composed of glass, polyvinylchloride (PVC), high-density polyethylene (HDPE), polypropylene, aluminum, and combinations thereof. Each was fitted with their associated screw caps or crimp style caps, as appropriate. Several containers that were tested contained a fused fluoropolymer liner associated with their caps which was meant to be an inert contact surface. However, the irradiation with the EB resulted in degradation of the fluoropolymer liner and formation of water-soluble perfluoroalkyl carboxylates (PFCAs). This was anticipated to interfere with the analysis of EB treated samples for detecting anticipated degradation product of PFOS and PFOA in the present work and therefore were not selected for use. Additionally, several containers and caps structurally failed, resulting in cracks, plastics embrittlement, caps fusing with glass, etc., and were ruled out. In the end we found that 20-mL clear borosilicate glass headspace vials with a 20 mm aluminum crimp seal and butyl rubber septum (without fluoropolymer liner) worked best, as shown in **Figure 8.** These containers and caps held up well to the EB treatment and maintained the integrity of the head space gases for analysis of potential volatile compounds, as demonstrated by stability of spiked perfluoro-2-butene (PF2B) gas into sealed vessels (controls) during the shipment and sample treatment process. The only change that occurred with such vials because of EB treatments was discoloration of the glass to amber colored, and at unusually high EB doses (above 1MGy) the butyl rubber liner of the cap fused to the glass and were difficult to open. However, under most EB treatment conditions they worked well.

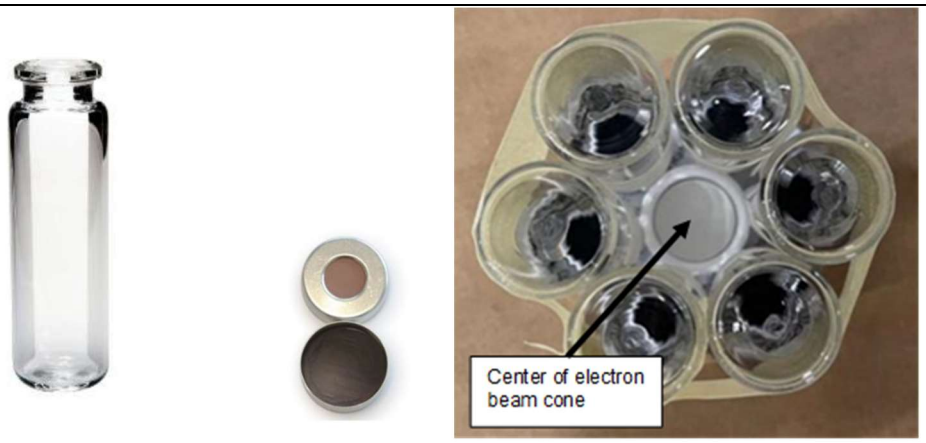

Figure 8. Test vessels used for EB irradiation experiments and carousel used to hold them for exposures.

A second task included as part of startup activities, and not included in the SOPO, was to develop a method of exposure for test vessels to the EB irradiation. This was implemented, as demonstrated in the pictures in Figure 9. For EB treatments at FNAL, the vials were placed on the sample platform (position 4), 135 cm from the beam exit from the accelerator window, where most samples are treated. A piece of aluminum foil was used as a secondary containment in case there was any leakage from the samples so that it would not go into the beam dump. The samples were placed with the seal side down to avoid any issues with the necking of the vessel or the aluminum lid limiting the e-beam dose delivered. Finally, the samples were positioned in a hexagonal pattern around the center of the beam to allow for processing of 6 samples at a time while maintaining uniform dose through the samples. The picture on the left in **Figure 9** shows the A2D2 experimental linear accellerator (LINAC) at FNAL in it's entirity minus some shielding and an aluminum 80cm x 80cm enclosure shown in the picture on the bottom left and right. The metal duct shown behind the sample in the picture in the right is exhaust designed to remove ozone generated in the process. In a system specifically designed for water treatement ozone production would be minimal to none. Some tested containers are also shown in the figure to the right. The accelerator is a repurposed medical accelerator that is operated at 10 MeV. It is a pulsed copper LINAC that allows change in the dose rate directly from 0.2 to 1.2 kilogray (KGy) per second. The beam of electrons exits the accelerator with a small spotsize on the order of millimeters (mm) in diameter. All of the sample work in this study occurred at position 4 shown in **Figure 9**. After traveling the 135 cm in air the spot size of the e-beam increases from millimeters in size to approximatly 10.3 centimeters. Samples were typically dosed maximally at 125 kGy per run. After each 125 kGy run some time was allowed for the samples to cool and the ozone to clear before the accelertor was entered. The dosimetry films are good up to 200 kG and a maximum temperature of 60 C, so sample temperatures were controleld below 60 C through treatments.

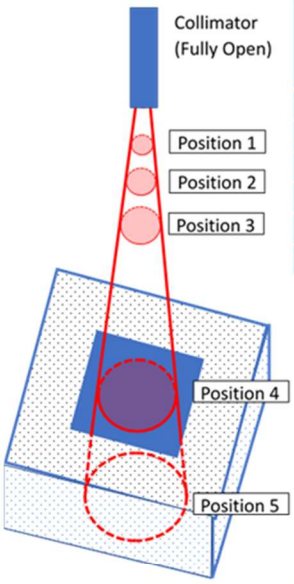

Setting	Power, kW	Dose Rate, kGy/kg-s
1	0.22	0.22
2	0.43	0.43
3	0.65	0.65
4	0.87	0.87
5	1.08	1.08
6	1.3	1.3

Position	Beam Diameter, cm	Distance from Collimator, cm
1	4.8	63
2	5.7	75
3	7.1	93
4	10.3	135
5	12.6	165

Figure 9. The A2D2 accelerator EB system configuration used to expose test vessels.

In addition to the A2D2 LINAC used at FNAL for most EB experiments, treatments at nominal dose rates of 15 kGy/sec and 30 kGy/sec were performed at E-Beam Service, Inc. (Lebanon, OH). E-Beam Services, Inc. utilizes a IBA Dynamitron EB accelerator with 150 kW capability shown in **Figure 10**. The Dynamitron is a direct current linear accelerator in which the beam of electrons is scanned at 100 Hz, operating at either 3 MeV or 4.5 MeV kinetic energy.

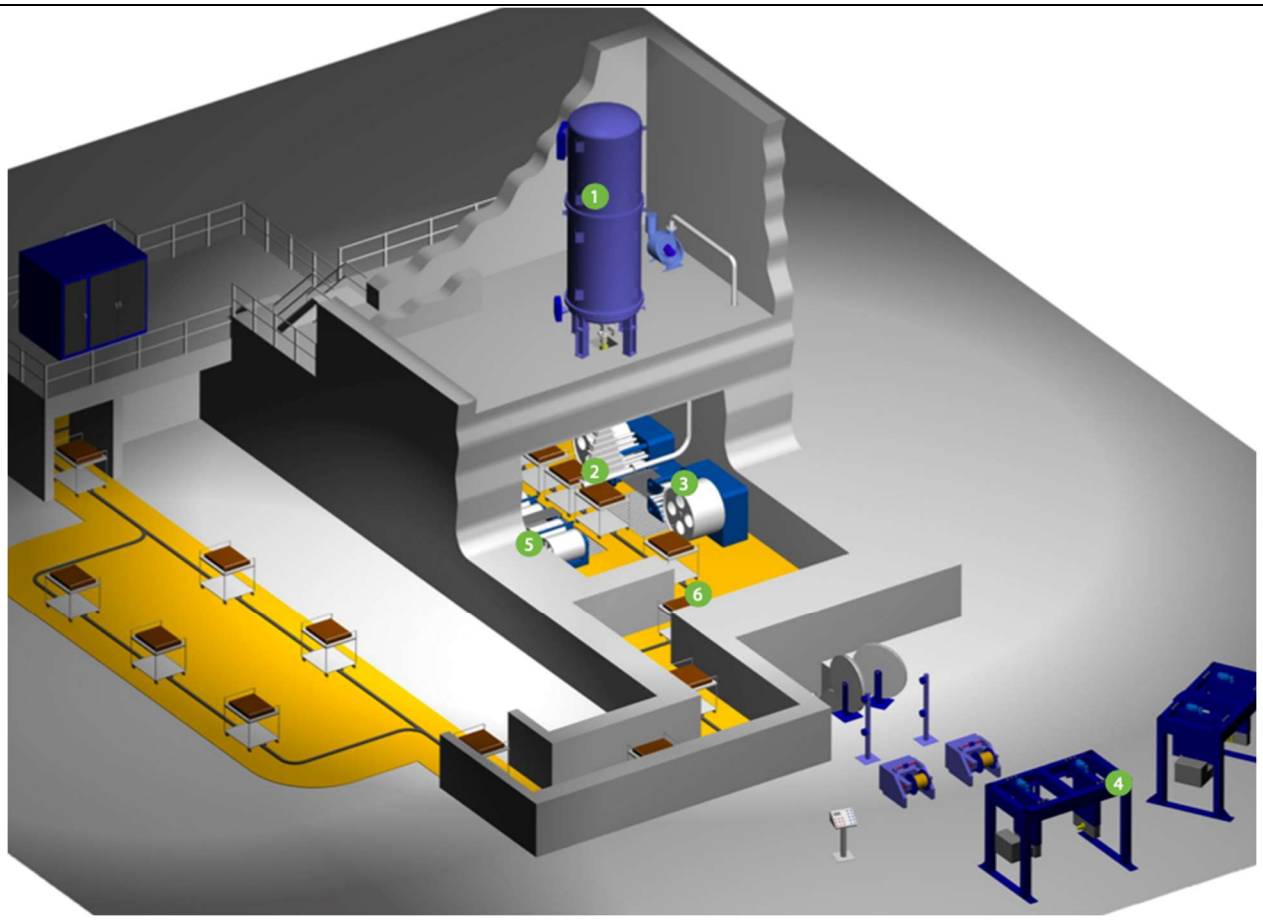

Figure 10. Dynamitron E-beam Facility Diagram. (1) Dynamitron, (2) Scanning Horn, (3) Capstan Underbeam, (4) Pay off and Take up Reels, (5) Small Wire Capstan, (6) Tray Conveyor System

Due to the lower energy of this accelerator, the depth/height of the water in the samples was proportionally adjusted to match the penetration depth of the electrons. The samples were prepared to accommodate the lowered penetration depth and ensuring uniform e-beam treatment of the samples.

The PFAS-water samples prepared by 3M were irradiated in two batches. All of the samples were irradiated to a nominal target dose of 500 kGy. Fifty-six samples were processed targeting a 15 kGy/sec instantaneous rate and thirty-two samples were processed targeting a 30 kGy/sec instantaneous rate.

For the irradiation targeting the instantaneous rate of 15 kGy/sec, settings of 4.5 MeV and 25 mA were used across a 40-inch scan. FNAL supplied dosimeters were placed on top of the samples. The dosimeters were on samples for passes 1-4, passes 5-8, passes 9-12, or passes 13-16. The target dose was 31.3 kGy per pass for a total of 16 passes (nominal 500 kGy total dose). The time between passes was estimated at 8.7 minutes. When the samples passed under the scan horn of the accelerator, the samples were 32 inches from the window. At this distance, the beamed area is approximately 23 cm. The samples were within the beamed area under the scan horn for 1.95 sec, resulting in a calculated dose rate of 16 kGy/sec when being dosed.

For the irradiation targeting the instantaneous rate of 30 kGy/sec, settings of 3.0 MeV and 50 mA were used across a 42-inch scan. FNAL supplied dosimeters were placed on top of the samples. The dosimeters were on samples for passes 1-4, passes 5-8, passes 9-12 or passes 13-15. The target dose was 33.3 kGy per pass for a total of 15 passes (nominal 500 kGy total dose). The time between passes was estimated at 4.5 minutes. When the samples passed under the scan horn of the accelerator, the samples were 32 inches from the window. At

that distance, the beamed area was approximately 23 cm. The samples were within the beamed area under the scan horn for 1.15 sec, resulting in a calculated dose rate of 29 kGy/sec when being dosed.

Testing Conditions

In Y1, water samples containing PFAS were prepared at 3M and typically treated by EB irradiation at FNAL. Hundreds of samples were prepared and treated as part of Y1 work. The prepared samples typically contained perfluoroctanesulfonate (PFOS) or perfluooctanoate (PFOA) at nominal concentration of 20 μg/L (ppb) or 20 mg/L (ppm). Additional samples were also prepared with other types of PFAS and were evaluated for degradation by EB and included identification of degradation intermediates. For preparations of PFAS solutions in water for EB treatments, care was taken to omit organic solvents either by directly preparing accurately weighed PFAS solid neat material in water solutions at desired pH, or allowing organic solvent to evaporate (for stocks prepared in methanol or acetontrile) prior to being resuspended in aqueous phase. For higher molecular weight PFAS, some issues in solubility was observerd and affected initial concentrations to be significantly different than intended concentrations.

Samples with PFOA and PFOS were typically treated with EB doses of 0 kGy (non-irradiated controls) and nominal 500 kGy, and all result normalized to the result of the non-irradiated controls. As part of the project objectives for Y1, Task 2, we evaluated effects of dose rate at 500 kGy with nominal dose rates of 0.015, 0.25 kGy/sec, or 1.2 kGy/sec at FNAL. Additional samples were sent to E-Beam Services, Inc. for EB treatments at nominal 15 kGy/sec and 30 kGy/sec**.** As additional subtasks for Y1, Task 2, the effect of total dose was also evaluated from 50 kGy to 1.6 MGy using a determined opitimal dose rate near 1.2 kGy/sec, the effects of pH-adjusting additives were also evaluated, including additon of nitric acid (HNO_3) to reduce the pH and sodium hydroxide (NaOH) to raise pH, and the effects of dissolved oxygen (DO) on degradation was evaluated. Most experiments were conducted under a headspace of argon (Ar) to minimize radical reactions with oxygen. From that work, optimal EB treatment conditions for PFOA and PFOS based on pH, dissolved oxygen, dose rate, total dose, as well as temperature were evaluated and defined. The parent PFAS compounds and water-soluble and volatile intermediate degradation products were identified and quantified by analytical procedures such as high-performance liquid chromatography with triple quadrapole mass specrometry (LC/MS/MS), gas chromatography with mass spectrometry (GC/MS) and ion chromatograpahy (IC). Intermediates were typically identified under sub-optimal EB conditions where degradation was incomplete. This is summarized below in Y1, Task 2 results. However, the Y1, Task 1 results for the health and environmental assessment phase came after achiving those data, but that is discussed first, below.

Y1: Task 1– Health/Environmental Assessment

Partially degraded intermediates might be created during electron beam treatment. While many studies have been published on the environmental concerns of PFASs, less data are available on the byproduct substances. The experimental results provided confirmation of the anticipated breakdown species of PFAS in water, and in some instances identified unexpected species.

PFAS Degradation Products by EB Treatment

As a result of Y1 work, both PFOA and PFOS were demonstratably removed from water by EB treatment, versus non-treated controls. The data indicated the addition of sodium hydroxide facilitated greater

losses, showing that increased pH aids degradation efficiency. This is consistent with the literature, indicating that in basic solutions (pH above 10), the hydroxyl radical and hydrogen peroxide dissociate in solution, which likely leaves the aqueous electrons (aka aqueous electron) as dominant species and should therefore have a stronger influence upon the chemistry. Also, the data indicated EB dose rate possibly affects efficiency and completeness of degradation, as described further below.

However, as part of the environmental health and safety assessment aspect, degradation products were determined analytically from most completed irradiation experiments. It was shown that loss of PFOA resulted in formation of lower molecular weight perfluorinated carboxylic acids only. For PFOS little to no degradation products were observed, possibly indicating complete degradation. Complete degradation was verified under the optimal condtions of pH 13 and 1.2 kGy/sec with 100% mass balance for inorganic fluoride from PFOA, and fluoride and sulfate from PFOS.

The degradation intermediates from PFOS and PFOA treated by EB were identified from treatments at sub-optimal conditions, in order to determine if any had exceedinglly hazardous properties. PFOA is a C_8 perfluoroalkyl carboxylate (PFCA), and the primary degradation intermediates from EB treatments, typically observed under sub-optimal test condtions, were lower molecular weight PFCAs, including: TFA (C_2), PFPA (C_3), PFBA (C_4), PFPeA (C_5), PFHxA (C_6)and PFHpA (C_7). These were identifed by LC/MS/MS analysis. The primary endproduct was identified as fluoride ion by IC analysis, with 100% mass balance to fluoride ion observed under optimal EB treatment conditions that were determined as part of the present work. No volatile fluorocarbons were observed from PFOA by headspace GC/MS analysis, ruling out potentially deleterous products such as perfluoroisobutylene (PFIB). The results suggested initial radical attack of the PFOA molecule occurred near the carboxylate functional group. This is supported by recently conducted ab initio computer simulations of e_{aq}^- reaction with PFOA [65]. It is likely that OH• is also involved in the unzipping secondary reactions following intitial attack by e_{aq}^-. A proposed degradation pathway for PFOA is shown below in **Figure 11**.

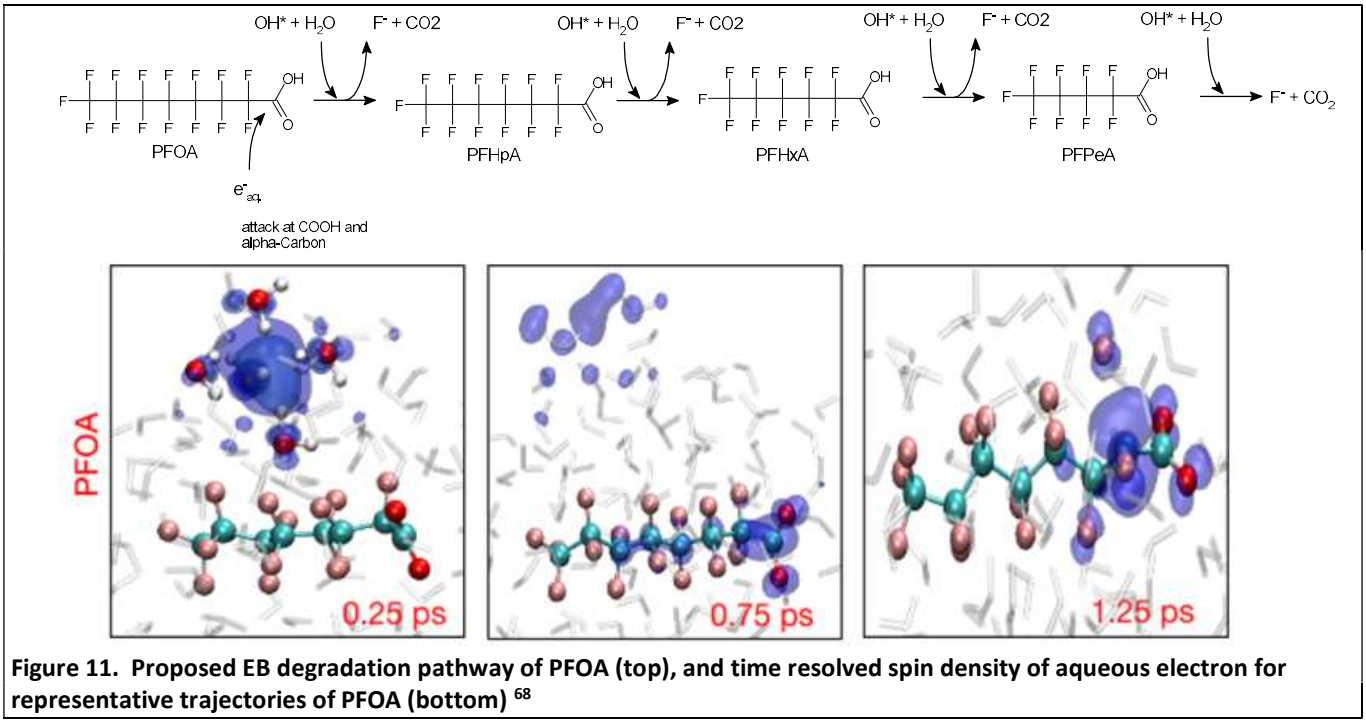

Figure 11. Proposed EB degradation pathway of PFOA (top), and time resolved spin density of aqueous electron for representative trajectories of PFOA (bottom) [68]

PFOS is a C_8 perfluoroalkyl sulfonate (PFSA), and major degradation intermediates from EB treatments were typically not present. Minor levels of water-soluble intermediates such as PFOA and lower molecular weight PFCAs were observed by LC/MS/MS analysis, but accounted for less than a few percent of the PFOS removed. Also, trace levels of volatile hydrofluorocarbons like trifluoromethane (C_1), pentafluoroethane (C_2), 1H-heptafloropropane (C_3) and 1H-nonafluorobutane (C_4) were also observed from PFOS by headspace GC/MS analysis, but again only accounted for small quantities of the PFOS removed. Analysis of PFOS reaction mixtures by high resolution LC-qTOF analysis also revealed the absence of any unknown water-soluble intermediate products. The vast majority of PFOS lost was typically observed simply as inorganic sulfate and fluoride ions, indicating likely role of highly unstable intermediate(s) after radical attack is initiated and which were not identified by the analytical methods employed. The observed low-level volatile fluorocarbons indicated radical attack by e_{aq}^- in the fluorocarbon tail, away from the sulfonate functional group. This is also supported by ab initio molecular dynamics simulations of aqueous electron reaction with PFOS [65]. It is possible that some minor e_{aq}^- attack occurs near the sulfonate functional group, resulting in formation of a C8 radical anion, which then undergoes reaction with water and/or hydroxyl radical and results in the series of low-level PFCAs, but most PFOS likely undergoes attack at the perfluorocarbon tail followed by rapid decomposition of some unstable intermediate(s) to ultimately produce fluoride and sulfate anion. A proposed degradation pathway for PFOS is shown below in **Figure 12.**

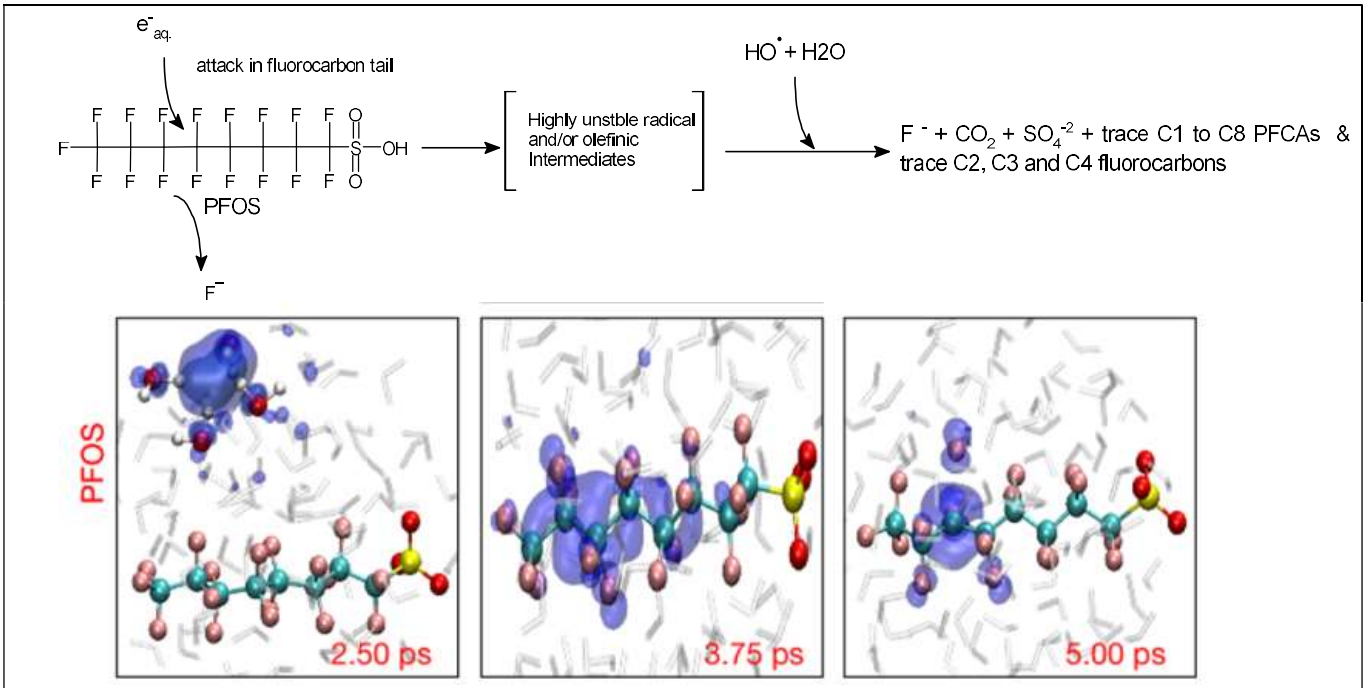

Figure 12. Proposed EB degradation of PFOS (top), and time resolved spin density of aqueous electron for representative trajectories of PFOS (bottom) [68]

PFAS Isomers and EB Treatment

PFAS such as PFOS and PFOA are produced as predominantly linear isomers. However, depending on the source production process, each can have a significant isomeric component as branched isomers. PFAS from

electrochemical fluorination (ECF) process can have a signficant branch isomer composition (20-30% w/w). PFAS produced by telomerizationo process typically result in primarly linear isomer composition[66]. Because the present study utilized ECF derived PFOS and PFOA for testing, during the analysis of samples in the present study the LC/MS/MS chromatographic conditions were usually capable to separate earlier eluting branched isomers from the linear isomer. As a result, a general observation was that most branched isomers were generally removed faster than the linear isomer, and this pattern was reflected in intermediate products. Similar observatoins have been noted for PFAS biotransformation studies and isomer patterns in biota where ADME properties are different for select isomers [67,68,69,70]. An example of this is shown in **Figure 13** for PFOS at different doses of EB irradiation relative to non-irradiated controls, along with a calibration standard of PFOS. The effect of 0.1N NaOH on chromatographic peak intensity is notable as well. Although not pursued in depth in the present work, it was previously identifed that there is a need to understand isomer profiles of PFAS during treatment processes due to different physicochemical properties and different rates of degradation [71]. While this could have an impact on the environmental and health assessment of EB treatment, it was not wholey addressed as part of the present study.

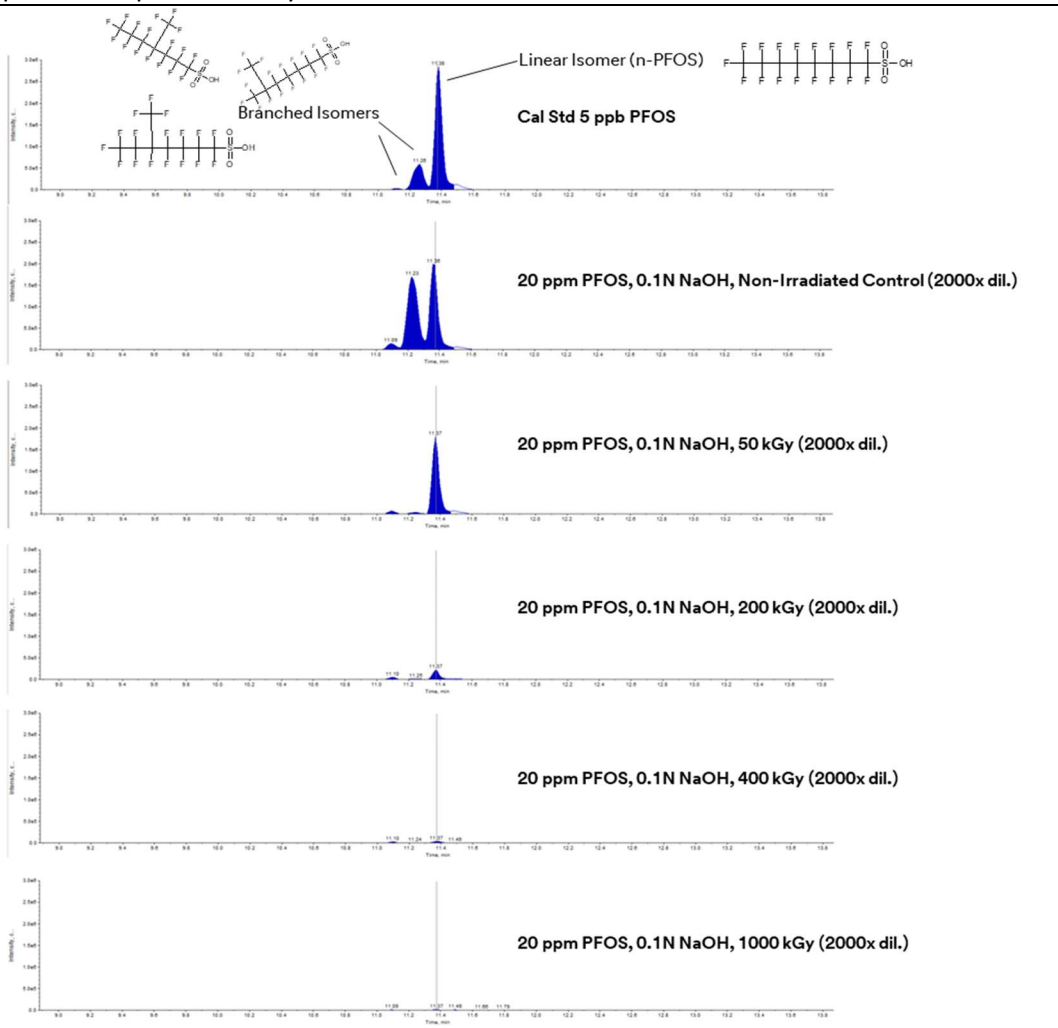

Figure 13. ECF-PFOS isomer changes observed due to EB treatment. Identified in the top chromatogram are methyl branched isomers and the linear (n-PFOS) isomer, however, there are 89 isomers of PFOS possible; but, the majority of branched isomers from ECF are methyl branched.

Additional PFAS Tested

As noted earlier, a significant amount of additonal work was performed which did not fall under any particular SOPO tasks. As part of that effort, twenty-four other PFAS than PFOA and PFOS were also evaluated in Y1, and included the compounds shown below in **Figure 14,** and further below in **Figure 19**. The degradation products observed from those in **Figure 14** were determined and are discussed. In many instances the products were identified as low molecular weight, environmentally persistent PFCAs, PFSAs or volatile fluorocarbons. The test results for each are briefly noted in **Figure 14**, but detailed further below. All were evaluated and considered pertinent to the health and environmental assessment as PFAS streams typically contain numerous PFAS and not just PFOA and PFOS. Furthermore, one PFAS in **Figure 14** is related to a legacy AFFF product and others are associated with current chemistries produced.

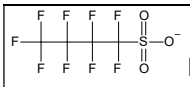
Perfluorobutane sulfonate, PFBS: 20-25% removal, products TFA, PFPA, PFBA, 1H-nonafluorobutane, 1H-heptafluoropropane, pentafluoroethane, trifluoromethane, sulfate and fluoride.

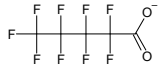
Perfluorobutanoate, PFBA: 100% removal, product fluoride ion

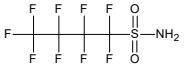
Perfluorobutane sulfonamide, FBSA: 20-25% removal, products PFBS, TFA, PFPA, PFBA, 1H-nonafluorobutane, 1H-heptafluoropropane, pentafluoroethane, and trifluoromethane, perfluorooctane, sulfate and fluoride.

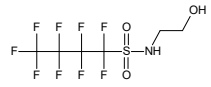
2-(perfluorobutanesulfonamido)ethanol, FBSE: 100% removal, products FBSA, PFBS PFPA, PFBA, 1H-nonafluorobutane, 1H-heptafluoropropane, pentafluoroethane, trifluoromethane, perfluorooctane, sulfate and fluoride

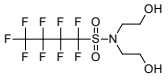
[(N,N-bis(2-hydroxyethyl)]perfluorobutanesulfonamide, FBSEE: 100% removal, products FBSA, PFBS PFPA, PFBA, 1H-nonafluorobutane, 1H-heptafluoropropane, pentafluoroethane, trifluoromethane, perfluorooctane, sulfate and fluoride

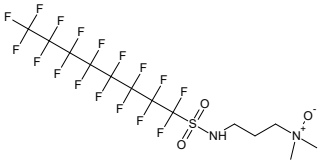
Perfluorooctanesulfonamido amine oxide, PFOSA-NO: 100% removal, similar products as from PFOS, largely sulfate and fluoride with trace-levels of PFCAs and hydrofluorocarbons.

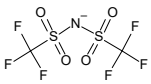
(Bis)Trifluoromethansulfonylimide, TFSI: 60% removal, products trifluoromethane sulfonate (TFMS), trifluoromethane, and sulfate and fluoride.

Figure 14. Other PFAS types evaluated in the present work. (Results at 500 kGy, 1.2 kGy/sec and pH 13 are shown and discussed).

Initially, the EB treatability of the C4 homologs of PFOS and PFOA, PFBS and PFBA, were evaluated. Both PFBS and PFBA were tested at nominal 20 ppm. PFBS showed removal efficiency of 20-25% under optimal treatment conditions of 500 kGy and 0.1N NaOH, but PFBA was 100% removed with formation of trace levels (< 1 mol%) of PFPA and TFA, but 99-100% mass balance to fluoride ion. The effectiveness of EB treatment for PFBS was greatly reduced compared PFBA or to the efficiency of removal of 20 ppm PFOS (99%) under the same conditions. The results for PFBS indicated a fluorocarbon chain length effect on EB treatability. The reasons for perfluoroalkyl chain length effects are not immediately apparent. Possible reasons could include differences in physical-chemical properties (i.e., solubility, surface tension, etc.), chemical structural differences (i.e., conformational limitations or steric hindrance for intra-molecular radical rearrangements), and cross-sectional dimension (molecule size) for interaction with aqueous electron. Degradation products from PFBS by LC/MS/MS were observed as low levels of trifluoroacetate (TFA), perfluoropropanoate (PFPA) and PFBA. The headspace analysis also revealed low levels of 1H-nonafluorobutane, 1H-heptafluoropropane, pentafluoroethane and trifluoromethane, suggesting C-C and C-S bond cleavage reactions occur for PFBS. Volatile products accounted for approximate 2.5 mol% of degraded PFBS. The observation of hydrofluorocarbons is notable because they typically have high global warming potentials (GWPs), as discussed further later. The results also showed that most of PFBS removed was converted to inorganic fluoride and sulfate. This was further evaluated, as discussed later, and confirmed with other short chain PFSAs.

The sulfonamide compound FBSA, like PFBS, was removed about 25-35% relative to non-irradiated controls. Degradation products measured by LC/MS/MS included PFBS, PFBA, PFPA and TFA. PFBS accounted for 3 mol% of degraded quantity of FBSA. PFBA was the major product at about 10 mol% of total products. Furthermore, volatile 1H-nonafluorobutane, heptafluoropropane, pentafluoroethane and trifluoromethane were observed in headspace gases, like PFBS results. Volatile products accounted for approximate 15 mol% of degraded FBSA. A surprising finding was formation of perfluorooctane, and which may offer some clues to the mechanism for perfluoroalkyl sulfonate degradation by EB, since perfluorooctane would have been formed from two perfluorobutyl radicals in proximity. Based on fluoride and sulfate, the FBSA removed was largely measured as sulfate and fluoride. Overall, the results indicate both S-N, C-S, C-C and C-F cleavage reactions occurred. The degradation pathway for FBSA and PFBS are shown below in **Figure 15**.

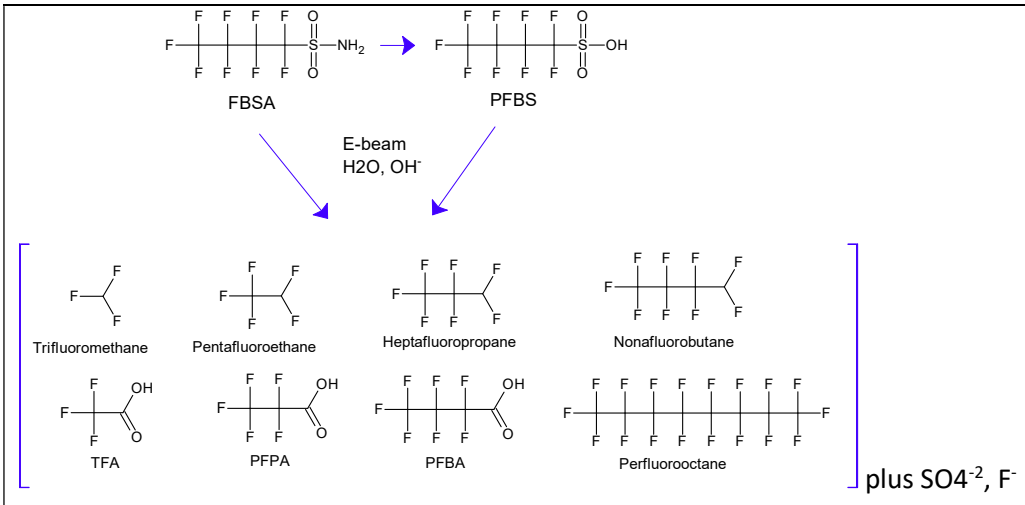

Figure 15. Degradation Products of FBSA and PFBS

Expanding further upon the perfluorobutanesulfonamide class of substances, FBSE and FBSEE were evaluated. Both FBSE and FBSEE showed 100% removal of parent substance. However, a significant amount of FBSA (major) and PFBS (minor) were formed, along with low levels of PFBA, PFPA and TFA. Like findings of FBSA, 1H-nonafluorobutane and perfluorooctane were significant from FBSE, with minor levels of heptafluoropropane, pentafluoroethane and trifluoromethane also observed. Volatile products accounted for approximately 2 mol% of degraded FBSE and 8 mol% of degraded FBSEE. Based on IC results, ~70% of FBSE fluorine was measured as fluoride and 76% of FBSE sulfonate was measured as sulfate anion. Results for degradation products indicate degradation reactions involving S-N, C-S, C-N, C-C and C-F cleavage, C-N and C-C cleavage reactions and C-F cleavage reactions occurring, to generate the products shown in **Figure 16.**

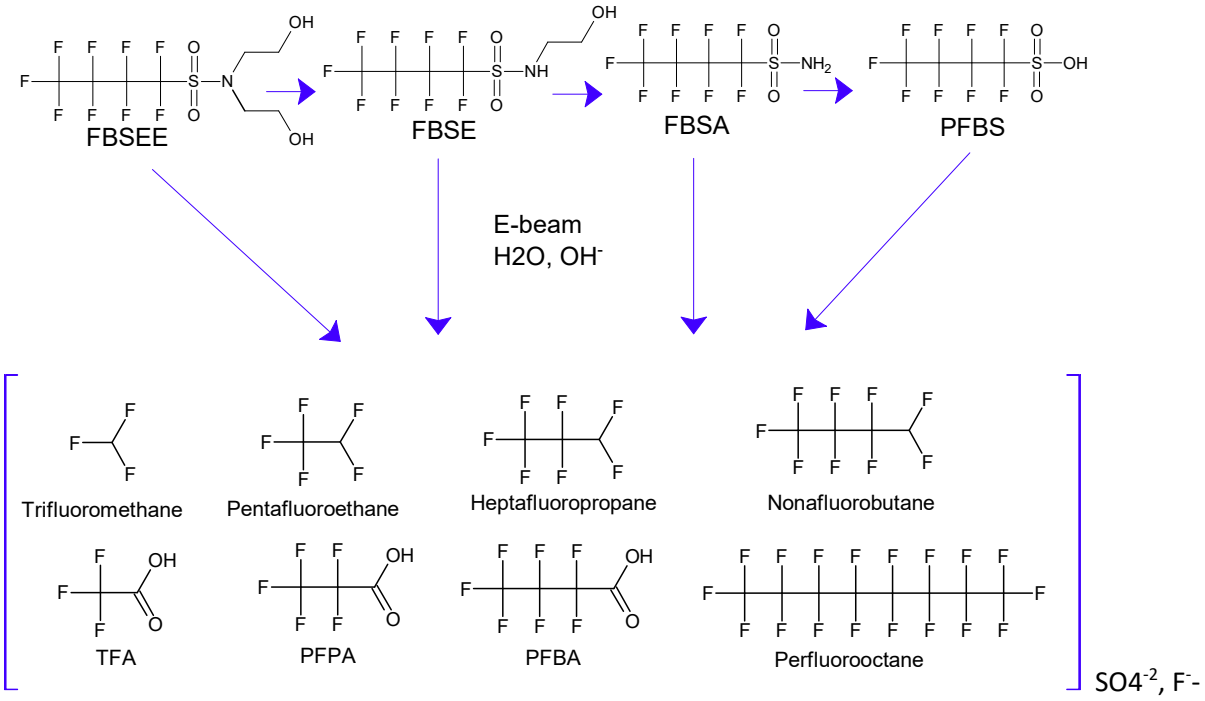

Figure 16. Degradation Products of FBSE and FBSEE

A legacy C8-based perfluorooctanesulfonamide compound used in select aqueous film-forming foam (AFFF) products, PFOSA-NO, was also tested for EB treatability. The PFOSA-NO demonstrated 100% removal. The EB treatment of PFOSA-NO did not form significant levels of PFAS degradation products, like observations with PFOS, with only trace TFA, PFPA, PFBA and PFPeA measured by LC/MS/MS. Headspace GC/MS results showed trace levels of 1H-nonafluorobutane, heptafluoropropane and trifluoromethane, suggesting a role of degradation initiating within the perfluorocarbon tail. Volatiles only accounted for 0.9 mol% of PFOSA-NO removed. From analysis of inorganics by IC, about 80% mass balance to fluoride was observed and about 115% mass balance for sulfate was observed, suggesting AOF was nearly completely degraded to inorganic products.

Finally, the compound TFSI (Li salt) was tested. The Li-TFSI is an electrolyte salt sold for use in lithium-ion battery manufacturing or the alkylamine salt is used as an ionic liquid antistatic agent for blending with high-performance polymers and thermoplastics in electronics, display and semiconductor applications [72,73]. Following EB treatment, the TFSI was removed about 60% and resulted in formation of low levels of trifluoromethane

sulfonate (TFMS) and accounted for 1-2 mol% of the total degraded parent. However, volatile trifluoromethane was observed and accounted for 9 mol% of degraded TFSI. Based on IC results, complete destruction to fluoride and sulfate were likely. The EB degradation pathway for TFSI is shown in **Figure 17**.

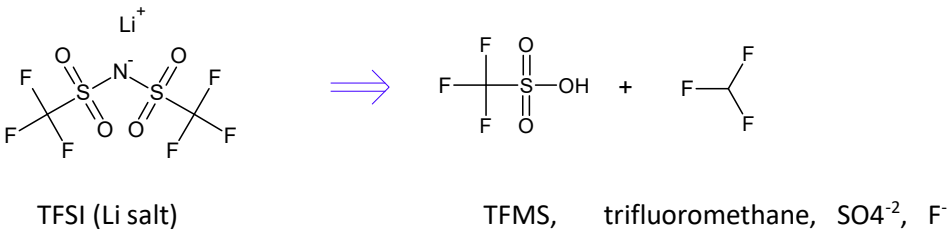

Figure 17. Degradation products of TFSI

Effect of Perfluorocarbon Chain Length on EB Treatability

Additional to the variety of PFAS tested, above, several PFCAs and PFSAs were evaluated. Early on we had observed that shorter pefluoroalkyl sulfonates (PFSAs) did not degrade as efficiently as PFOS under the conditions optimized for PFOS and PFOA. This was largely obtained from testing with PFOS that also contained low levels of the shorter chain homolog impurities perfluorohexane sulfonate (PFHxS) and perfluorobutane sulfonate (PFBS), both of which were determined analyticaly as part of the LC/MS/MS analysis. The results of their removal relative to non-irradiated controls is shown in the **Figure 18**.

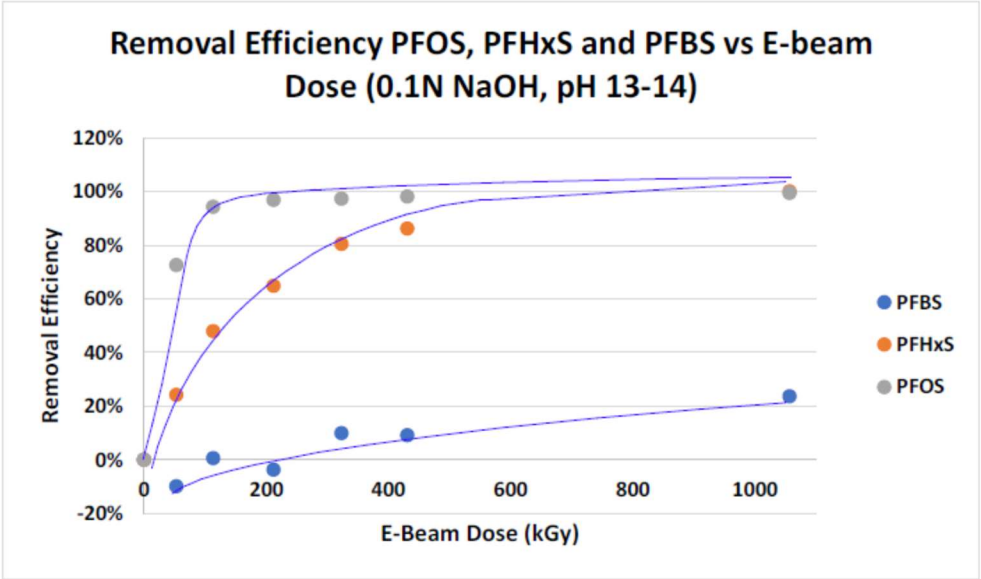

Figure 18. Effect of perfluorocarbon chain length on perfluoroalkyl sulfonate treatment by EB (removal efficiency based on concentrations measured in EB treated samples versus non-irradiated controls

Following that finding, additonal tests with a broad variety of fluorocarbon chain length PFCAs and PFSAs was then conducted to further define this effect and to identify limitations of EB treatments for other PFAS expected to be co-present with PFOS and PFOA. Those tests were conducted under EB conditions optimized for PFOA and PFOS and provided insight into the kinetics and rates of degradation of PFCA and PFSA compounds, as well as limitations and areas for future improvements. In that work, it was identified that low molecular weight PFSAs such as trifluoromethane sulfonate (C_1), perfluoroethane sulfonate (C_2), and perfluoropropane sulfonate (C_3) were largely impervious to EB treatments, and perflurobutane sulfonate (C_4) was poorly degraded with only approximately 25% removal.

As part of the continued effort to evaluate other PFAS than PFOA and PFOS for both the health/environmental assessment, as well as to understand limits of EB treatment for other PFAS, we tested ten PFSAs ranging from C1 to C10, and nine PFCAs ranging from C2 to C10 perfluorocarbon chain length. Those were as follows: trifluoromethanesulfonate (TFMS, C1), perfluoroethanesulfonate (C2, PFES), perfluoropropanesulfonate (PFPS, C3), perfluorobutanesulfonate (PFBS, C4), perfluoropentanesulfonate (PFPeS, C5), perfluorohexanesulfonate (PFHxS, C6), perfluoroheptanesulfonate (PFHpS, C7), perfluorooctanesulfonate (PFOS, C8), perfluorononanesulfonate (PFNS, C9) and Perfluorodecanesulfonate (PFDS, C10), and trifluoroacetate (TFA, C2), perfluoropropanoate (PFPA, C3), perfluorobutanoate (PFBA, C4), perfluoropentanoate (PFPeA, C5), perfluorohexanoate (PFHxA, C6), perfluoroheptanoate (PFHpA, C7), perfluorooctanoate (PFOA, C8), perfluorononanoate(PFNA, C9) and perfluorodecanoate (PFDA, C10). The chemical structures of the PFCAs and PFSAs tested are shown in **Figure 19**. Those sample sets were treated with 0.1N NaOH and at nominal 1.2 kGy/sec for nominal doses of 0 kGy (control), 50 kGy, 100 kGy, 250 kGy, 500 kGy, 750 kGy, 1000 kGy and 1600 kGy. 1600 kGy was the highest achievable dose before integrity of test vessels was compromised and only performed on solutions with PFSAs. The samples were analyzed by quantitative LC/MS/MS after treatments to only determine the levels of PFAS parent substance remaining.

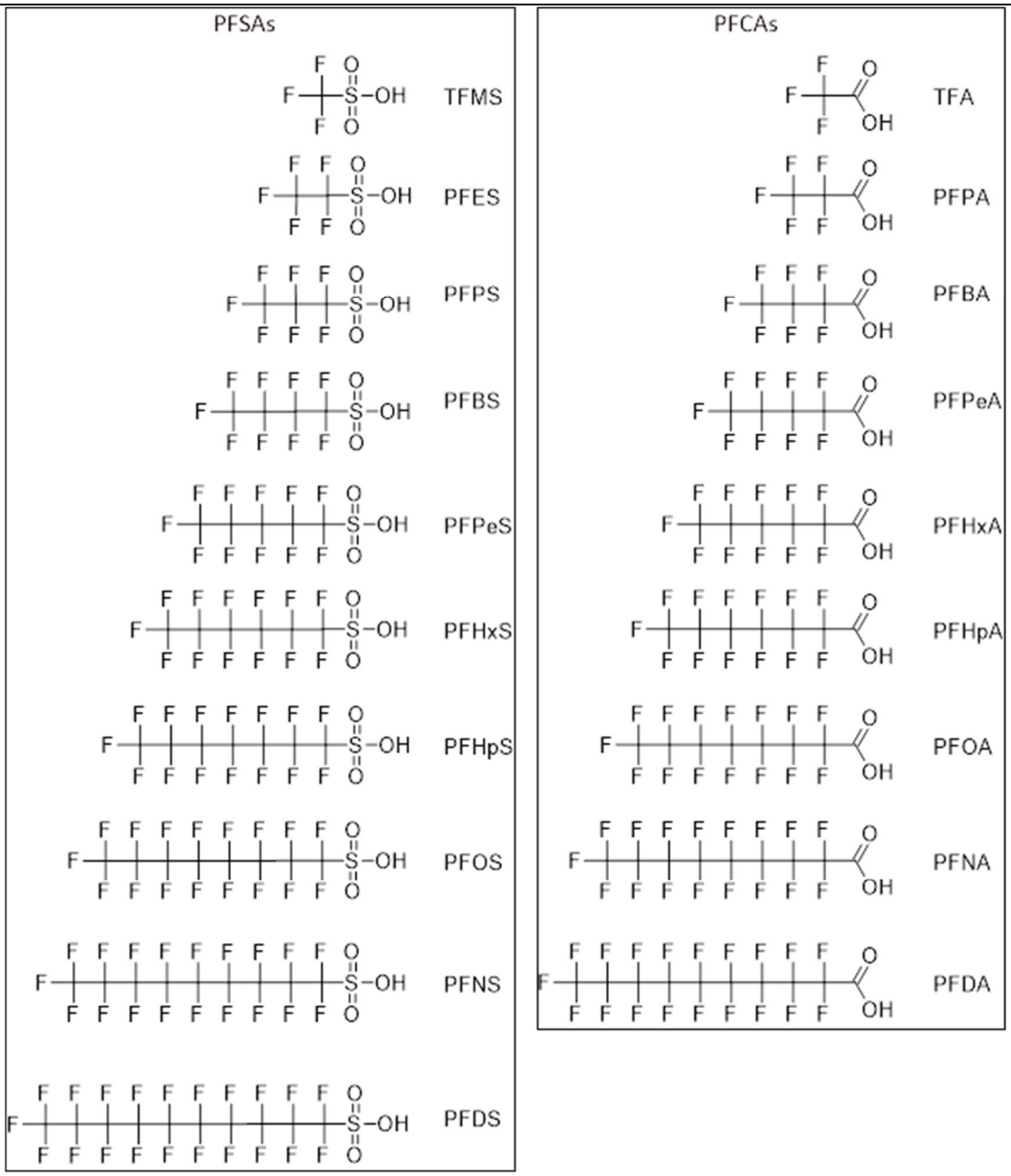

Figure 19. Perfluoralkylsulfonates (PFSAs) and perfluoroalkyl carboxylates (PFCAs) tested for EB treatability.

The results from analysis of EB treated PFSAs and PFCAs corroborated the earlier results showing that the low MW, short chain PFSAs like PFBS and smaller, were less effectively treated by e-beam, while short chain PFCAs were still efficiently removed, as shown below in **Figure 20** and **Figure 21**. From the results, short chain PFSAs are less susceptible to EB treatment than short chain PFCAs. Also, PFOS and PFOA appear to be the most amenable to EB treatment, which could reflect the fact that the conditions were optimized to PFOA and PFOS. The higher molecular weight PFNS, PFDS, PFNA and PFDA were less effectively degraded by EB relative to PFOS and PFOA but could in part have been related to lower water solubility of those substances. The PFNS and PFDS concentrations in test samples were significantly lower than the targeted concentrations due to possible losses

to container walls during initial solution preparation which resulted in the targeted concentration not being achieved in final test samples.

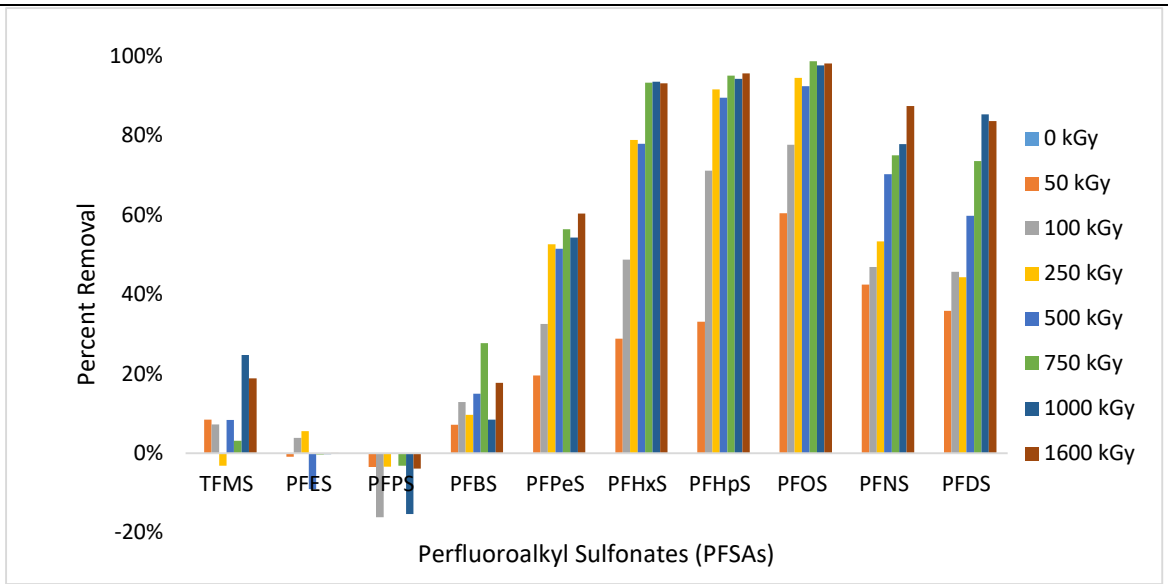

Figure 20. Effect of perfluorocarbon chain length on e-beam treatment of perfluoroalkyl sulfonates**.**

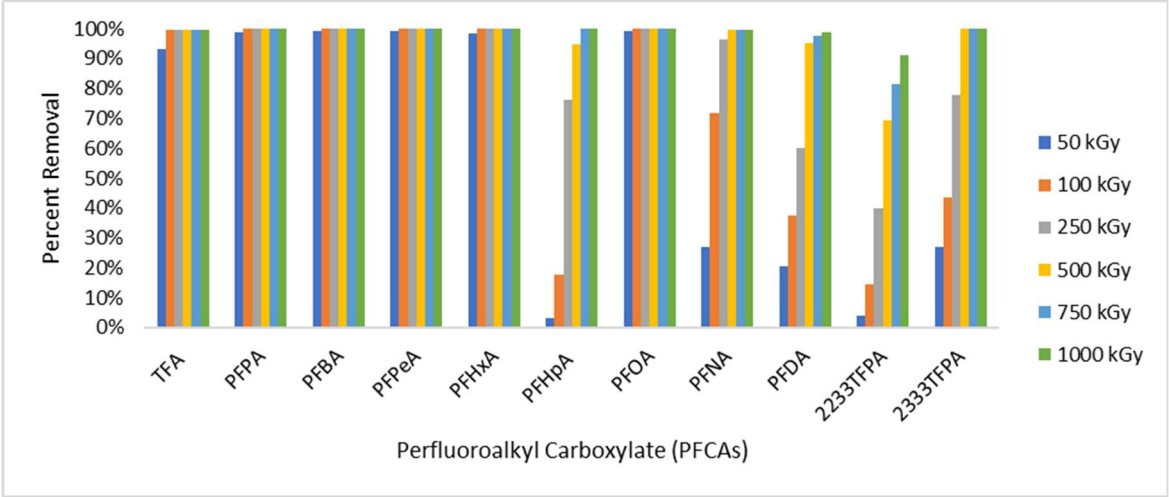

Figure 21. Effect of perfluorocarbon chain length on e-beam treatment of perfluoroalkyl carboxylates. ***Note: PFHpA data skewed because it was fortified at 10-times the expected level due to preparation error.***

Also, consistent with our data from earlier testing the loss of parent compound from these experiments typically appeared pseudo first-order. Therefore, first order reaction rates and half-life times based on the best fit data, typically the first 4 to 6 datapoints, were calculated for all the PFCAs and PFSAs tested. The calculated first-order kinetic rates and half-time lives for PFSAs and PFCAs are shown in **Table 1** and **Table 2,** respectively. Based on the observed rates, EB provides for some of the fastest known destruction of PFAS in water relative to other destruction techniques [74]It is noteworthy that the kinetic profiles of most PFSAs appeared to change after the first 4 to 6 data points, possibly indicating that radicals were present in excess early on, but then rates possibly switch to second-order kinetics after depletion of radical concentrations.

Table 1. E-beam degradation kinetic data for fluorinated carboxylates (PFCAs)

Perfluorinated carbons	1	2	3	4	5	6	7	8	9	10
Tested Concentration (mg/L)	1.01 ppm	1.00 ppm	1.00 ppm	1.00 ppm	0.600 ppm	1.00 ppm	0.600 ppm	1.00 ppm	0.600 ppm*	0.600 ppm*
E-beam Dose	TFMS	PFES	PFPS	PFBS	PFPeS	PFHxS	PFHpS	PFOS	PFNS	PFDS
	Percent Removal of PFCA Test Substance									
0 kGy	0%	0%	0%	0%	0%	0%	0%	0%	0%	0%
50 kGy	8.4%	-0.9%	-3.5%	7.1%	19.5%	28.8%	33.1%	60.4%	42.4%	35.9%
100 kGy	7.3%	3.8%	-16.1%	12.9%	32.5%	48.8%	71.1%	77.6%	46.8%	45.7%
250 kGy	-3.2%	5.6%	-3.4%	9.6%	52.6%	78.8%	91.6%	94.4%	53.3%	44.3%
500 kGy	8.4%	-9.1%	-0.1%	15.0%	51.5%	77.9%	89.5%	92.3%	70.2%	59.7%
750 kGy	3.2%	-0.3%	-3.2%	27.7%	56.4%	93.3%	95.0%	98.6%	75.0%	73.5%
1000 kGy	24.7%	-0.2%	-15.3%	8.5%	54.3%	93.5%	94.2%	97.6%	77.8%	85.3%
1600 kGy	18.9%	0.0%	-3.9%	17.7%	60.3%	93.1%	95.6%	98.1%	87.4%	83.6%
Measured Concentration in non-treated control (ppm); results normalized to this value	**1.05**	**1.03**	**0.896**	**1.12**	**0.633**	**1.04**	**0.477**	**1.69**	**0.100**	**0.0230**
% removal at last kinetic point in plot	18.9%	NA	NA	27.7%	52.6%	78.8%	91.6%	94.4%	75.0%	73.5%
# points in 1st order kinetic plot	8	NA	NA	6	4	4	4	4	5	5
e-beam dose at last point in plot (kGy)	1601	NA	NA	716	267	267	257	256	717	717
last time point in curve fit (seconds)	1334	NA	NA	597	223	223	214	213	598	598
1st order rate constant (k); ln(uM) vs time (seconds) plot to get slope	-0.00016006	NA	NA	-0.000424	-0.00321	*-0.00688*	-0.0117	-0.0125	-0.00158	0
1s order half-life time (seconds)	**4330**	NA	NA	**1634**	**216**	**101**	**59.2**	**55.4**	**439**	**468**
1s order half-life time (minutes)	**72.16**	NA	NA	**27.2**	**3.60**	**1.68**	**0.987**	**0.923**	**7.31**	**7.80**

*; PFNS and PFDS loss observed and likely caused by binding to containers during solution preps
NA; degradation was not observed to perform kinetic calculations

Table 2. E-beam degradation kinetic data for fluorinated carboxylates (PFCAs)

Perfluorinated carbons	1	2	3	4	5	6	7	8	9	0	1
Tested Concentration (mg/L)	1.00 ppm	1.01 ppm	1.01 ppm	1.00 ppm	1.00 ppm	10.1*	1.00 ppm	1.02 ppm	1.01ppm*	1.01 ppm*	1.00 ppm
Nominal Dose	TFA	PFPA	PFBA	PFPeA	PFHxA	PFHpA	PFOA	PFNA	PFDA	2233TFPA	2333TFPA
	Percent Removal of PFCA Test Substance										
50 kGy	93.0%	98.7%	99.1%	99.1%	98.4%	3.3%	99.1%	27%	20%	4%	27%
100 kGy	99.8%	100%	100.0%	100.0%	100.0%	17.7%	99.9%	72%	38%	15%	44%
250 kGy	99.8%	100%	100.0%	100.0%	100.0%	76.1%	100.0%	97%	60%	40%	78%
500 kGy	99.8%	100%	100.0%	100.0%	100.0%	95.0%	100.0%	100%	95%	69%	100%
750 kGy	100%	100%	100.0%	100.0%	100.0%	99.9%	100.0%	100%	98%	81%	100%
1000 kGy	100%	100%	100.0%	100.0%	100.0%	100.0%	99.9%	100%	99%	91%	100%
Measured Concentration in non-treated control (ng/mL; ppb); results normalized to this value	***571***	*1260*	***1365***	***1105***	***936***	***9740****	***841***	***622***	***1345***	*993*	*638*
% removal at last kinetic point in plot	99.8%	100.0%	100.0%	100.0%	100.0%	**99.9%**	99.9%	99.8%	98.1%	91.1%	99.6%
# points in 1st order kinetic plot	3	3	3	3	3	***6***	3	5	7	7	7
e-beam dose at last point in plot	104 kGy	104 kGy	104 kGy	102 kGy	102 kGy	***765 kGy***	102 kGy	514 kGY	938 kGy	941 kGy	941 kGy
1st order rate constant (k); ln(uM) vs time (seconds) plot to get slope	-0.0816	-0.0955	-0.0884	-0.0949	-0.0946	-0.0105	-0.0832	-0.0151	-0.00551	0	-0.00722
1st order half-life time (seconds)	**8.5**	**7.3**	**7.8**	**7.3**	**7.3**	**66.0**	**8.3**	**45.9**	**125.8**	**229.5**	**96.0**
1st order half-life time (minutes)	**0.142**	**0.121**	**0.131**	**0.122**	**0.122**	**1.10**	**0.14**	**0.76**	**2.10**	**3.82**	**1.60**

*; PFHpA data indicates a solution prep occurred and 10-times the intended level was spiked into the samples, skewing kinetic calculations

In addition to PFCAs, two polyfluorinated propanoic acids (2333-TFPA and 2233-TFPA) were evaluated. Compared to the perfluorinated propanoic acid (PFPA), the loss of the polyfluorinated equivalents indicated reduced degradation, as shown in **Figure 22**. This was postulated to be due to disruption of the electron

withdrawing inductive effect of the perfluorocarbon tail and lowering the reactivity of the carbon-carbon bond at the carboxylate functional group. This also suggested there is less influence on PFAS recalcitrance to EB treatment because of shielding of the carbon backbone by the fluorine atoms, since replacing fluorine with hydrogen would be expected to reduce the shielding effect. The apparent removal of one fluorine and replacement with hydrogen on the terminal carbon (2233-TFPA) was a stronger factor to recalcitrance than replacing the fluorine on the middle carbon (2333-TFPA).

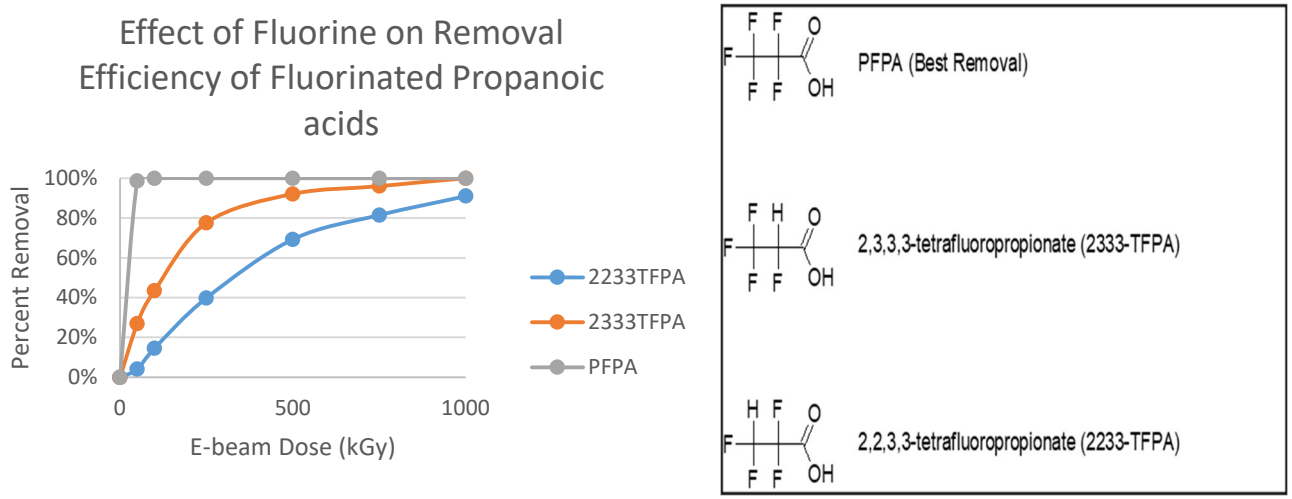

Figure 22. Effect of Fluorine replacement with hydrogen on EB treatability of fluorinated propanoic acids.

Pertinent to the health and environmental assessment task, a select few samples were fortified with 0.5% methanol as a potential hydroxyl radical scavengers to evaluate the role of hydroxyl radical in the degradation of PFOA and PFOS. Both PFOA and PFOS were removed the same as samples without methanol, as discussed later under Y1, Task 2, Subtask 2.4-Other Additive. Aside from the observation that PFOA and PFOS were removed efficiently in the presence of methanol, possibly suggesting a role of the aqueous electron in degradation of both and a lesser role of hydroxyl radical, another observation from those samples was that a significant gas pressure build up occurred in samples containing methanol and appeared to release a fuming gas when opened. Out of concern for possible HF, the gas was analyzed gas-phase Fourier Transform Infrared (FTIR) analysis. The gas-phase FTIR analysis showed that hydrofluoric acid (HF) was not formed in those reactions, supporting the environmental and health assesment of potential hazardous fluorinated substances. However, the gas was determined to be largely composed of carbon monoxide, carbon dioxide and methane. Such gases, if formed from co-present alcohols or other dissolved organics, could require abatement during EB treatment. Methanol or other hydrocarbon alcohols such as ethanol are also pertinent because they may be present in IE regeneration wash waters. Treatment of spent IE wash solutions was determined as a good fit for EB treatment from the present work. If hydrocarbon alcohols are not first reclaimed from the spent regeneration solutions prior to the EB treatment, they could generate gases which could be toxic or flammable.

Summary of Y1, Task 1- Health and Environmental Assessment.

In no instance were the intermediate products or endproducts from EB treatments result in any compounds of which would have resuted in a NO-GO decision as it pertained to a health or environmental hazard, albeit the toxicological and ecotoxicological data for several of the identified PFAS intermediates and endproducts are not well established. Some of the observed degradation products were of potential

environmental concern, notably short chain PFCAs are persistent in the environment and volatile hydrofluorocarbons identified have high global warming potential (GWP) values. For example the GWP for trifluoromethane, pentafloroethane and heptafluoropropane, which were observed from some EB treatments, are 14800, 3500, and 3220 CO_2 equivalents for a 100 year time horizon[75,76]. These findings iterate the need to operate under optimal EB conditions for complete destruction, possibly tailored for specific types of PFAS, in which the PFAS is completely destroyed and minimizing formation of fluorocarbon-based intermediate products and endproducts. An alternative would be to recapture low level intermediate products after EB treatment and recycle them through the EB process to complete their degradation, or for volatile hydrofluorocarbons they might be abated by incineration using a thermal oxidizer system, but would add significantly to the cost of treatment.

Y1: Task 2 Results – Optimal E-beam Dose and Additive Concentration

Subtask 2.1: Dose Rate

Dose rate at FNAL's A2D2 accelerator can be varied from 0.2 to 1.2 kGy/sec, but it is expected that most treatment will be performed at the highest dose rate to minimize the treatment time. Dose rate effects are often related to high dose rates which are typically delivered by e-beam accelerators versus other sources of ionizing radiation. Hence, e-beam treatment is usually identified as radiation processing at high dose rates. The water radiolysis process based on high energy electrons has been described as more economical and effective for large scale applications as compared to other methods applied for the removal of emerging contaminants. High dose rates affect radiolysis yields by increasing the radical interaction probability. Small number of experiments will focus on determining if there are any dose rate effects associated with the treatment. We will investigate the chemistry effects at three dose rates – 0.2 kGy/sec (low), 0.6 kGy/sec (medium) and 1.2 kGy/sec (high).

Water samples contained perfluoroctanesulfonate (PFOS) or perfluooctanoate (PFOA) at nominal concentration of 20 μg/L (ppb) or 20 mg/L (ppm). All samples were prepared with a headspace of argon to minimize potential radical reactions with molecular oxygen. Samples were treated at EB doses of 0 kGy (non-irradiated controls), or nominal 500 kGy with nominal dose rates of 0.2 kGy/sec and 1.2 kGy/sec at FNAL. Additional samples were sent to E-Beam Services, Inc. for EB treatments of nominal 500 kGy total dose with dose rates of 15 kGy/sec and 30kGy/sec. Additonal dose rate treatments were perfromed later for 20 ppm solutions only, to supplement the data with dose rates at 0.025 kGy/sec and 0.15 kGy/sec, by using aluminum shielding to attenuate the dose rate. While the dose rate of electrons was decreased via the alumnium, x-rays were produced in the aluminum which may have had some effects in destruction of PFAS.

As a result of the experimental work, data on dose rate indicated that higher dose rates generally resulted in lowered degradation efficiency, as shown in **Figure 23** for PFOA ad PFOS at 20 ppm test concentration and
pH 13.

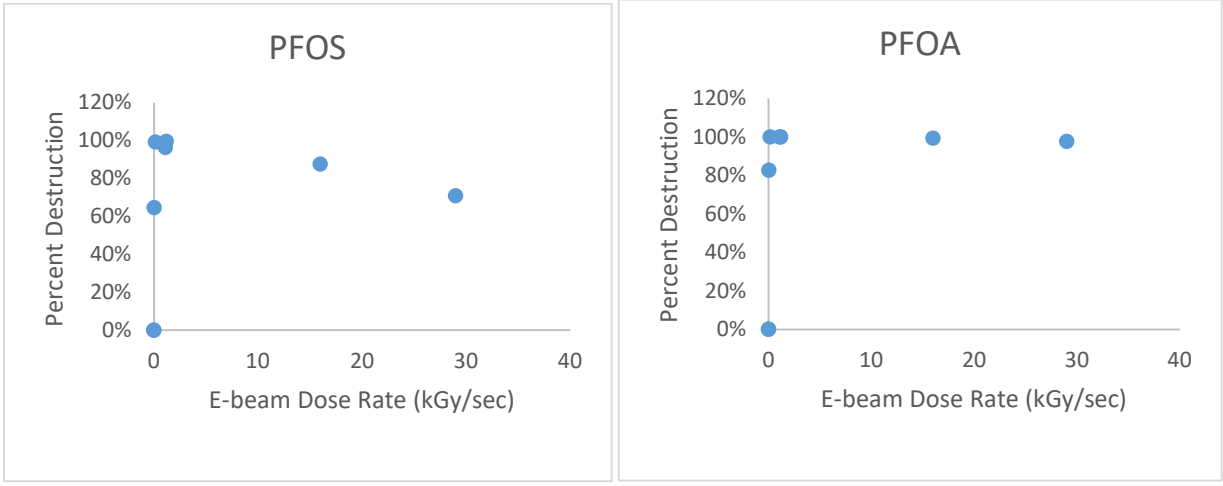

Figure 23. EB treatment of 20 ppm PFOS (left) and 20 ppm PFOA (right) versus applied e-beam dose rate at pH 13 and 500 kGy delivered dose. Percent destruction indicates sum of parent and intermediate degradation products destroyed.

The improved degradation of PFOA and PFOS at lower dose rates was attributed to kinetics of desired radical formation from radiolysis of water at low EB dose rates that enables a more efficient reaction with the PFOS and PFOA in aqueous solution. Dose rate and pH effects were largely tested in parallel experiments, and the effect of dose rate was different under acidic conditions than basic conditions, as shown in **Table 3**. Under basic conditions degradation of PFOA and PFOS was better at the lower dose rates, but, under acidic conditions this response appeared to be opposite for PFOA.

Table 3. Effect of E-beam Dose Rate and pH Altering Additives (NaOH, HNO_3)

Additive	pH	e-beam dose rate (kGy/sec)	Total Absorbed Dose (kGy)	Percent Removal of 20 ppm PFOA	Percent Removal of 20 ppm PFOS
0.01% Nitric Acid	4	0	0	0.0%	0.0%
0.01% Nitric Acid	4	1.2	536	33.0%	29.9%
0.01% Nitric Acid	4	15	557	39.2%	23.4%
0.01% Nitric Acid	4	30	565	49.8%	10.0%
no additive (water only)	7	0	0	0.0%	0.0%
no additive (water only)	7	1.2	536	47.9%	47.9%
no additive (water only)	7	15	557	11.8%	43.3%
no additive (water only)	7	30	565	15.9%	34.5%
0.01M Sodium Hydroxide	10	0	0	0.0%	0.0%
0.01M Sodium Hydroxide	10	1.2	536	99.9%	89.7%
0.01M Sodium Hydroxide	10	15	557	76.7%	53.6%
0.01M Sodium Hydroxide	10	30	565	65.5%	47.3%
0.1M Sodium Hydroxide	13	0	0	0.0%	0.0%
0.1M Sodium Hydroxide	13	1.2	536	**100%**	**99.6%**
0.1M Sodium Hydroxide	13	15	557	99.4%	87.6%
0.1M Sodium Hydroxide	13	30	566	97.6%	70.9%

From the present work, it was determined that an optimal EB condition for 100% removal of PFOA and PFOS was 0.1 M NaOH (pH 13) in conjunction with a dose rate close to 1 kGy/sec. However, significant removal of both PFOA (99.9%) and PFOS (89.7%) did occur with 0.01 molar NaOH (pH 10) indicating an optimal concentration may be between 0.1 M and 0.01M NaOH. The optimal degradation of PFOS and PFOA by EB at high pH indicates a critical role of e_{aq}^-, as discussed in greater detail later herein. The defluorination and subsequent degradation of PFOA and PFOS by g e_{aq}^- generated from sulfite mediated UV photochemical systems have been shown[77,78].

As part of the Y1, Task 2 work, we also evaluated the optimal EB dose in the presence of 0.1 M NaOH and optimal dose rate near 1 kGy/sec. We delivered doses of nominal 50, 100, 200, 300, 400, and 1000 kGy to solutions of 20 ppm PFOS or PFOA. The results showed that PFOA and PFOS were optimally removed at EB doses as in the range 200-300 kGy, as shown in **Figure 24**. This provided needed information on the optimal energy input for efficient degradation of these two PFAS in water.

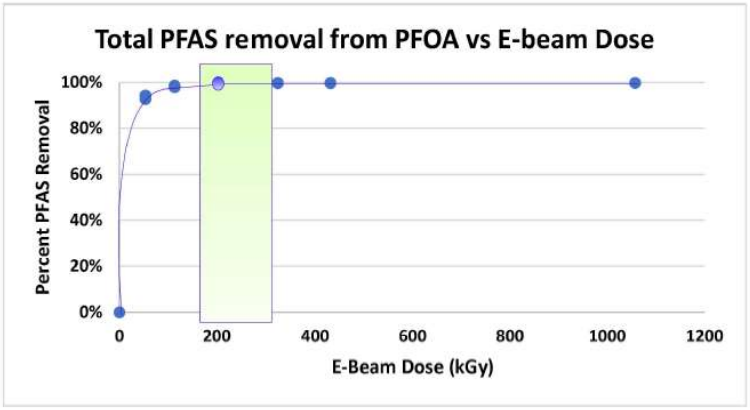

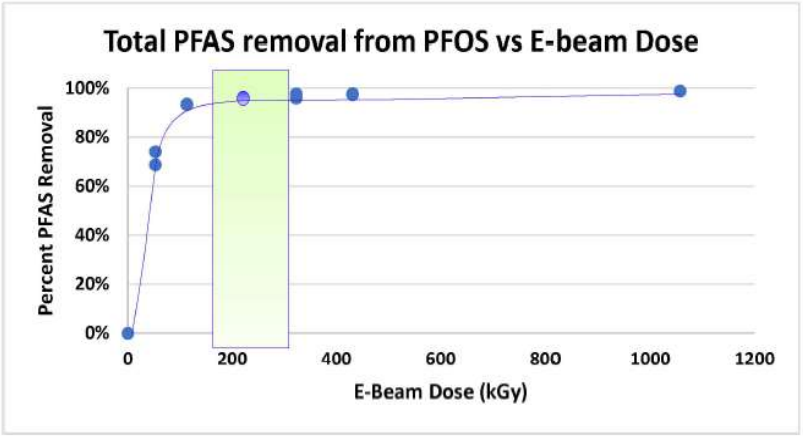

Figure 24. Effect of EB dose on total PFAS removal for 20 ppm PFOA (top) and 20 ppm PFOS (bottom). The optimal dose of 200-300 kGy is shaded.

The concept of electric energy per order (EEo), determined in units of kWh/m^3/order, was first developed as a means of evaluating energy requirement of UV-based advanced oxidation processes (AOPs) for degradation of pollutants, and has been applied as measure of efficiency evaluating PFAS destructive methods [79]. A means for calculating EEo for EB applications with PFAS was shown as a better parameter than *G*-value for

inter-study comparisons[80]. In that work, the calculated EEo values for EB were estimated to be in the range of 31-176 kWh/m^3/order and appeared to be a promising approach versus EEo values for other destructive technologies with PFAS (range 5-9595 kWh/m3/order). In the present work, the EEo values were calculated for PFOS (range 26-133 kwh/m^3/order) and PFOA (range 9-73 kWh/m^3/dose) after treatment under optimized conditions, as shown in **Figure 25**. The EEo values were even lower than previously estimated, and further confirm EB as a viable technology for PFAS treatment.

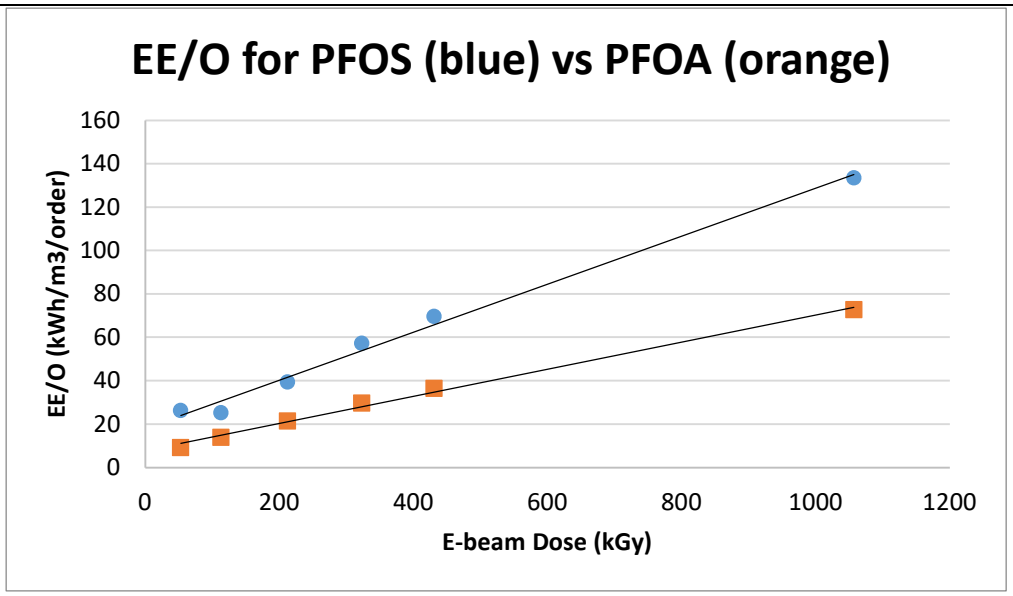

Figure 25. Calculated EEo values for PFOS and PFOA under optimal EB treatment conditions

Subtask 2.2: Effect of Dissolved Oxygen

In Y1, as part of Task 2, methods of creating samples with variable dissolved oxygen (DO) levels were developed at 3M to evaluate the effects of DO on EB treatment. This was performed under the assumption that DO would be a potential scavenger of aqueous electron and hydrogen radical and could interfere with the EB treatment. We also tested the replacement of argon (Ar) gas with nitrogen (N_2) gas for purging the DO to reduce costs of treatment. The results of testing at 20 ppm PFOS or 20 ppm PFOA under variable DO concentrations, with optimized test conditions of 0.1N NaOH (pH 13) and approximately 1 kGy/sec with 500 kGy dose are shown in **Figure 26**. The correlation for PFOS removal and PFOA removal versus DO concentration were different. Interestingly, PFOS was removed at 65% with DO at saturating levels, and near 100% removed at DO below 1-2 mg/L. The correlation of PFOS loss versus DO concentration appeared to be sigmoidal, or multi-order. In contrast, PFOA removal was more sensitive to DO with about 20% removal at saturating concentrations and 100% removal at DO below 1-2 mg/L. The correlation of PFOA removal versus DO concentration appeared to be second order, not sigmoidal like PFOS. Overall, the results with PFOS and PFOA indicate that the removal of DO to approximately 1-2 mg/L (or about 15% of saturation), is sufficient and that further removal of DO is not required. Further, our results showed that nitrogen gas also an effective gas for purging DO out of solution for EB treatments (not shown). These results provide further insight into understanding the differing mechanism of EB degradation of PFOA vs. PFOS, given their different sensitivities to DO.

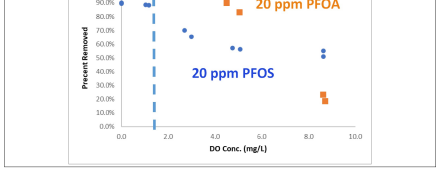

Figure 26. Effect of dissolved oxygen on PFOA (orange squares) and PFOS (blue circles) removal by EB.

Subtask 2.3: Chemical Additives NaOH & HNO_3

The effects of pH-adjusting additives were evaluated on PFAS destruction by EB. This was done in parallel with dose rate experiments, as reported earlier in **Table 3**. The additon of nitric acid (HNO_3) to reduce the pH to 4, and addition of sodium hydroxide (NaOH) to raise the pH to 10 and 13, had a significant effect on EB treatabilty of PFOS and PFOA, as shown in **Figure 27.** The reasons for this are described below.

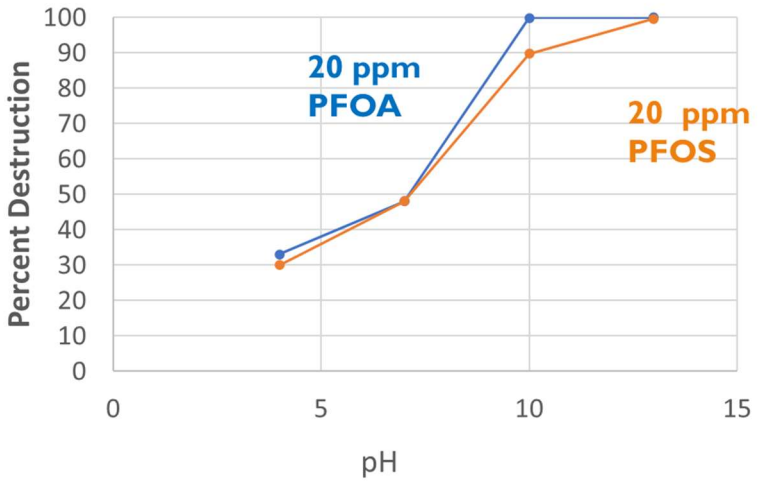

Figure 27. Effect of pH on EB treatment of PFOS and PFOS.

The EB water radiolysis is often measured as the *G* parameter, or *G*-value, and was summarized well by Siwek and Edgecock [81]. For water radiolysis, the *G*-value is the number of free radicals created per 100 eV of

energy deposited into the water. For water radiolysis under neutral pH conditions, the main radicals formed after EB interaction with water are shown in the top equation in **Figure 28**. The *G*-value can be converted to SI units of μmol/J to estimate the concentrations of the radical species in solution and calculated by the second equation shown at the bottom of **Figure 28**. Since the formed radicals and e_{aq} can also react with the products of water ($H3O^+$, OH^-), the pH can significantly affect their yields (*G*-values), as shown in **Figure 29**. Overall, the optimal degradation of PFAS by EB at high pH indicates a critical role of e_{aq}^- and less dependence on $OH^\bullet$. This was further supported by the addition of methanol as a hydroxyl radical, discussed below in the Y1, Task2, Subtask 2.4 section regarding other additives.

$5\ H_2O \rightarrow [2.7]\ OH^\bullet + [2.6]\ e_{aq}^- + [0.6]\ H^\bullet + [2.6]\ H3O^+ + [0.45]\ H_2 + [0.7]\ H_2O_2$

$C_{RC} = [D \times G\text{-}value_{RC}]$

where C_{RC} is the reactive chemical (i.e., radical) concentration in μmole/kg, *D* is the applied dose (J/kg), and $G\text{-}value_{RC}$ is the G-value of the reactive compound in μmole/J

Figure 28. G-values for radicals generated by EB water radiolysis (top), and equation for calculating concentrations of radicals formed (bottom) [70].

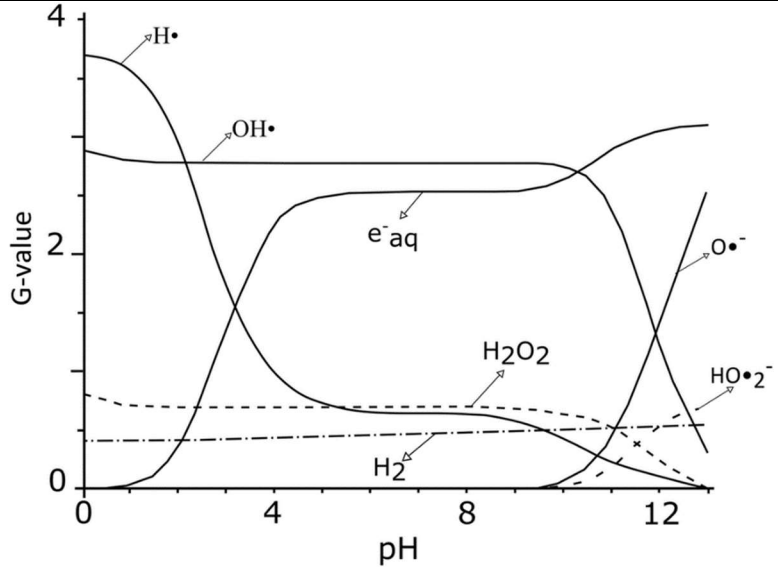

Figure 29. Impact of pH on EB directed water radiolysis products [81].

Effect of Initial PFAS Concentration

The effect of initial PFAS concertation was tested on both PFOS and PFOA. This was determined for both water and water with 0.1N NaOH (pH 13). Concentrations prepared were at nominal 0.2, 2, 20, 200, 2000, 20000 and 200000 ppb of each. Analytical results for the 0.2 ppb concentration were unreliable at such low level and were excluded from the results in the **Table 4 and Table 5**, below.

Table 4. Effect of PFOS initial concentration on EB treatability				
Nominal Prepared Conc. (ppb)	**pH Condition**	**Measured Initial conc. (ppb)**	**log (initial conc)**	**% removal**
2	water (pH 7)	1.82	0.26	77%
20	water (pH 7)	12.9	1.11	83%
200	water (pH 7)	134	2.13	76%
2000	water (pH 7)	1630	3.21	82%
20,000	water (pH 7)	15100	4.18	66%
200,000	water (pH 7)	158000	5.20	41%
2	0.1N NaOH (pH 13)	1.18	0.07	78%
20	0.1N NaOH (pH 13)	7.88	0.90	93%
200	0.1N NaOH (pH 13)	84.4	1.93	96%
2000	0.1N NaOH (pH 13)	1460	3.16	98%
20,000	0.1N NaOH (pH 13)	13200	4.12	100%

Table 5.Effect of PFOA initial concentration on EB treatability				
nominal (ppb)	**pH Condition**	**Measured Initial conc. (ppb)**	**log (initial conc)**	**% removal**
2	water (pH 7)	1.76	0.24	97%
20	water (pH 7)	16.1	1.21	98%
200	water (pH 7)	156	2.19	98%
2000	water (pH 7)	1740	3.24	92%
20,000	water (pH 7)	18270	4.26	67%
200,000	water (pH 7)	176400	5.25	44%
2	0.1N NaOH (pH 13)	3	0.42	100%
20	0.1N NaOH (pH 13)	13	1.10	100%
200	0.1N NaOH (pH 13)	164	2.22	100%
2000	0.1N NaOH (pH 13)	1540	3.19	100%
20,000	0.1N NaOH (pH 13)	18600	4.27	100%
200,000	0.1N NaOH (pH 13)	177000	5.25	100%

Effect of Water Depth in Test Vessel

Although samples were prepared with an ideal depth of nominal 3-cm and based on expected depth-dose curves for 9-10 MeV electrons, the irregular shape of the test vessels and inverted position during treatments suggested depth was not uniform and could have impacted the results. So, we prepared samples at varying volumes of 4.5-mL, 9-mL, 13.5-mL, 15-mL, and 18-mL to achieve nominal liquid depths of 1.5-cm, 3-cm, 4.5-cm, 5-cm and 6-cm. The results were used to essentially generate depth-dose curves for our test vessels, as shown in **Figure 30**, below. The result indicated the 9-mL volume to achieve nominal 3 cm depth was optimal.

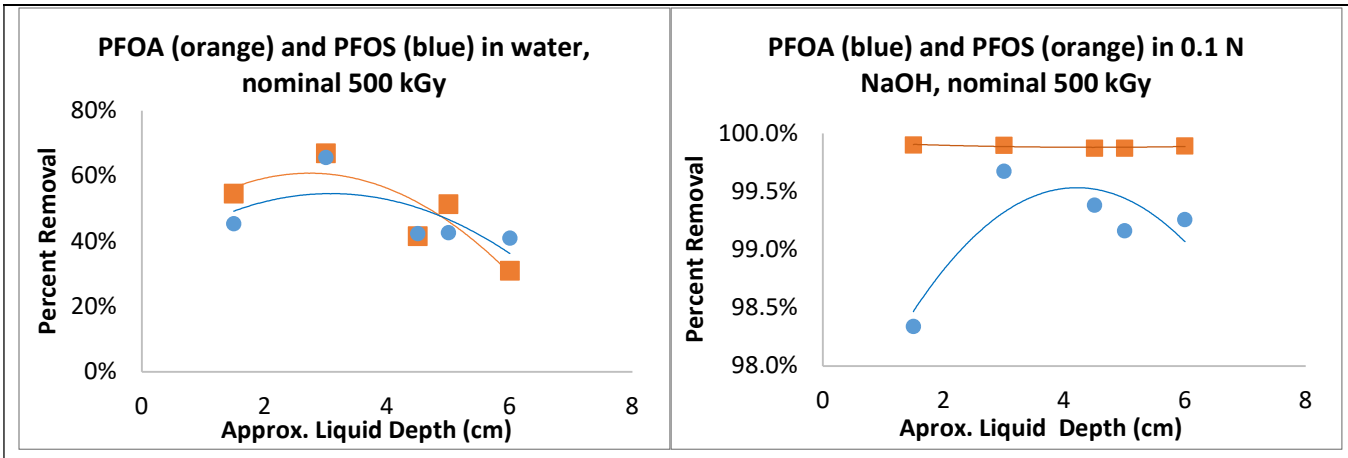

Figure 30. Depth dose curves for EB treated test vessels used in the present study.

Effect of Temperature

Although most samples during treatment were not controlled for temperature, the temperatures did warm during treatment cycles. In some instances, the dosimetry films failed and indicating temperatures exceeding 60-70°C, a failure point for the films used. Iterative treatment followed by cool down period was typically employed to maintain samples below the fail temperature of the films and avoided boiling of the samples which would have resulted in test vessel failure. However, the impact of temperature on EB treatment remained largely unknown in most treatments. To evaluate temperature effects, the EB treatment of test samples with PFOS at 20 ppm and EB doses of 250 kGy and 500 kGy were performed in a temperature-controlled water bath maintained at fixed temperatures between 20-80°C. The results showed that there was a temperature dependence, with best treatment at the highest temperature of 80°C, as shown in **Figure 31**. This was speculated to be due to increased diffusion rates at the higher temperatures.

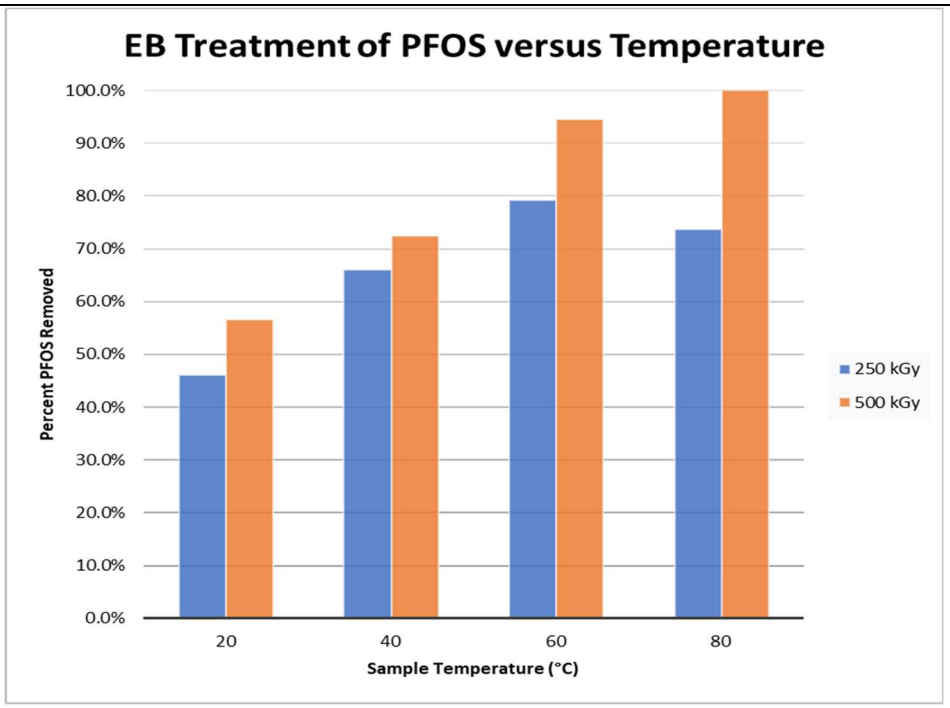

Figure 31.Effect of water temperature on EB treatability.

We theorized that most radical formation does not occur in proximity to the dissolved PFAS molecules in water, given there are approximately 5- to 6-orders of magnitude more water molecules than PFAS molecules at a 20-ppm concentration. Therefore, the radicals must diffuse to the PFAS before reacting with surround radicals and water molecules. This is illustrated in **Figure 32** showing that at 200 kGy, there are roughly seven aqueous electrons formed in proximity to a single PFAS molecule volume of water with nominal three dimensions of 112 water molecules each. If rates are limited by diffusion and improved by temperature, it may be reasonable to consider stirring or ultrasonics to facilitate increased rates of reactions.

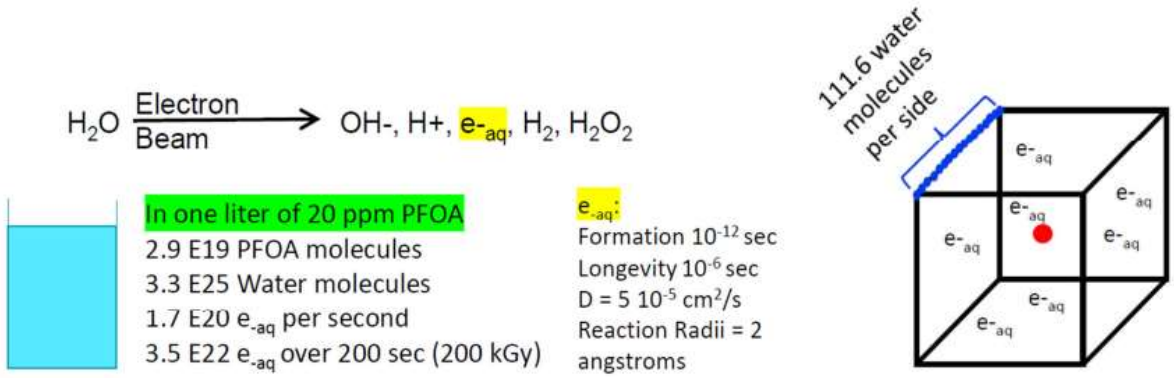

Figure 32. Proximity effects of radicals and PFAS in water lending to a diffusion limited process.

Subtask 2.4: Other Potential Chemical Additives

Methanol Additive

As noted earlier in the Y1, Task 1 section, for a select few samples, 0.5% methanol was added as a hydroxyl radical scavengers to evaluate the role of hydroxyl radical in the degradation of PFOA and PFOS. In water with 0.5% (v/v) methanol present, 90% of PFOA was removed verus 48% removed in water alone, and 57% of PFOS was removed with methanol, versus 48% removed in water alone. Both were removed better with methanol, supporting a role of the aqueous electron in degradation of both PFOA and PFOS and a lesser role of hydroxyl radical. This is shown in **Table 6,** below.

Table 6. Effect of Methanol on EB Treatment of PFOS and PFOA

Description	kGy/sec	Dose (kGy)	ng/mL (ppb)										Avg. % Parent Removed
			TFA	PFPA	PFBA	PFPeA	PFHxA	PFHpA	PFOA	PFBS	PFHxS	PFOS	
PFOA in water, 500 kGY	1.2	536	583	119	118	151	376	1054	9300	0.643	< 0.200	< 4.64	48%
PFOA in water, 500 kGY	1.2	536	545	99.3	92.9	121	318	854	9650	0.712	< 0.200	< 4.64	
PFOA in water, Control	**0**	**0**	**56.9**	**< 5.00**	**36.5**	**5.94**	**88.6**	**118**	**18800**	**0.647**	**< 0.200**	**< 4.64**	**N**
PFOA in water, Control	**0**	**0**	**22.6**	**< 5.00**	**4.93**	**5.23**	**87.9**	**121**	**17600**	**0.680**	**< 0.200**	**< 4.64**	**NA**
PFOA in 0.5% MeOH, 500 kGY	1.2	547	27.9	19.1	11.1	6.26	21.3	31.2	1880	0.861	< 0.200	< 4.64	90%
PFOA in 0.5% MeOH, 500 kGY	1.2	547	30.3	19.3	12.1	7.61	25.5	35.6	2050	0.582	< 0.200	< 4.64	
PFOA in 0.5% MeOH, Control	0	0	< 10.0	< 5.00	6.53	5.17	91.1	125	19600	0.777	< 0.200	< 4.64	N
PFOA in 0.5% MeOH, Control	0	0	< 10.0	< 5.00	4.99	4.17	95.0	127	21400	0.737	< 0.200	< 4.64	NA
PFOS in water, 500 kGY	1.2	525	287	39.3	32.2	21.8	14.6	12.9	73.4	15.1	3.43	9540	48%
PFOS in water, 500 kGY	1.2	525	382	37.0	31.0	22.1	15	13.0	70.8	14.8	3.32	8500	
PFOS in water, Control	0	0	18.6	< 5.00	< 1.00	< 1.00	< 2.00	< 1.00	0.376	16.3	4.13	18680	N
PFOS in water, Control	0	0	12.2	< 5.00	< 1.00	< 1.00	< 2.00	< 1.00	0.496	16.1	4.18	15940	NA
PFOS in 0.5% MeOH, 500 kGY	1.2	547	22.3	5.77	7.79	4.82	9.20	7.31	47.4	15.6	8.23	8060	57%
PFOS in 0.5% MeOH, 500 kGY	1.2	547	25.2	6.00	7.60	4.28	9.06	7.28	46.4	15.1	7.23	7390	
PFOS in 0.5% MeOH, Control	0	0	< 10.0	< 5.00	< 1.00	< 1.00	< 2.00	< 1.00	0.536	17.1	3.98	18300	N
PFOS in 0.5% MeOH, Control	0	0	< 10.0	< 5.00	< 1.00	< 1.00	< 2.00	< 1.00	0.328	15.8	4.15	17400	NA

Another observation from those samples was that a significant gas build up occurred in samples containing methanol. The gas was shown to be composed of carbon monoxide, carbon dioxide and methane by gas-phase Fourier Transform Infrared (FTIR) analysis. The gas-phase FTIR analysis also showed that hydrofluoric acid (HF) was not formed in those reactions, supporting the environmental and health assesment for hazardous fluorinated substances. The inclusion of a hydrocarbon alcohol is pertinent to the health/environmental assesment because, for example, alcohols may be present in IE regeneration wash waters. Such gases, if formed from co-present alcohols, could require abatement when EB treating IE regeneration wash water if the hydrocarbon alcohol is not first reclaimed from the solution prior to the EB treatment. The determined lack of hazardous HF suggests that any released fluorine from PFOA and PFOS by EB treatment was released in the form of fluoride ion.

Titanium Dioxide (TiO2) and Hexagonal Boron Nitride (hBN) Additives

Titanium dioxide (TiO2) and hexagonal boron nitride (hBN) with 254nm ultraviolet light (UV_{254}) have been reported to facilitate the photocatalytic degradation of PFOA, possibly facilitated by hydroxyl radical, but have been generally less effectively for PFOS[82,83]. Early on in our work, we tested TiO2 and hBN, each at 2.5 g/L, with 20 ppb PFOS and PFOA, which indicated a slight improvement over solutions without the additives. However, repeat experiments at 20 ppm did not confirm the early observation and it was deduced that neither

additive stimulated degradation by EB that was sufficiently to pursue them further. The earlier observations were assumed due to variance due to analytical measurement error. The experimental results from the 20 ppm with 2.5 g/L of TiO2 or 2.5 g/L hBN are shown below in **Table 7** and **Table 8**, respectively. In all, it was found that TiO2 or hBN did not improve EB degradability of PFOS or PFOA in water.

Other additives discussed that might facilitate improved degradation, but which were not tested and are possibly for future testing, could include Fenton reagent, zero valent iron, hydroxyl radical scavengers, and alternative acids and bases as pH altering additives.

Table 7. Results with Titanium Dioxide (TiO2)

Description	kGy	PFOA (ng/mL)	Total PFAS (uM)	% PFOA removed	% PFAS removed
Water + PFOA + TiO2 (not treated)	0	17860	44.0	0.00%	0.00%
Water + PFOA + TiO2	538	7380	28.8	58.7%	34.5%
Water + PFOA + TiO2 + 0.1N NaOH	524	4.72	0.1	99.97%	99.9%
Water + PFOA (no additive, no treatment)	0	18200	45.2	0.00%	0.00%
Water + PFOA (no additive, 1.2 kGy/s ~500 kGy)	536	9475	33.4	47.9%	26.1%
Water + PFOA (no additive, no treatment, 0.1N NaOH	0	18800	46.2	0.00%	0.00%
Water + PFOA (no additive, 1.2 kGy/s ~500 kGy), 0.1N NaOH	536	0.859	0.00287	100.0%	100.0%
Water + PFOS + TiO2 (not treated)	0	12980	26.1	0.00%	0.00%
Water + PFOS + TiO2	538	7000	18.3	46.1%	29.9%
Water + PFOS + TiO2 + 0.1N NaOH	524	90.6	0.2	99.3%	99.1%
Water + PFOS (no additive, no treatment)	0	17310	34.9	**0.00%**	-0.58%
Water + PFOS (no additive, 1.2 kGy/s ~500 kGy)	536	9020	21.82	47.9%	37.1%
Water + PFOS (no additive, no treatment, 0.1N NaOH	0	14010	28.1	0.00%	0.00%
Water + PFOS (no additive, 1.2 kGy/s ~500 kGy), 0.1N NaOH	525	58.55	0.117	99.6%	99.6%

Table 8. Results with Hexagonal Boronitride (hBN) Additive

Description	kGy	PFOA (ng/mL)	Total PFAS (uM)	% PFOA removed	% PFAS removed
Water + PFOA + hBN (not treated)	0	18460	45.4	0.00%	0.00%
Water + PFOA + hBN	538	16440	52.6	10.9%	-16.0%
Water + PFOA + hBN + 0.1N NaOH	524	7.86	0.0	100.0%	99.9%
Water + PFOA (no additive, no treatment)	0	18200	45.2	0.00%	0.00%
Water + PFOA (no additive, 1.2 kGy/s ~500 kGy)	536	9475	33.4	47.9%	26.1%
Water + PFOA (no additive, no treatment, 0.1N NaOH	0	18800	46.2	0.00%	0.00%
Water + PFOA (no additive, 1.2 kGy/s ~500 kGy), 0.1N NaOH	536	0.859	0.00287	100.0%	100.0%
Water + PFOS + hBN (not treated)	0	14820	29.8	0.00%	0.00%
Water + PFOS + hBN	538	6100	15.4	58.8%	48.3%
Water + PFOS + hBN + 0.1N NaOH	524	250	0.6	98.3%	98.1%
Water + PFOS (no additive, no treatment)	0	17310	34.9	**0.00%**	-0.58%
Water + PFOS (no additive, 1.2 kGy/s ~500 kGy)	536	9020	21.82	47.9%	37.1%
Water + PFOS (no additive, no treatment, 0.1N NaOH	0	14010	28.1	0.00%	0.00%
Water + PFOS (no additive, 1.2 kGy/s ~500 kGy), 0.1N NaOH	525	58.55	0.117	99.6%	99.6%

Y1: Task 3 Results – Process Flow Specification

As part of the original project objectives, the year 1 task 3 objective was to provide information and detailed analysis of at least one conventional water treatment technology for PFAS, likely GAC at that time. The information gathered was to include total life cycle energy demand and costs associated with the use of that conventional water treatment technology. Also, based on the results from the Y1 experimental testing, we would determine where in the water treatment system EB technology would be a good fit. The planned comparison would utilize enumeration of monetary costs, energy usage, and as necessary other factors such as logistics and regulatory constraints in the evaluation with the ultimate deliverable of a calculated lifetime energy requirement and treatment cost. The determined energy and cost would serve as the metric to be used for evaluating the accelerator-based methods in Y2.

It is noteworthy that in the early concepts of our work which envisioned EB treatment of PFAS in water as a potential replacement technology for conventional treatment technology, it was not known if GAC reactivation was efficient at destroying PFAS and was assumed it was not, therefore EB could fill an unmet need. However, information in the scientific literature published during the present study have shown that reactivation can result in complete destruction of bound PFAS from GAC solids, and this does affect the scope of using EB as a potential replacement technology for GAC. Overall, we now believe EB treatment would not be a good replacement for GAC technologies in most situations, rather it would be better suited as a supplement to other technologies like reverse osmosis and ion exchange for PFAS removal from high concentration waste streams generated from those technologies. This is in part because of our findings that PFAS removal by EB is best suited for more concentrated PFAS streams, not the more dilute streams commonly found with most wastewater, groundwater and drinking water treatment applications. Since similar amounts of energy are needed to break down concentrated versus dilute waste streams it is more cost efficient to use EB to break down concentrated streams.

There are great complexities surrounding GAC production which make evaluation nearly impossible from an original material source (i.e. mined coal, coconut shells, etc.) to final end point (i.e. reactivation, disposal, etc.), for a full life cycle evaluation to be performed. We were only able to gain limited information from 3M's supplier of GAC, Calgon Carbon Corp. (C3) that is used at several of its locations and relied on data provided in the form of scant personal communications and publicly available pamphlets and presentations. This is in part due to proprietary nature of such information by CalgonCarbon Corp. which is withheld for competitive reasons. We have acquired more detailed cost and energy requirements related to installation and operation of a GAC groundwater PFAS treatment system that 3M operates in Minnesota, USA. This information was obtained from 3M's water remediation group who oversees installation, operation, and maintenance of such facilities. It is the data for that system that is our basis for comparison to estimated EB cost and energy requirements calculated utilizing calculations/algorithms developed as part of the present project in an Excel spreadsheet. We are primarily utilizing information associated with one facility because it operates at flow rates comparable to treatment flow rates that are realistic for EB treatment based on our Y1 experimental results.

For water treatment at various of its facilities, 3M utilizes a reactivated GAC material called DSR C which is provided from Calgon Carbon Corporation (Calgon) [84]. The size, complexity and treatment specifications of 3M's GAC systems can vary depending upon PFAS concentration requiring treatment, PFAS chemistries present, discharge permit requirements, volumes of water requiring treatment, etc. 3M is in process of implementing additional removal technologies in tandem with GAC at some of its facilities, including IE and RO, to aid in removal of PFAS which are not as efficiently removed by GAC. However, during the present work those treatment technologies were too early in their implementation stages to provide a reliable cost & energy evaluation, therefore the evaluation herein is focused solely on GAC for removal of PFOS and PFOA from groundwater in a pump and treat mode. Also, it was recently demonstrated that with high temperature

reactivation followed by off-gas treatment, the adsorbed PFAS can be destroyed greater than 99.9% [85], and the reactivated carbon is then more cost-effectively recycled for reuse. In this manner, the use of GAC (with thermal reactivation) process may be considered a removal and destruction technology [86].

Cost & Energy Estimation for GAC Treatment

Non-chemical activated GAC is produced by a high energy thermal process. The overall cost and energy requirements for its production involves many facets including mining, in the case of lignite (coal), or raw material purchase in the case of coconut shell or wood, material washing, thermal activation, size sorting, transportation, and thermal reactivation when applicable. The costs also include onetime infrastructure capital expenses for equipment and facilities, costs associated with the continuous operation and maintenance (O&M) including electrical, water, sewer, and natural gas, costs for personnel salaries, and corporate overhead costs. The total costs are difficult to compile on an individual component basis and are expected to vary from manufacturer to manufacturer. Also, such information is generally proprietary for competitive reasons. However, the total costs may be reflected in the billed US$ amount per pound of GAC that 3M incurs for Calgon's DSR C material, as described in the cost analysis below. Further, Calgon operated with a profit margin of about 18% in 2021, based on publicly available information, and this can be subtracted from the cost 3M incurs to estimate a GAC production, transport, and reactivation cost in $US. Additionally, over the last 5 years Calgon has published annual price increases ranging from 5-25% due to material shortages, so the cost of GAC treatment is expected to continue to rise as material shortages continue.

The DSR C product is initially derived from virgin GAC generated by heat activation process and is sourced from a combination of coconut shell and mined lignite (coal). Natural gas is the primary fuel used for the activation and reactivation processes for generating DSR C. When the DSR C adsorptive capacity has been exhausted at 3M's Oakdale, MN facility, it is returned to Calgon for thermal reactivation at 950°C (1742 °F) at either their Neville Island, PA plant or their Catlettsburg, KY plant. Based on information provided by Calgon (personal communication), the thermal energy requirement for virgin GAC production and the reactivation of spent GAC are roughly 11-13 million BTU per metric ton (MMBUT/MT) and 7.5-8.5 MMBTU/MT, respectively. This may vary somewhat based on activity desired, moisture level of the spent GAC, spent GAC quality and other factors. Reactivation process results in a burn-off rate of about 10-15% of the GAC solids, and a lowered adsorptive capacity to remove contaminants due to decreased GAC pore surface area following the thermal reactivation process. Therefore, reactivated GAC is typically supplemented with 10-15% (w/w) virgin GAC to compensate for those losses and is not considered 100% recyclable. This study used the highest reactivated carbon value of 10 MMBTU/MT to capture the fact that virgin GAC supplements the burned off reactivated carbon at a rate of 10-15%. It is noteworthy that the monetary costs for GAC production used herein do not include additional potential costs related to environmental impacts from deforestation for wood or coconut, mining for coal, or impacts for sourcing other carbon materials. Also, they do not consider potential costs such as environmental impacts of carbon dioxide and other emissions associated with mining, transportation, activation/reactivation, and facility operations.

Aside from the cost of producing the GAC material, there are the additional costs incurred by 3M, including capital expenses for construction of the treatment facility, annual O&M costs including electricity, water and sewer, miscellaneous O&M costs, salaries for operations personnel, and overhead costs of managing those facilities. While the land where the facilities are typically located may be preowned property of 3M, an estimated property purchase cost of 10% the capital expense for the treatment facility construction was used. Because the 3M Oakdale, MN facility was built in 2010, the average annual US inflation rate for the years 2010-2022 (2.52%) was used to estimate the capital cost to build the equivalent facility in 2022. Also, 3M paid

$1.10/lb. for DSR C in 2022. The Oakdale facility treats contaminated groundwater at a former disposal site and operates at a rate of 65 gallon per minute (gpm). The treatment results in removal of PFOS and PFOA at ~97% efficiency, as described further below. The system is comprised of two 10,000 lb. GAC tanks, a lead tank, and a lag tank. The lead tank is exchanged quarterly on an annual basis, and the lead tank is exchanged annually, for total of five 10,000 lb. exchanges (50,000 lbs./annually). The frequency of exchange is due to several factors, largely driven by flow rates and analytical testing of the influent and effluent for determination of breakthrough times. Breakthrough times are largely driven by the moderate levels of PFAS being treated at this specific site as well as presence of co-contaminants, measured in the form of total organic carbon (TOC) which also deplete the absorption capacity of the GAC. A general flow diagram of 3M's Oakdale GAC treatment system is shown in **Figure 33**.

The estimated O&M cost of operating the 3M GAC system calculated significantly higher than typical cost of GAC incurred for municipal drinking water treatment used to remove bad tastes or odors, which is typically in the range of 10 cents to 1 dollar per 1000 gallons ($0.0001 to $0.001 per gallon) treated (with capital expense included) [87]. Additional expenses are accrued due to the electrical requirements of the groundwater pumping system, as well as cost of sewer which are typically not incurred by municipal systems. The capital expense is also considered higher due to the full installation of a GAC system for PFAS removal, where installation of municipal GAC systems for odor/taste removal often utilizes existing equipment, such as replacing sand-based gravity filters with GAC. Finally, the simple economy of scales makes GAC treatment at municipal systems (often operating at tens to hundreds of millions of gallons per day) versus the small scale of the 3M pump and treat system at 93,600 gal/day (34,164,000 gal/year). Based only on O&M ($US) and energy (kWh), the cost for the GAC treatment system at the 3M facility was estimated at $0.0093/gal annually or 0.012 kWh/gal treated, using the actual data for the facility. Adding capital cost of $3.3 million (2022 estimated), split equally over an estimated 20-year facility lifetime, the cost increased to $0.014/gallon treated at the facility.

Conversions:

1 metric ton = 2,205 lbs.
1 MMBTU = 293 kWh

Capital Cost (one time):

3M Oakdale, MN Facility Capital Expense, (facility & property 2010):	*$2,500,000 (3M internal communication)*	
3M Oakdale, MN Facility Capital Expense, (facility & property, adj 2022)	**$3,260,000**	($163,000/y; 20-year life)

Annual Costs:

O&M (annual expenses, 2022 $US):	Dollar Cost	Energy Cost
Water:	$ 6,000	
Sewer:	$ 52,000	
Electricity[a]	$ 33,600	352,000 kWh
Miscellaneous Mechanical/Electrical:	$ 30,000	
Operations Personnel:	$ 135,000	
GAC Replacement (annual, 50,000 lbs.)@ $US 1.10/lb.:	$ 60,000	66,440 kWh [b]
Annual Total O&M Cost	$ 316,600	420,000 kWh [c]
Annual treatment cost per gallon (34,164,000 gallons annually):	0.00927 $/gal.	0.0123 kWh/gal.
Annual treatment cost per kg PFOA/PFOS removed (11.5 kg annually):	27,530 $/kg	36,521 kWh/kg

[a] Energy (kWh) and annual electric cost ($US) based on energy bill for March-April 2019, cost adjusted for US average inflation rate to 2022 dollars. Note: costs in other states and prices for domestic, commercial, and industrial electricity will vary.
[b] Estimated energy for production and use of 50,000 lbs of DSR C reactivated carbon (annual replacement), using value of 10 MMBTU/MT, or 227 MMBTU for 50,000 lbs., calculates at 66,440 kWh annually.
[c] Total energy consumption was estimated at 418,440 kWh. Assuming minor missed energy inputs, this estimate is rounded up to 420,000 kWh annually.

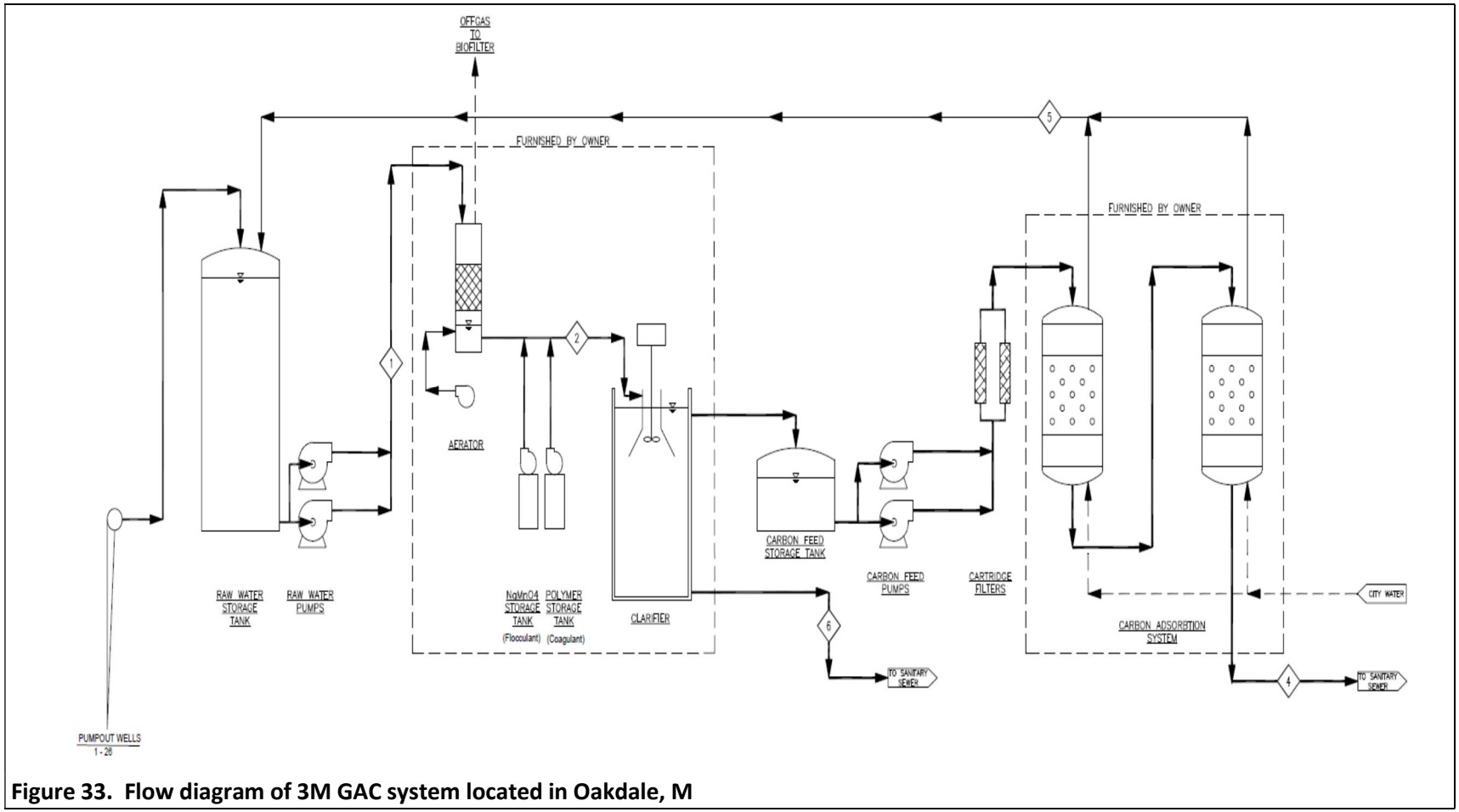

Figure 33. Flow diagram of 3M GAC system located in Oakdale, M

The 3M facility operates at 34,164,000 gallons per year. Based on monthly sampling between 2014 and 2022, the average influent concentration of PFOA and PFOS, combined concentration, was 91.5 μg/L. The site does not operate with a targeted discharge limit; however, treatment results in a 97% removal efficiency of PFOA/PFOS with an average effluent concentration of 2.72 μg/L combined. Based on 129,310,750 L/year and removal of 88.8 μg/L of PFOA and PFOS, combined, equates to removal of 11.5 kg of combined PFOA/PFOS annually. Based on annual operating cost for the facility, excluding capital cost, the GAC treatment calculated at $27,530 per kilogram of PFOA/PFOS removed. Per unit of energy, it was 36,521 kWh per kilogram of PFOA/PFOS treated. The system design specifications, when installed, were for operations capable of a maximum flow rate at 120 gpm, so those costs could be lower if operated at full capacity, assuming all O&M expenses, except personnel costs, would increase proportionally with the flow rate increase. Also noteworthy, estimated cost does not include additional expenses for analytical testing/monitoring of PFAS in influent and effluent, which can be substantial depending on monitoring frequency and number of PFAS analytes monitored. It is expected that an EB system would require similar monitoring costs to GAC, hence would offset in a head-to-head comparison of GAC versus EB.

Cost and Energy Estimation for Electron Beam Treatment

In Y1, systematic investigations in the present study have been conducted to optimize the treatment procedures for PFAS removal. These comprehensive experiments evaluated the influence of various parameters, such as dose rate, total dose, and the presence of additives. The findings revealed that applying a total dose of 200 kGy, administered at a dose rate below 10 kGy/s to a 20 ppm PFAS solution with a pH level of 10-13, resulted in a PFAS removal efficiency ranging from 85% to 99%. In Y2, the design of the accelerator was elucidated. Having ascertained the efficiency of the accelerator, it is feasible to compute the cost associated with PFAS removal. To facilitate this calculation, certain treatment conditions are postulated and employed in the estimation of PFAS removal costs:

1. The pH level of the water body is elevated to a range of 11-12 before treatment and subsequently neutralized to 8.5. The costs of achieving pH levels of 11, 11.5, and 12 will be assessed to determine the most economically efficient pH level for treatment.
2. A quantity of 2 ppm nitrogen is introduced into the water body to eliminate solvated oxygen, a prerequisite for optimal PFAS removal efficiency.
3. A total dose of 200 kGy is administered to the water body, with the beam rastered to ensure homogenous distribution and a dose rate maintained below 10 kGy/s.

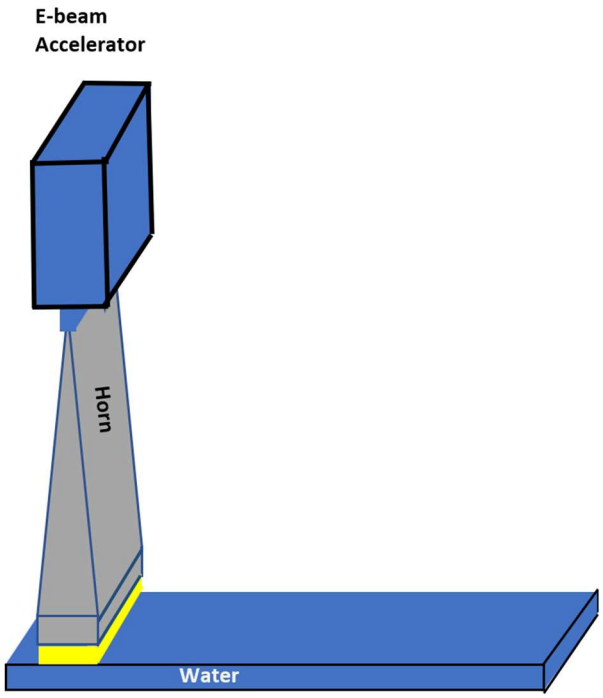

Figure 34. E-beam treatment schematic

Figure 34 depicts a simplified schematic representation of the water treatment process, in which an EB is directed toward the water flow from above. The beam power and dose requirements dictate the flow rate, corresponding to the water volume treated per unit of time. According to the findings of this study, a total dose of 200 kGy is necessitated for effective PFAS removal. The following equation provides the volume of water treated per unit of time, expressed in gallons per hour (Gal/h). This assumes a certain depth of water and width of water stream that was used in the accelerator beam delivery system design.

$$\text{Flow rate(Gal/h)} = \text{beam power[kW]} \times \text{Beam deliver efficiency} \times 4.76\ \text{Gal/h}$$

How the beam power is delivered to the water body can constitute a significant source of loss, reflecting the extent to which the beam is actively engaged in treating the water body. This is called beam delivery efficiency above. For example, in the configuration depicted in **Figure 34**, the water depth is 3 cm and only 80% of the beam energy is imparted to the water flow. Consequently, the 100/400 kW accelerator system can treat water at 380/1520 gallons per hour (Gal/h).

In administering a 200 kGy treatment to 1 gallon of water, 0.0175 kWh of energy is delivered to the water body. Utilizing this conversion factor, the electricity cost for treating each gallon of water can be determined through the subsequent equation.

$$\text{per gallon cost(\$/Gal)} = \text{electricity price [\$/kWh]} \times 0.0175 \text{accelerator efficiency [\%]} \times \text{beam deliver efficiency [\%]}\ \$/\text{Gal}$$

The accelerator efficiency is shown in the accelerator analysis section. Employing the configuration depicted in **Figure 34**, the beam delivery efficiency amounts to only 80%. As the Rhodotron is the preeminent commercially available accelerator system it is examines. Concurrently, the SRF accelerator system, currently under development, is acknowledged as the most promising solution for applications of this kind. Accelerator

efficiencies are rounded to 5% here as this is only a rough calculation. The electricity price is postulated to be $0.083/kWh, reflecting the average industrial electricity price in the US as of January 2023. In addition to the energy the accelerator consumes, a 5-kW power expenditure is presumed for the beam delivery system. For the accelerator system operating at 100/400 kW, the beam delivery system contributes an additional treatment cost of $0.0011/gal and $0.0003/gal, respectively. **Table 9** presents the costs associated with treating water with different accelerator systems.

Table 9. Accelerator energy cost.

Accelerator Efficiency	Accelerator Type	Beam delivers efficiency	Power cost per gallon treated $/gal
25%	Rhodotron @ 100 kW	80%	0.087
45%	Rhodotron @ 400 kW SRF @ 100 kW	80%	0.048
65%	SRF @ 400 kW Magnetron SRF @ 100 kW	80%	0.034
80%	Magnetron SRF @ 400 kW	80%	0.027

To attain high removal efficiency, the pH level of the water body necessitates adjustment. A 50% sodium hydroxide solution is employed to elevate the pH level of the water at $0.23 per pound. After the electron beam treatment, a 93% sulfuric acid solution neutralizes the water at $0.18 per pound. In addition to the pH adjustment, dissolved oxygen must be eliminated from the EB treated water using nitrogen. Nitrogen cost of $1.5 per 100 cubic feet equates to an additional $0.00003 per gallon of treated water.

The efficiency of PFAS removal varies with pH. To minimize PFAS removal costs, an optimized pH level should be selected. **Table 10** shows the costs associated with elevating and subsequently balancing the pH level. As observed in **Table 10,** when the pH level is increased from 11 to 13, an additional 4% of PFAS is removed; however, the cost escalates nearly 100-fold.

At a pH level of 13, the additive cost per gallon of water is comparable to the energy cost derived from **Table 10**. Presuming a 65% accelerator efficiency, the cost of PFAS removal is calculated. The optimized pH level is determined to lie between 11 to 12, as shown in **Figure 35**.

Table 10. Additive cost analysis to increase and then neutralize PH level.

PH	PFAS Removal rate @ 20 ppm level	Additive cost per gallon treated $/Gal	Additive cost per kg PFAS removed $/kg	Cost per kg PFAS removed @ 65% accelerator efficiency $/kg
10	88.43%	2.3E-05	0.34	418.2
10.5	92.41%	7.3E-05	1.04	400.91
11	95.55%	0.00023	3.21	389.3
11.5	97.86%	0.00073	9.88	387.48
12	99.33%	0.0023	30.91	402.92
12.5	99.97%	0.0073	96.78	466.41
13	99.77%	0.023	307.85	678.21

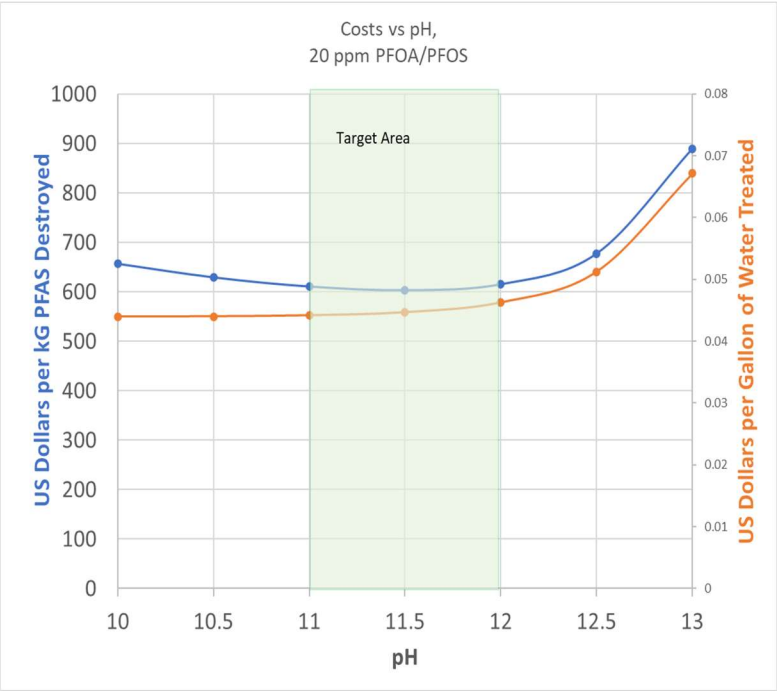

Figure 35. Cost of PFAS treatment by EB versus pH

Typically, the annual maintenance cost for an accelerator amounts to 1% of the overall accelerator cost. Given a $10 million investment in the accelerator system, the maintenance cost for the accelerator system is estimated at $100,000. Assuming a 90% operational time for continuous 24/7 operations, the total cost of electron beam treatment is computed. **Table 11** shows the cost of water treatment for each accelerator system at a pH level of 11.5 and a 20 ppm PFAS concentration. The analysis encompasses accelerator power consumption, additive expenses, and maintenance costs.

Table 11. water treatment cost @ PH level 11.5 and 20 ppm PFAS concentration

Accelerator systems	Accelerator efficiency	Water treatment cost $/Gal	PFAS removal cost $/kg
Rhodotron @ 100 kW	25%	0.122	1653.1
Rhodotron @ 400 kW	45%	0.058	780.94
SRF @ 100 kW	45%	0.084	1129.53
SRF @ 400 kW	65%	0.043	579.57
Magnetron SRF @ 100 kW	65%	0.069	928.16
Magnetron SRF @ 400 kW	80%	0.037	494.62

Owing to maintenance costs, higher accelerator power considerably reduces the cost of treatment. As illustrated in **Table 11**, the 400-kW accelerator system is effectively half the PFAS removal cost of a 100 kW system. Accelerator efficiency constitutes another significant factor that can substantially decrease treatment

costs. An increase of approximately 20% in accelerator efficiency can be attained by elevating the accelerator power from 100 kW to 400 kW. An additional 20% increment can be achieved by implementing SRF technology. Lastly, integrating a magnetron with the SRF accelerator can facilitate a further 20% increment.
In addition to accelerator efficiency, advancements in beam-water interface development can contribute to reduced treatment costs. The calculations for **Table 11** assume an 80% beam-water interaction efficiency. Developing an enhanced beam-water interface capable of utilizing 100% of the beam energy is feasible. With such a system, the costs presented could be diminished by another 20%.

One of our early concepts for best fit of EB technology to removal of PFAS from water was possibly as replacement for conventional treatment, but after cost and energy analysis this did not appear to be practical except at high concentrations. However, the frequently changing regulatory landscape, may influence this decision in the future. On June 15th 2022 the U.S. EPA announced it was updating their lifetime drinking water health advisory levels (HALs) for perfluorooctane sulfonate (PFOS) and perfluorooctanoate (PFOA) from the previous 2016 HAL of 70 ppt, combined concentration for PFOA and PFOS, to 0.02 ppt and 0.004 ppt for PFOS and PFOA, respectively[88], and the USEPA added interim HALs for PFBS (2000 ppt) and hexafluoropropylene dimer acid, also known as Gen-X (10 ppt), indicating growing emphasis on replacement chemistries. More recently in March of 2023, the USEPA changed direction and proposed a US National Primary Drinking Water Regulation for PFOA and PFOS at 4 ppt, individually [89], and further confounded the water treatment technology outlook. Based on such recent actions, it is increasing unclear if conventional water treatment technologies will effectively remove PFAS from drinking water to below regulatory levels. The final standard is certain to impact the PFAS treatment technology landscape in a manner which has yet to be completely defined.

Based on our research findings we have come to realize that EB is best suited for treatment of more concentrated PFAS streams and less suited for dilute PFAS concentrations such as those found in groundwater or drinking water where removal is for PFAS levels in the low ppb to part-per-trillion (ppt) concentration ranges. Such more concentrated PFAS streams can be found in direct wastewater from fluorochemical production processes, or from reject water from RO systems or IE regeneration wash waters. The primary driver for this decision is that our research has shown the EB treatment for removal of PFOA and PFOS in water appears to follow pseudo-first order removal kinetics. For example, the PFOA removal percentage at 2 μg/L (ppb) was the same as 20 mg/L (ppm), a concentration range over 5 orders magnitude. When considering a total PFAS mass destruction efficiency per unit of cost or energy, it makes sense to destroy as much of the PFAS mass as possible with the minimum cost and energy input. As an example of this concept, consider the treatment of one liter water with 0.002 mg/L (2 ppb, 2 μg total in one liter) PFOA treated with an EB dose of 500 kGy. Without the optimizing additive NaOH, the PFOA is reduced in concentration by about ½ to achieve 0.001 mg/L, and the PFOA mass destroyed in the one-liter sample is 1 μg . However, if treating one liter of a 20 mg/L solution of PFOA with the same EB dose of 500 kGy, we again observe ½ the PFOA concentration removed to get 10 mg/L, or 10 mg (10,000 μg) destroyed. On a mass basis 10,000-times more PFOA mass was destroyed by the same EB treatment at the higher concentration than at the lower concentration. This effectiveness is driven to 100% destruction by the addition of NaOH additive. The benefit of EB over conventional sequestration treatments such as GAC is not in cost per gallon treated, but cost per mass of PFAS removed, with the added benefit of PFAS destruction by EB.

Recommended Best Fit(s) for E-Beam Treatment of PFAS

Electron Beam Treatment of RO Reject Water or IE Regenerant

As mentioned above, it makes more sense from a cost and energy efficiency standpoint to use EB treatment as a supplement to a conventional PFAS sequestration technology such as RO, IE or GAC by treating

the concentrated waste streams from those technologies. Currently, such streams require secondary treatment or disposal of the wastes they generate. A simple demonstration schematic is shown below in **Figure 36** for EB treatment of RO reject water containing high-concentration PFAS.

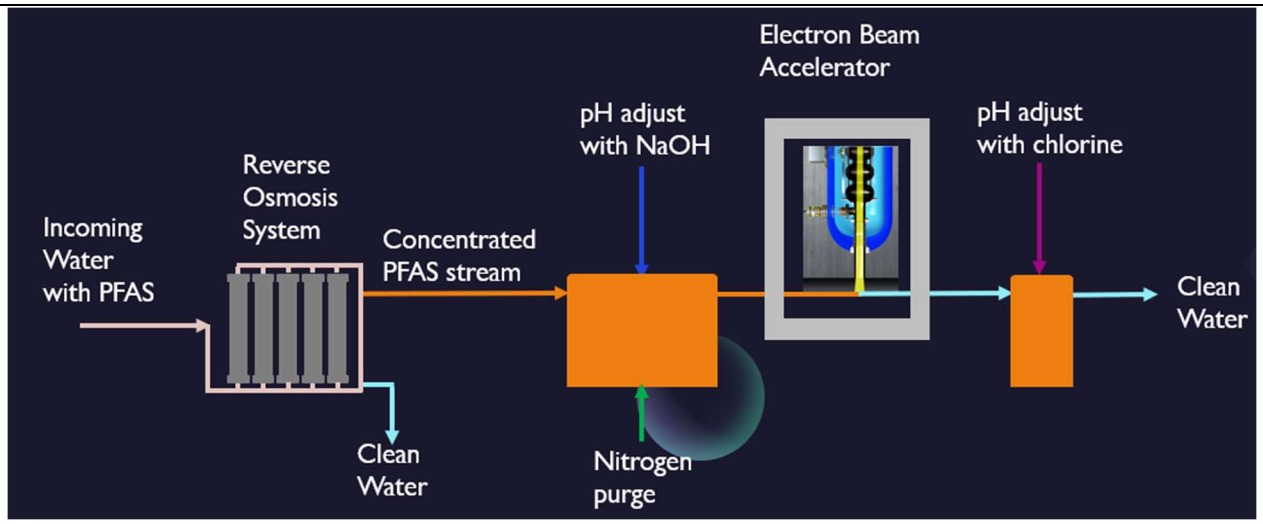

Figure 36. Proposed EB Best Fit: Supplement for RO Reject Water Treatment Shown

In April-May of 2022 3M and ECT2[90] conducted pilot scale testing of a combined chemical flocculation→GAC→RO→regenerable IE system, with alcohol distillation recovery system for the spent IE regenerant. The alcohol recovery system's still bottoms are a high salt content brine slurry. The system was designed for removal of mixed PFAS from wastewater at a 3M fluorochemical manufacturing facility, where the pilot scale testing was performed. PFAS concentrations were originally determined at the 3M EHS Laboratory for the pilot testing work. However, the remaing sample volumes were used to prepare EB treatment samples. Samples were prepared by dilution at 10x to pH 13 with 0.1N NaOH and then treatment at nominal 500 kGy at 1 kGy/sec. It is noteworthy that some PFAS concentrations exceeded 1100 ppm initially (110 ppm in diluted EB treated samples), yet achieved 100% removal, and others were not high in the system due to GAC removal (i.e. PFOA and PFOS) and diluted samples did not give a result above the low limits of measurement and were then not determined for percent removal (ND). The results are show below in **Table 12.** The final concentrations after EB treatment are shown after being adjusted for the 10x dilution to compare to original concentrations. Overall the wastestreams did not contain high levels of PFOA or PFOS, as they were largely removed by GAC prior to treamtne. These results show that EB can treat RO reject water, IE wash waters, and even distillation still bottoms with high salt content. PFBA was observed to increase after treatment of RO reject water, and could possibly have been formed from EB degradaton of an unknown PFBA precursor.

Table 12. EB Treatment of RO reject, IE wash water and alcohol distillation still bottoms.

Sample Type	before EB treatment (ppb); conc in original samples							
	PFOA	PFPeA	PFBA	PFPA	TFA	PFOS	PFHxS	PFBS
WW-RO-REJECT	3.19	39.6	990	4470	248	11.3	4.59	33.5
EGEN WW-FINAL SPENT REGEN COMPOSITE	< 0.0242	368	41800	94800	4590	0.137	< 0.0253	22.4
R316-REGENERANT FLUSH	< 0.0242	1110	124000	225000	6000	0.135	0.129	35.6
DIST WW-STILL BOTTOMS	0.38	9050	200000	1140000	19700	0.297	0.129	288

Sample Type	After EB treatment (ppb); adjused for dilution for treatment							
	PFOA	PFPeA	PFBA	PFPA	TFA	PFOS	PFHxS	PFBS
WW-RO-REJECT	< 10.0	11.5	1395	1113	250	3.51	2.81	31.7
EGEN WW-FINAL SPENT REGEN COMPOSITE	< 10.0	< 10.0	136	< 20.0	< 100	<1.85	< 2.00	14.0
R316-REGENERANT FLUSH	< 10.0	< 10.0	654	< 20.0	< 100	<1.85	< 2.00	27.0
DIST WW-STILL BOTTOMS	< 10.0	< 10.0	21.0	196	300	<1.85	< 2.00	213

Sample Type	Percent Removed by EB Treatment							
	PFOA	PFPeA	PFBA	PFPA	TFA	PFOS	PFHxS	PFBS
WW-RO-REJECT	ND	71.0%	↑	75.1%	0%	68.9%	38.8%	5.4%
EGEN WW-FINAL SPENT REGEN COMPOSITE	ND	> 97.0%	99.7%	100%	> 97.8%	ND	ND	37.5%
R316-REGENERANT FLUSH	ND	> 99.0%	99.5%	100%	> 98.3%	ND	ND	24.2%
DIST WW-STILL BOTTOMS	ND	> 99.9%	99.9%	100%	98.5%	ND	ND	26.0%

ND; not determined.

Groundwater Treatment by Electron Beam

Although not identified as a first best fit for EB, the treatment of PFAS contaminated groundwater could be another option, especially if PFAS concentrations are higher such as might be expected at former PFAS disposal sites, in landfill leachate, or for AFFF contaminated groundwater located near firefighter training areas at military installations, commercial airports, etc. We obtained a PFAS contaminated groundwater sample in June 2022 from a capped former PFAS disposal site at a 3M facility in Decatur, AL. At that location, groundwater has been physically contained by sheet piling driven to the bedrock and capped off and is pumped and treated by GAC at the site. The groundwater is subsequently pumped and treated by GAC. We diluted the groundwater samples 10-fold to 0.1N NaOH (pH 13) and EB treated at 500 kGy at nominal 1 kGy/sec. The results demonstrated that EB can be applied to groundwater samples with high levels of PFAS, as shown in **Table 13.** EB Treatment of PFAS Laden Groundwater (concentrations in ppb)**.** In all, for the PFCAs and PFSAs analyzed, there was > 85% removal of all PFAS compounds in the groundwater, except PFBS.

Table 13. EB Treatment of PFAS Laden Groundwater (concentrations in ppb)

Sample Description	PFOA	PFHpA	PFHxA	PFPeA	PFBA	PFPA	TFA	PFOS	PFHxS	PFBS
DAL GW-GRS04 Before EB; 10x dil with 0.1N NaOH	456	302	1528	424	540	524	72.4	206	666	193
DAL GW-GRS04 After EB;10x dil with 0.1N NaOH	< 1	< 1	< 1	< 1	< 1	< 2	< 10	5.54	81.2	155
% Removal	99.8%	99.7%	99.9%	99.8%	99.8%	99.8%	86.2%	97.3%	87.8%	19.7%

Y2: Task 1 – Evaluation of Up to three E-beam Technologies for PFAS Treatment

Electron Beam Accelerator Technology

Electron beam technology is a versatile and precise scientific tool with wide ranging industrial applications. Electron beam accelerators are used for driving industrial chemistries, medical sterilization, welding, 3D printing, surface modification of materials, printing, environmental remediation, and water treatment among others. Electron beam accelerators take electrons and accelerate them to high energies, under vacuum, at nearly the speed of light and direct them for deposition in the desired target.

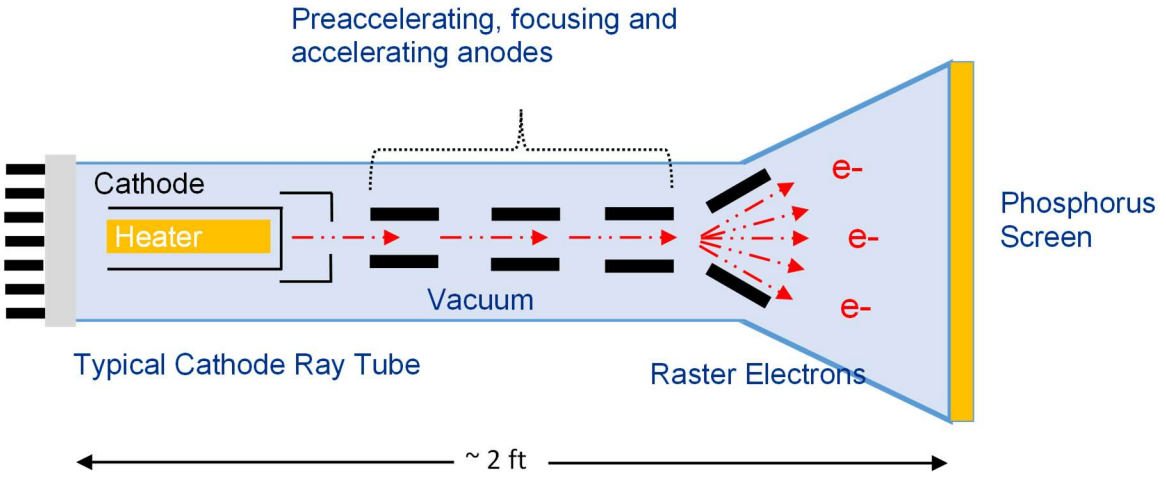

Figure 37. An example of a simple electron beam accelerator, the cathode ray tube, commonly found in televisions and monitors before LEDs.

Figure 37 above shows a cathode ray tube (CRT) accelerator. In a CRT the electrons from the wall are used to heat up a piece of metal which then emits them into the vacuum chamber where they are focused, accelerated and then steered onto a phosphorus screen to create an image. Over the roughly 2 foot length of the CRT the electrons would only reach an energy of 10s of keV above the resting state before hitting the screen.

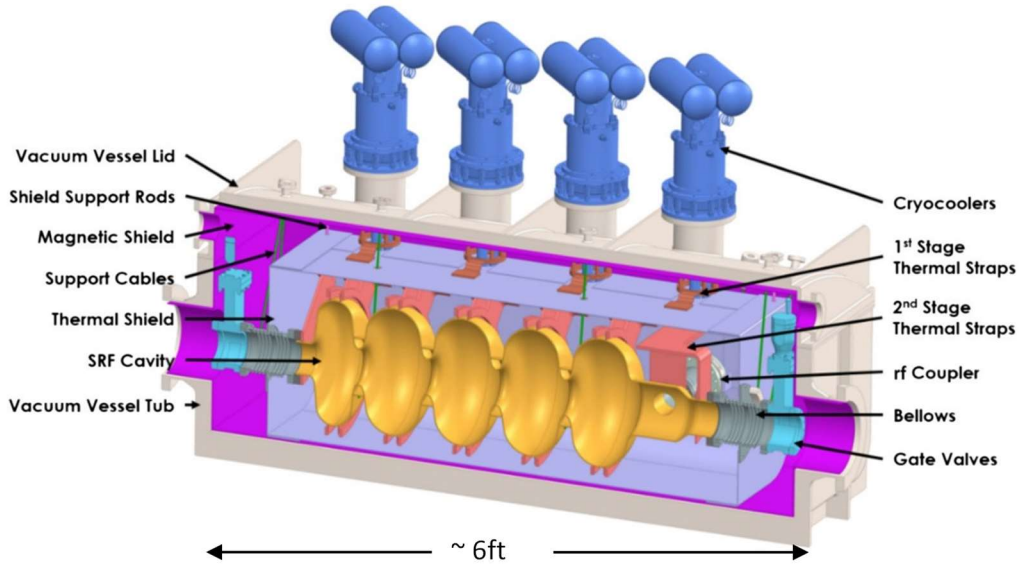

Figure 38. Compact 650 MHz electron beam accelerator being developed at Fermilab for commercial applications.

For comparison, the kind of accelerator we are discussing in this work is shown in Figure 38**,** above. Like the CRT electrons from the wall are injected into the accelerator, but here the electrons are accelerated on a 650 MHz radio frequency wave. For this accelerator shown the electrons can reach an energy of 10 MeV in the roughly 6 feet length of the accelerator. At 10 MeV energy the electrons can penetrate roughly 5 cms into water. This accelerator is superconducting and the SRF cavities are made from niobium with a thin layer on the inside of niobium three tin (Nb_3Sn). To reach the superconducting state the accelerator must be cooled to around 4 Kelvin. Therefore, some of the design of the accelerator involves shielding the accelerator from the outside room temperature. The bulk of the design of this accelerator is in fact based around minimizing heat generated during operation so that cryogenic cooling costs are minimized.

The reason the accelerator is designed to produce 10 MeV electrons is that it gives you the maximum penetration depth into the target, in this case water, without having to worry about activating the target. The electrons will produce X-rays and for this reason a shielding enclosure must be provided around the accelerator. **Figure 39,** below, shows a typical electron beam accelerator with beam delivery system, enclosure, and conveyor belt. The beam delivery system consists of magnets that bend the beam and shape it to hit the target. The conveyor system here is just an illustrative example that would be replaced by a flowing water stream for PFAS destruction.

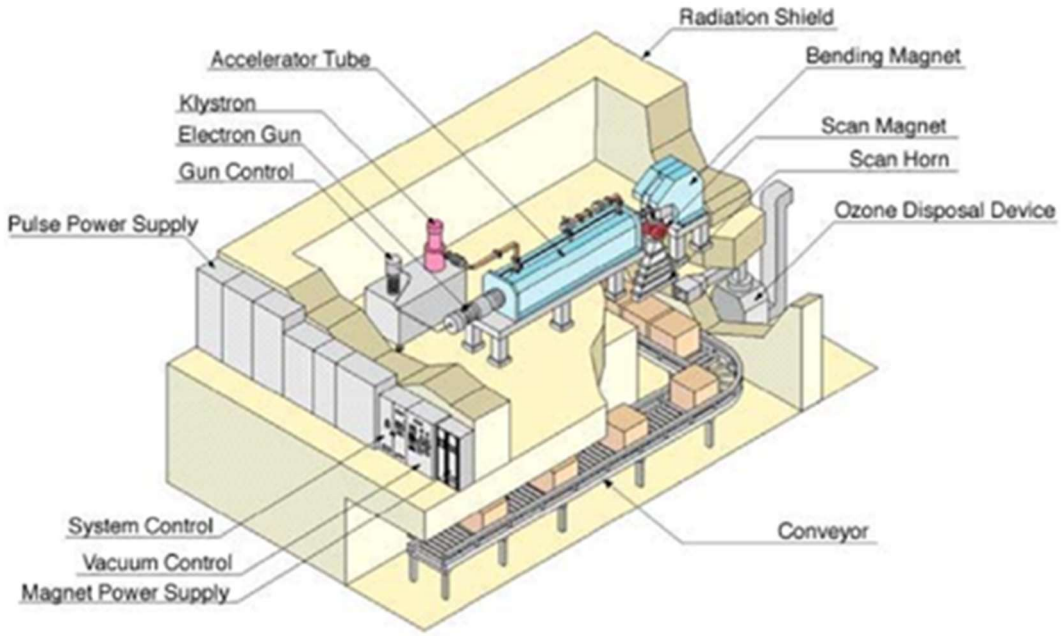

Figure 39. **Layout of electron beam accelerator treatment facility.**

For the purposes of this study, 5 different electron beam accelerators were examined. The primary attributes of interest were:

- Accelerator Efficiency – which largely determines operating costs
- Accelerator Cost
- Accelerator Reliability

Additional attributes of interest include:

- Simplicity/Ease of Operation
- Repairability (in situ)
- Rugged - works in the industrial environment
- Footprint - small sizes available to fit into existing installation

Electron Beam Accelerator Efficiency

After this brief introduction to electron beam accelerators, a more thorough examination on accelerator efficiency is needed. Electron beam accelerators are known for their high energy efficiency because of their direct energy conversion, precise focusing, instantaneous operation, and limited secondary waste generation. These features make them attractive for a wide range of industrial and scientific applications where efficient and

controlled energy delivery is essential. High efficiency is essential to reduce energy and operating costs and to allow for treatment of high mass flow rates. High efficiency in high degree is determined by acceleration efficiency η_{acc}, which may be determined as a ratio of the beam power P_{beam} to input RF power P_{RF} necessary to maintain accelerating RF field. For room-temperature accelerators, it depends on the beam loading and Ohmic loss,

$$\eta_{acc} = \frac{P_{beam}}{P_{RF}} = \frac{UI}{UI+U^2/R} = \frac{1}{1+U/(RI)}$$

where U is the beam energy and I is the beam current and *R* is the accelerator shunt impedance,

$$R = \frac{R}{Q} Q_0,$$

Where R/Q is characteristic impedance, which is determined by the acceleration structure geometry, and Q_0 is the unloaded quality factor. Acceleration efficiency increases with the beam loading or with the beam current or the beam power.

Beam loading at fixed average power, or average beam current at fixed energy, may be increased using two means. The first is operation in the pulsed regime with a relevant duty factor (DF, also known as beam on time). In pulsed mode operation the percent of time that there is current going through the accelerator is small, in part to prevent the accelerator from overheating. One example of a pulsed accelerator is the linear industrial accelerator IMPELA[91], based on a room-temperature 1.3 GHz SW acceleration structure, see **Figure 40**. Another example of a pulsed electron accelerator is the ILU-14 [3,4] based on 176 MHz bi-periodic SW structure, seen in **Figure 41** [92,93].

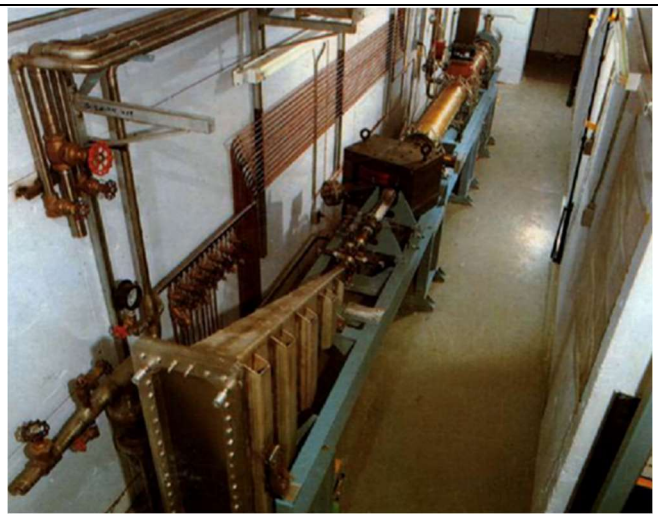

Figure 40. **Industrial accelerator IMPELA. Beam energy is 10 MEV, beam power is 25 kW, 5 % duty factor (typically 200 us pulse lengths at 250 pps)**

Figure 41. Industrial accelerator ILU-14. Electron beam energy is up to 10 MEV, beam power is 50 kW.

In this case of pulsed mode operation, the average beam power is:

$$P_{beam} = UI_{av} = UI \cdot DF$$

where I now is the pulsed beam current. Acceleration efficiency for pulsed mode operation in this case is calculated with:

$$\eta_{acc} = \frac{1}{1+DF \cdot U/(RI)}.$$

Typically for pulsed mode operation a high-power RF source, modulator and associated equipment are needed. These items increase the cost of the system and its footprint. Also, the high beam current may cause problems with the beam dynamics and beam interception in the accretion system.

The other acceleration mode, which is fundamentally different than pulsed accelerators, is one where the beam passes many times through the same acceleration structure (cavity, periodic structure, etc.), returning the beam to the cavity entrance after each pass. Examples of this include the microtron or Rhodotron seen in **Figure 42** [94]. In a Rhodotron, the beam is accelerated many times in the TEM RF field of a half-wave resonator (HWR). In this case, operating in the CW regime with a smaller beam current at the same average power is possible. The acceleration structure voltage, in this case, is $U_a = U/n$, where n is the number of the beam turns. Acceleration efficiency, in this case, is:

$$\eta_{acc} = \frac{1}{1 + U/(nRI)}$$

However, in this case, the beam optics may limit the beam power because of possible current interception in the magnet system, which returns the beam to the acceleration structure at each turn. Careful optics optimization and control of the beam injection energy increase may mitigate the problem. While the Rhodotron is advantageous in some areas, unfortunately the HWR cavity used can have high loss because of how the RF fields are concentrated on the internal electrode. Utilization of conical cavities, widely used for SRF HWR[95], may reduce these loses by as much as 2 times.

Figure 42. Rhodotron, IBA, beam energy 5-10 MeV, beam power up to 700 kW

Another way to increase acceleration efficiency is to use a superconducting RF structure[96]. The SRF structure, seen in **Figure 38**, has an unloaded quality factor and an associated shunt impedance that is up to 1e6 times higher than a similar room temperature (RT) structure.

Considering that the refrigeration efficiency,η_{ref} seen in the equation below, is 1 e-3 to 1 e-4, the SRF accelerator gives a radical reduction in Ohmic loss and, therefore, an efficiency increase. At Fermilab, several compact industrial linacs are under development, providing 10 MeV of the beam energy at the beam power of 100s of kW. The linac is based on an Nb cavity with Nb_3Sn coating, which allows operation at temperatures > 4 K with very high unloaded Q, up to $2e10^7$. Q is a measure of energy efficiency of the accelerator. The Nb_3Sn coating can go to the superconducting state at around 17-18 degrees Kelvin, compared to niobium at 9 degrees Kelvin. In turn the Nb_3Sn allows conduction cooling and compact cryo-coolers instead of cumbersome refrigerators and liquid He systems. In this case,

$$\eta_{acc} = \frac{1}{1 + U/(\eta_{ref} RI)}$$

The wall-grid efficiency, which determines the operation cost, depends to a high degree on the RF source efficiency, which depends on the RF source operation frequency type. Note that optimal operation frequency depends on the accelerator type.

Accelerator Technologies Compared

Given a short overview on electron beam accelerator technology and how energy efficiency is determined the different electron beam accelerators being compared for PFAS destruction in water is discussed.

All electron beam accelerators were compared (see **Table 14**) at a beam energy of 10 MeV. 10 MeV was chosen because at this energy you don't have to worry about activation of the water or species in it. Also, there is a decent penetration depth with the bulk of the energy being deposited in the top 3 cms of water.

Table 14. **Parameters of the options for 10 MeV accelerators operating at 100 and 400 kW power.**

		SRF Nb_3Sn	**IMPELA**	**IMPELA**	**ILU-14**	**RHODOTRON**
Frequency	MHz	1300	1300	1300	176	107.5
Length	m	1	3.25	3.25	5.5	2
Energy	MeV	10	10	10	10	10
Average beam power	kW	100/400	100/400	100/400	100/400	100/400
Duty Factor	%	100	5	25	5	100
Pulsed beam power	kW	N/A	2000/8000	400/1600	2000/8000	N/A
Power for refrigeration	kW	40	N/A	N/A	N/A	N/A
Pulsed Ohmic loss in the linac	kW	N/A	540	540	2400	N/A
Pulsed input RF power	kW	N/A	2540/8540	1540	4400/10400	N/A
Average input RF power	kW	100/400	127/427	235/535	220/520	336
Average Ohmic losses	kW	N/A	27	135	120	86
Pulsed beam current	mA	10/40	200/800	40/160	200/800	10/40

Table 14 summarizes the operating parameters of different accelerator technologies operating at 10 MeV. This information was collected from literature, manufacturers and internal publications and information at Fermilab. The first column is for the superconducting accelerator being designed and built at Fermi. Fermi is currently working on a 10 MeV 650 MHz and 1.3 GHz accelerator. While the 650 MHz accelerator will be more energy efficient than the 1.3 GHz accelerator, the 1.3 GHz platform was examined because of availability of resources. The 650 MHz geometry is seen in **Figure 38.** Above. and the 1.3 GHz design is fully detailed in a section below. Of note is that the SRF accelerator is continuous wave, being that the duty factor is 100%. As discussed above the SRF accelerator, with proper design, can accelerator the electron without loss but at the parasitic cost of refrigeration.

The next two columns in the table are IMPELA accelerators that are also operating at 1.3 GHz but they are room temperature and pulsed. The difference between the two IMPELA designs is one is examined at 5% duty

factor and the other at 25%. To deliver the same average power between the two, the 5% duty factor must deliver 5 times as much power per pulse which requires special power handling/conditioning equipment. The way the power is pulsed can have a big effect on the over-losses to heat and therefore energy efficiency.

The 4th accelerator in the table, the ILU-14, is another linear pulsed accelerator, but unlike the IMPELA the operating frequency is much lower at 176 MHz. The lower frequency can potentially offer energy efficiency gains. This is the last of the linear accelerators that are compared.

The final electron beam accelerator shown in **Table 14** is the Rhodotron. The primary difference in the design of the Rhodotron is that it is a circular accelerator where each electron takes multiple passes through the accelerator before it leaves at 10 MeV energy. This accelerator and the SRF Nb_3Sn are the only two operating at 100% duty factor. The Rhodotron is the only of the accelerators listed that can be purchased today.

Parameters considered for the options presented in **Table 14** are discussed below. The overall efficiency of industrial accelerators, η_{acc} , is determined by the following factors captured in the equation below[97]:

- Efficiency $\eta_{AC\rightarrow DC}$ of the conversion from AC to DC; typically, the efficiency of transformers and rectifiers is higher than 95%.
- Efficiency of the RF source $\eta_{DC\rightarrow RF}$ including additional power for the gun heater and electromagnets for vacuum tubes (this power is typically small compared to other parameters).
- The need for equipment cooling. A chiller adds additional power overhead ξ_{chill} ~ 15% of the power dissipated in the tube.
- Input power determined by the tube gain K (in dB); the input power is ~0.001-5% of the output RF power, depending on the tube type.
- Transmission line efficiency η_{trans}; for industrial linacs, where the RF source is typically placed next to the accelerator, it is close to 100% for the case if the RF tube is connected to the linac directly.
- Accelerator cavity efficiency $\eta_{RF\rightarrow beam}$; for SRF linac operated in the CW regime it may be close to 100% if the cavity is matched to the line. Note that in a pulsed regime, $\eta_{RF\rightarrow beam}$ is smaller because of the filling time, RF source timing off-set, the modulator off-set, etc.
- Efficiency of the electron injector η_{inj}, how the electrons get from the incoming power source to the vacuum of the accelerator.
- Efficiency of the cavity cryogenic cooling η_{cooler}, which in turn is determined by the RF losses P_{loss} in the cavity and cooling efficiency. For cryo-plant (2K) it is about 1-1.3e^{-3}, for cryo-coolers (~ 4 K) it is 1-1.5^{e-4}.

The total accelerator system efficiency may be calculated using the following formula:

$$\eta_{acc}^{-1} = 1 + \left({}^{1}/_{\eta_{\mathrm{RF}\to\mathrm{beam}}} - 1\right)(1 + \xi_{chill}) +$$

$$+ \frac{\left[\left(\frac{1}{\eta_{DC\to RF}} - 1\right)(1 + \xi_{chill}) + (1 - \eta_{trans}) + \frac{1}{\eta_{DC\to RF}}\left(\frac{1}{\eta_{AC\to DC}} - 1\right) + 10^{-0.1K}\right]}{(\eta_{acc}\eta_{trans})}$$

$$+ \frac{P_{inj}\left(\frac{1}{\eta_{inj}} - 1\right)}{P_{beam}} + \frac{P_{loss}}{P_{beam}\eta_{cooler}}$$

The energy consumption diagram for a typical CW accelerator is shown in **Figure 43,** below.

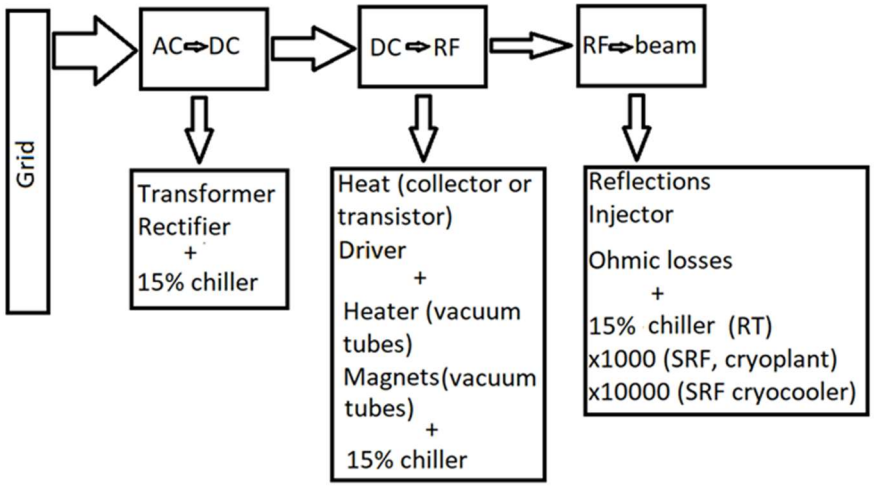

Figure 43. **Power consumption diagram for CW accelerator.**

The overall efficiency of an industrial accelerator is determined to a high degree by the efficiency of RF sources, especially for SRF accelerators. Considering an SRF 650 MHz, 10 MeV, 100/400 kW linac based on the Nb_3Sn technology, we may expect the unloaded quality factor Q_0 of up to $3e^{10}$ at 5-6 MeV/m at 4.5 K, and R/Q of up to 670 Ohm/m. This means that for a cavity length of ~1.6 m, the total surface Ohmic loss is 3 W. If the cryo-cooler efficiency is $\gtrsim 1e\text{-}^{4}$, the total power necessary for the cooling system is $\lesssim$ 40 kW. If one assumes that the power required to excite the RF source is small and that the losses in the electron injector are small, the formula is simplified:

$$\eta_{acc}^{-1} = 1 + \left(\frac{1}{\eta_{DC\to RF}} - 1\right)(1 + \xi_{chill}) + \frac{1}{\eta_{DC\to RF}}\left(\frac{1}{\eta_{AC\to DC}} - 1\right) + \frac{P_{loss}}{P_{beam}\eta_{cooler}}$$

In this case, the overall efficiency of the complete SRF system is determined by the efficiency of the RF source. The efficiency of the different accelerators from **Table 14** is shown in **Figure 44** for 100 kW and **Figure 45** for 400kW, below.

Figure 44. Wall-plug efficiency versus RF source efficiency for 100 kW

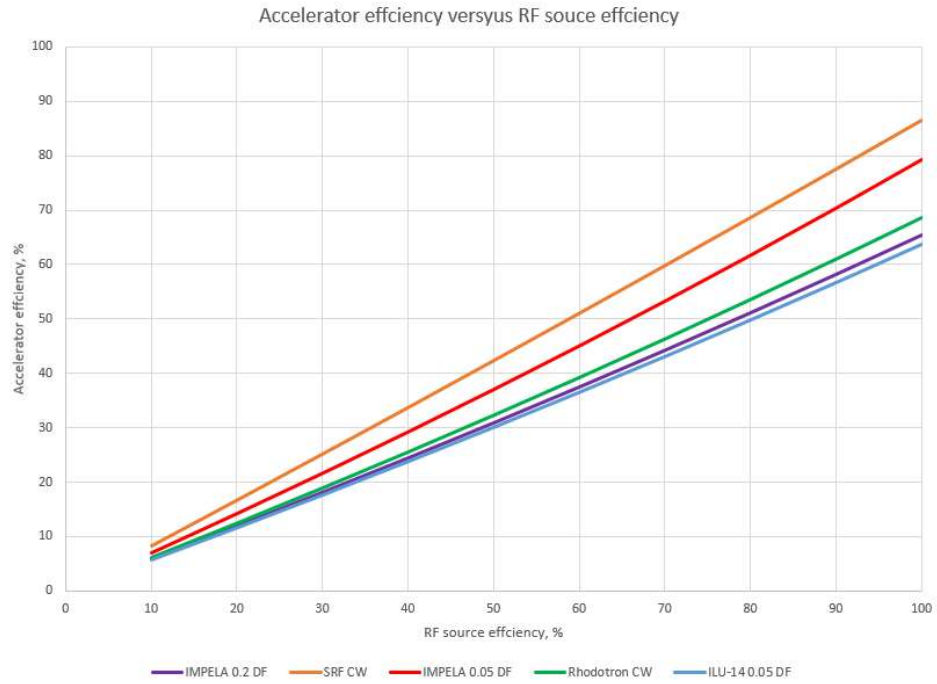

Figure 45. Wall-plug efficiency versus RF source efficiency for 400 kW

The following assumptions are made here (Note that industrial linacs do not need power overhead for amplitude control.):

1. Chiller overhead is 15 %.
2. For IMPELA and Rhodotron, the RF source has a 10% overhead for the line loss.
3. For SRF and ILU-14 linac, the source is placed close to the linac, and the line loss causes no overhead.
4. A 40 kV injector is used for SRF linac and IMPELA.
5. The SRF linac needs 40 kW from the grid for refrigeration; detailed further below.

Figure 44 and **Figure 45** show the wall-plug efficiency for all these options as a function of the RF source efficiency for the average beam power of 100 kW and 400 kW, respectively. With considerably low beam loading, the overall efficiency of the SRF option is considerably higher than the efficiency of all RT options. The 5% duty factor IMPELA option had the second highest efficiency, but as noted earlier needs considerably high pulsed power, over 2.5 MW. Fortunately, the 1.3 GHz RF sources requiring both high pulsed and average power are readily available from industry. For example, the CPI VKL7796 klystron has a pulsed power of 4 MW at an average power of 300 kW[98]. The efficiency of this tube is about 40%, and one may expect a wall plug efficiency of 25%. The footprint of this RF system may be significantly larger than other options because it needs a high-power modulator and pulsed transformer. The low-frequency option of ILU-14 has lower efficiency because of lower acceleration efficiency, which takes place because of higher Ohmic loss. Considering the efficiency of a gridded tube of ~60-65%, one may expect a very low wall plug efficiency of about 20%.

The efficiency of the gridded tube employed for the Rhodotron is the same as for ILU-14. It is about 60-65%, also giving a low wall-plug efficiency 25-27%. In contrast to the ILU-14, the Rhodotron operates in CW mode and does not need a high-power modulator or a pulsed transformer. CW operation at this power allows for utilization of ~250 kW Solid State amplifiers (SSA), the footprint for this power is large, but because the RF station is placed outside the accelerator shielding, it may not influence the cost of facility. Recent advances in SSA technology may allow efficiency of 80-90% in frequency ranges up to 650 MHz (see **Figure 46**), although R&D is still necessary to achieve these parameters at high power. Together with a conical HWR, SSA technology may give a wall plug efficiency for a Rhodotron of up to 45-50%. With the same RF source, the SRF linac efficiency is 20-25% higher than all RT choices (except the 5% duty factor IMPELA). The operation frequency and CW operation of the SRF linac enable self-exciting mode operation with a magnetron[96]. Magnetron efficiency may reach 90%, which pushes the wall-plug efficiency of the SRF linac to 65%.

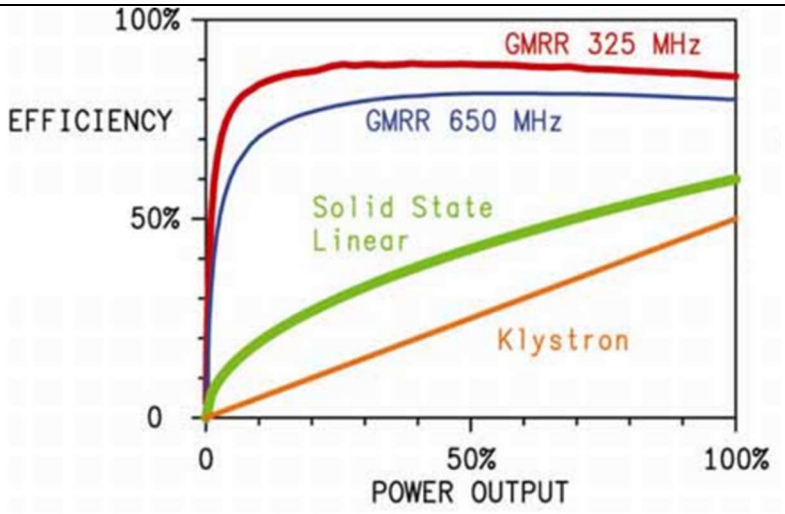

Figure 46. **Efficiency versus the output power for the SSA based on modern GMRR technology [99].**

In **Figure 45**, for accelerators at 400 kW average power, the SRF option still has the highest efficiency. The 5% duty factor IMPELA option, which has the second highest efficiency, needs 8.5 MW of pulsed power at >400 kW average power. Such a power supply is not available form industry currently. The other 3 RT linac options have about the same efficiency. Considering available RF sources, one may exclude the low duty factor IMPELA option, and count on other RT accelerators which may provide efficiency of ~40% compared to the SRF option efficiency of ~80%.

Also noteworthy is the fact that the Rhodotron based on conical HWRs and state-of-the art SSA power supplies may provide up to 65% wall plug efficiency, but R&D is necessary. The Rhodotron, which is much more compact than the high duty factor IMPELA and ILU-14 options, is the most preferable option before SRF technology appears on the market. High power options of the Rhodotron are currently available on the market, which make it even preferable now. With improvement to the optics and potentially increasing the injection energy the Rhodotron can potentially make 1 MW of power. However, the SRF may provide much higher efficiency for the power level of up to 1 MW. The results of all the accelerators examined for efficiency are summarized in the **Table yyy2**.

Summary of accelerator comparison work

In **Table 15** it is shown that the SRF accelerator is the best option for 10 MeV, high power (>100 kW) operations. As the power increases so does the energy efficiency so more powerful machines are preferred. At 400 kW of power on the order of a 15% increase in efficiency may be had in going from a klystron power supply to a magnetron. Magnetrons may need to be developed for a specific required power, frequency, and duty factor. While SRF accelerators are the most energy efficient, they are still on the pathway to being commercially available. Rhodotrons are available on the market today and are the most efficient of currently available technologies. For the purposes of the rest of the study and report the SRF and Rhodotron technologies are evaluated and compared to conventional water treatment technologies like GAC for treatment of PFAS in water. The other accelerator technologies evaluated have low efficiencies or are not technically feasible (or both).

Table 15. Wall-plug efficiency of the industrial accelerators for 100 kW and 400 kW of the beam power.

Power, kW	SRF magnetron	SRF	IMPELA 0.05DF	IMPELA 0.2 DF	Rhodotron Moden SSA	Rhodotron	ILU-14
100	65	40	25	20	35	25	20
400	80	65	N/A	40	65	40	40

Y2: Task 2 – Technical Evaluation and Cost Analysis of E-beam Technologies

As the SRF system examined in the previous section had the highest energy efficiency a complete preliminary technical design will be developed based on Fermilab exiting technologies to the point a cost to construct analysis can be done. This information will be used to compare to the currently commercially available Rhodotron costs. And finally, the accelerator technologies will be compared to GAC water treatment systems for PFAS. One of the biggest drivers of accelerator cost and efficiency is the RF power supply technology and it will be discussed first.

Cost estimate for the RF system.

The major cost of the accelerator system is based on the RF power source. As demonstrated in previous calculations, each accelerator system requires different RF power sources. Because the cost of RF power supply generally grows linearly with the RF power, the RF power source cost is generally measured in $/W. The $/W number includes the power supply and associated cooling system for the RF station. The key features of the RF system are efficiency, longevity, and footprint. The three relevant power supplies Klystron, traditional SSA and magnetron will be analyzed.

Klystrons:

The klystrons are the only choice available for the IMPELA and ILU-14 accelerator systems. They are the only RF system providing peak power requirements with a reasonable footprint. The Klystron's cost estimation here is based on a 2015 quote for a large high energy physics project (the XFEL at DESY in Hamburg, Germany). The inflation and exchange rate are combined to a 1.5 adjustment factor. **Table 16** below shows the cost of different klystron systems from the 2015 quotes. For pulse mode operation of the IMPELA and ILU-14, high power modulators and pulsed transformers are needed. The 2015 quote includes the cost of the modulators and pulsed transformers. The cost of such a modulator and pulsed transformer is $2M on top of the RF station. This negatively effects the usefulness of this type of accelerator and RF power supply combination. The klystron generally has a design efficiency of around 65%. For the 5% DF IMPELA accelerator, much higher peak power is required, such as provided by the CPI VKL7796. The klystrons that satisfy such low DF and high peak power only have efficiency of around 40%. Because of the low efficiency of the high peak power klystron at 1.3 GHz frequency, the 5% DF IMPELA shows no advantage in efficiency. Because the 5% DF IMPELA option is less efficient and costs more (need higher power klystron and larger modulator and pulsed power transformer), further cost analysis is not conducted for this option. The CPI VKL7796 cost was not quoted.

The footprint of a high-power klystron is generally on the order of 1m×1m×2m. **Figure 47** shows a typical high-power klystron. **Figure 48** shows a typical HV modulator necessary for pulsed accelerator operation. **Figure 49**

shows a dimension of a typical pulsed power transformer. The modulator and pulsed transformer require extra 2m×1m×2m space.

Figure 47. VKP-7958A 1MW CW 700 MHz Klystron for DESY[100]

Figure 48. HV modulator[101]

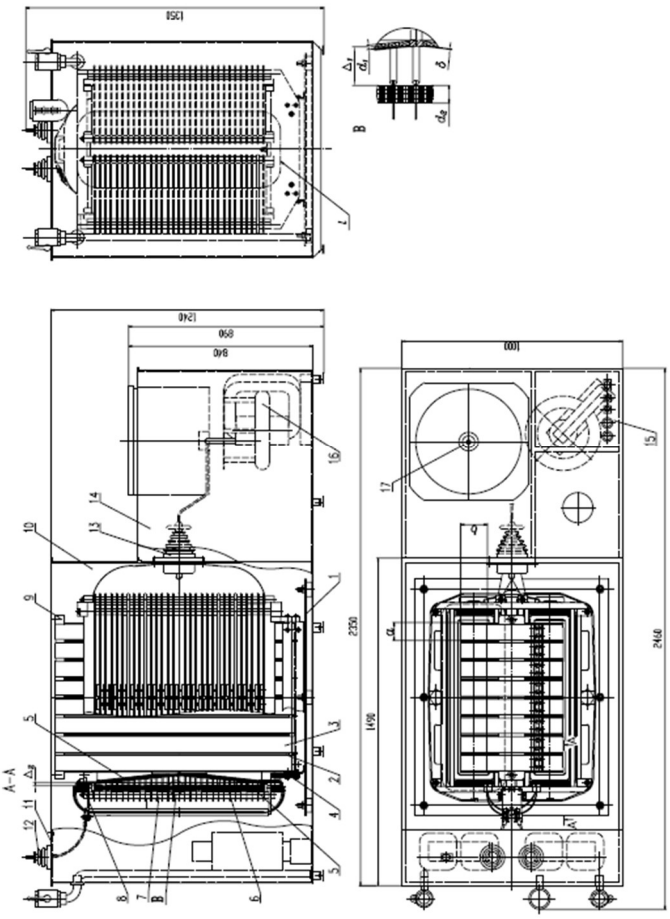

Figure 49. **Pulse Transformer design.**[102]

Table 16. Quoted price for the Klystron based on XFEL project.

Klystron	Power, kW	Cost 2015, M€	Cost 2023, M$	Cost 2023, $/W
E3736H	150	0.55-0.65	0.83-0.98	5.5-6.5
TH1802	150	0.7-0.8	1.05-1.2	7-8
VKL-8301	150	1.1	1.65	11
TH 2104C	75	0.3-0.4	0.45-0.6	6-8
Modulator				
AMPEGON	N/A	1	1.5	N/A
PPT		1	1.5	
Pulsed Transformer				
ABB	N/A	0.25-0.35	0.38-0.53	

SSA:

The SSAs are a suitable choice for CW operation only. They are widely available in the broadcasting industry. SSA was quoted from R&K. The quoted price is available in **Table 17**.

Table 17. Quoted price for the SSA from R&K Company Limited[103].

R&K 1.3 GHz	Cost, K$	Cost $/W
20kW	290	14.5
16kW	250	15.6
8kW	135	16.9

Also based on conversions with SSA supplier Gatesair[104], a majority of the commercial SSA designs don't consider efficiency a top priority. In consequence, most of the available SSA efficiency are in the 40-45% range. By minor improvement, the efficiencies of current SSAs are expected in the 40-50% range. Though, SSA technology is underdeveloped, potentially future SSAs could reach 70-80% efficiency[99]. **Figure 50** is a Gatesair Maxiva™ ULXTE 30kW transmitter, and the rack is about 1m×.5m×2m. The footprint of the SSA grows linearly with power. A 100 kW SSA station will consume 4 racks shown in **Figure 50**. A 400 kW SSA station will consume 16 racks.

Figure 50. **Gatesair Maxiva™ ULXTE 30kW transmitter**

Magnetrons:

Magnetrons are a choice viable for CW operation at L-band frequency, so only the SRF accelerator can utilize magnetrons[96,105]. The magnetron is the most efficient RF power source currently available for the accelerators discussed. The 100kW L-band magnetron tube at 896, 915, 922, 929 MHz is listed at 12,000$ online at Mega Industries[106]. A magnetron requires tubes that typically have a life span that is 3000-8000 hours. A magnetron tube change is required at each failure. To compare cost, 11 magnetron tubes are included to achieve a similar life span of the Klystron and SSA. While some Klystrons have been evidenced to last over 100,000 hours, under industrial use conditions it is likely the lifetime will be decreased. The magnetron cost is the lowest at 1-2 $/W[97].

Table 18 shows a summary of all 3 RF power supply choices. The magnetron is shown to be the most cost effective by far as well as the most energy efficient. Unfortunately, magnetrons may need further development for the power, duty factor and frequency of the accelerators detailed. Magnetrons also have bulbs that must be changed periodically. Klystrons are the next most cost effective but have associated ancillary equipment that is expensive and large. The SSAs are the most expensive but are modular and have the potential with development to increase their efficiency significantly.

Table 18. RF power source comparison

	Cost $/W	Longevity hours	Efficiency %	Footprint m	Suitable accelerator system	availability	Other cost
Klystron	7-10	>40000	45-65	1×1×2 extra 1×2×2 cabinet for Modulator and PPT	All systems	Commercially available	Modulator and PPT 3M
SSA	15-20	>40000	40-50	1×2×5	Rhodotron SRF	Commercially available	none
Modern SSA			70-80		Rhodotron SRF	R&D required	none
magnetron	1-2	<8000	>80	.5×.5×1	SRF	R&D required	none

SRF compact accelerator design for cost analysis

With RF power supply costs detailed the cost of the overall most efficient accelerator, Fermilab's compact SRF accelerator is detailed. The Nb_3Sn-coated superconducting radiofrequency (SRF) cavity can deliver extremely high rf to beam efficiency (> 90%) at 4K[96]. The 4K operating temperature for the *Nb_3Sn* SRF cavity enabled conduction-cooling technology. A 10 *W/m* conduction-cool 650Mhz SRF cavity was demonstrated at Fermilab IARC[91]. These technologies enabled the utilization of SRF technology without cumbersome and large liquid Helium plants. As demonstrated in the efficiency analysis, the SRF technology-based accelerator outperforms the room-temperature accelerators by a large margin. At the same time, because of the high accelerating gradient achieved by the SRF cavity (10 W/m), the SRF accelerator could be much more compact.

The IARC at Fermilab has been developing a higher-power mid-energy compact SRF linac[96]. The conceptual design of a 650Mhz, 10MeV, 1MW linac was done for water treatment. The accelerator presented herein is based and expanded on from this work. Though this study focuses on 100kW and 400kW beams, it is logical to design the accelerator power as high as possible when concerned about energy efficiency. The higher power leads to better accelerator efficiency. Also, increasing accelerator power mainly consists of increasing the cost of the RF power source. The cost increment of other accelerator components from 100kW to 1MW is relatively small. Therefore, the 100kW and 400kW accelerators are achieved by scaling down the RF power source. The accelerator design in this project is incentivized by the 1 MW design. The SRF accelerator discussed in the accelerator efficiency sections above was a Fermilab design of a 1.3 GHz accelerator because this

compared more directly with the other RT accelerators at 1.3 GHz. The 650 MHz design that is discussed in this section is in fact more energy efficient than the 1.3 GHz design at 10 MeV and high power.

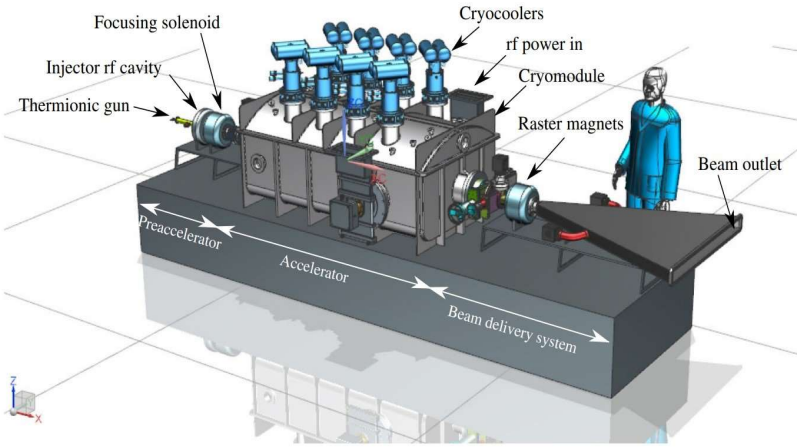

Figure 51. **Accelerator layout of the SRF compact accelerator with general beam delivery system.**

The overall layout of the SRF compact accelerator is shown in **Figure 51**. The pre-accelerator system consists of a room temperature electron source. The accelerator is a conduction-cooled accelerating structure, which operates under cryogenic temperature (around 4 K). The beam delivery system operates under room temperature and shapes the beam spot to the desired form and delivers the beam to the water flow.

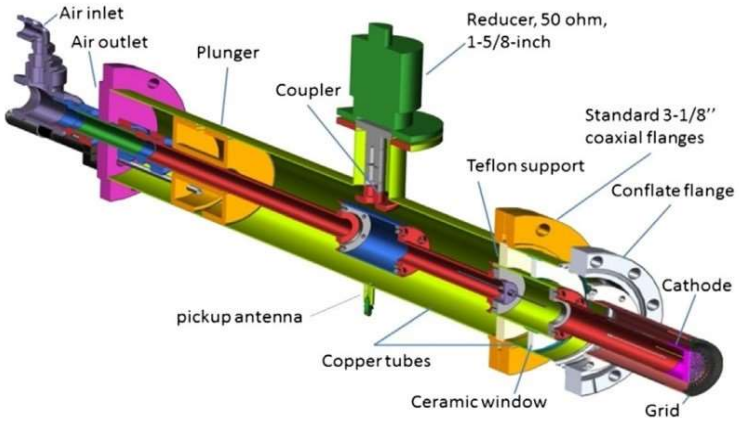

Figure 52. **The RF gun components.**

Based on operational experience, RF guns based on thermionic cathodes are cost-effective, simple, and reliable electron sources[107]. The thermionic cathodes generate electrons. The RF gun provides the initial boost to the electron beam. **Figure 52** is the RF gun design. The design parameters are listed in **Table 19**.

Table 19. **RF gun design parameters**

Gun Parameters	Value
Cathode Diameter	12.7 *mm*
Current Density	2.35 A/cm^2
Cathode Temperature	950-1200 C°
DC Bias Voltage	2.6 *kV*
Output Energy	3.5 *keV*
Bunch RMS Size	<15°
Energy RMS Size	<25%

The RF gun generates up to a 100 mA electron beam at 3.5 keV. To maximize beam capture, the beam must be accelerated to $\beta = 1$ before injecting into the SRF cavity. The injector cavity accelerates the electron beam to 300 keV. **Figure 53** shows the injector cavity design. **Table 20** shows the injector design parameters.

Table 20. The injector cavity design parameters

Dimension	Value	RF parameters	Value
φ_{cavity}	308 mm	Vout	300 kV
$\varphi_{aperture}$	35 mm	R/Q	178 Ω
R_1	20 mm	Q_0	19000
R_2	24 mm	Rshunt	3.4 MΩ
Lgap	29.6 mm	RF loss	11.6 kW
Lcavity	68.2 mm	Es,max	14.5 MV/m

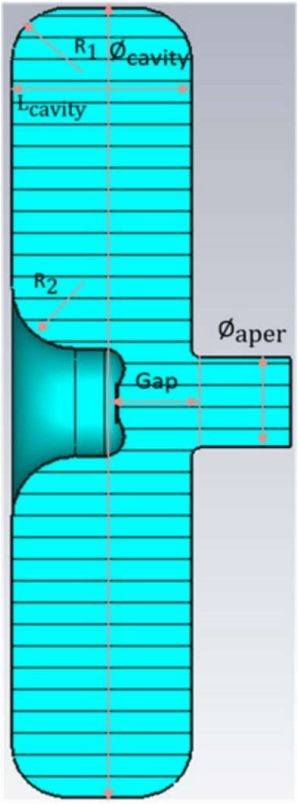

Figure 53. **The injector cavity design[96].**

The beam must be focused to match the SRF cavity's transverse optics. A solenoid is implemented between the injector and SRF cavities to focus the beam. The focusing solenoid needs to provide proper focusing, be compact, and produce a minimum remnant magnetic field to avoid reducing the Q_0 in the SRF cavity. The focusing solenoid design parameters are shown in **Table 21.**

Table 21. **Parameters of the focusing solenoid at the SRF cavity inlet.**

Solenoid Parameters	Value
Coil ID/OD	50/120mm
Coil length	90 mm
Peak field on the axis	0.025 T
Current density	0.4 A/mm^2
Focusing strength	6×10^{-5} T^{2}m

The pre-accelerator section for the compact SRF accelerator system up to the focusing solenoid has now been detailed. The main accelerator portion of the system is sealed inside the cryostat and kept under cryogenic temperature for superconducting operation. **Figure 54** demonstrates the cryostat design. The cryomodule utilizes eight two-stage cryocoolers (**Figure 54** shows half of the cryomodule) and a single-layer thermal and magnetic shield. The thermal shield is connected to the 50 K cooling stage. The thermal and magnetic shield insulates ambient thermal radiations and intercepts heat transmitted through the RF couplers and the beamline ports. The cryocooler, a Cryomech PT420, which offers a 2.0 W cooling capacity at 4.2K, is used to cool the main bulk of the SRF cavity. The Cryomech PT425, which offers a 2.5 W cooling capacity at 4.2K, enhances the cooling capacity for the RF couplers. The RF couplers are one of the biggest sources of heat generation in the accelerator.

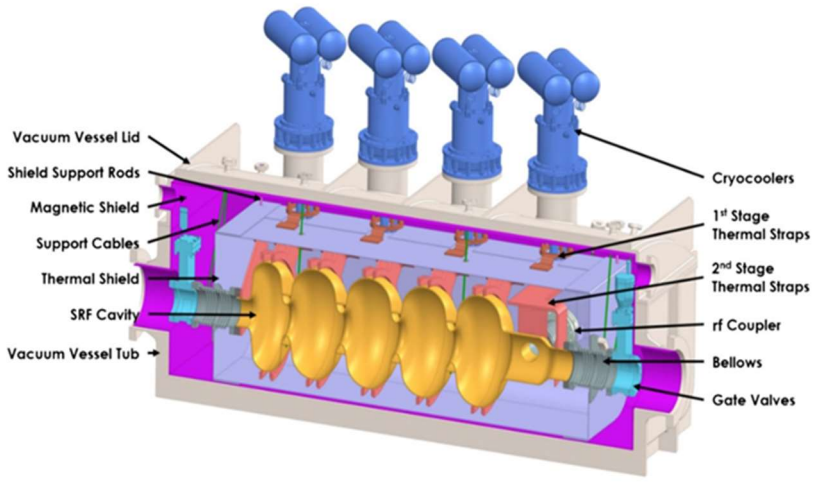

Figure 54. **Cross-section of the cryostats.**

Figure 55 demonstrates the cavity design for the accelerator. The five-cell cavity has the first cell smaller to compensate for the low β of the injected electron beam. The last cell is larger than cells 2, 3, and 4 to out-propagate higher order modes and achieve high cavity coupling. The design parameters are listed in **Table 22**.

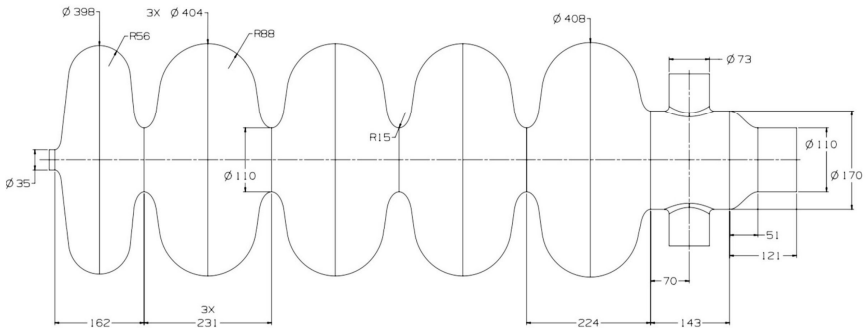

Figure 55. The SRF cavity dimension with coupler port. All measurements are in mm[96].

Table 22. Design parameters for the 650 MHz 5-cell cavity[96].

Cavity Parameters	Value
Normalized shunt impedance *R/Q*	634 Ω
Geometry factor *G*	262 Ω
Dissipated power P_{diss} at 10 MeV	$0.6R_s$ [nΩ] W
Peak surface electric field $E_{s,peak}$	17.5 MV/m
Peak surface magnetic field $B_{s,peak}$	36.5 mT

To feed 100 kW(or 400 kW) of RF power into the SRF cavity, the RF coupler is necessary. The RF coupler penetrates from the air to high vacuum and from room temperature to the cryotemperature. The RF coupler design is shown in **Figure 56**.

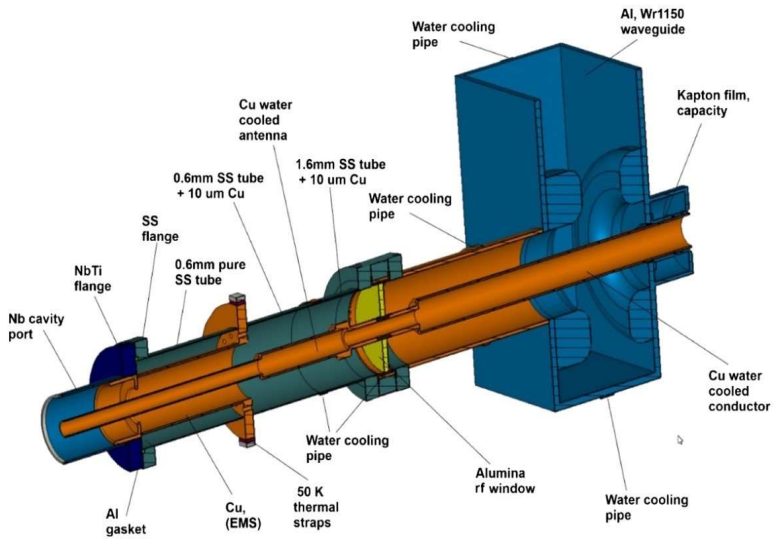

Figure 56. Cut view of the coupler configuration.

The coupler design for this project is motivated by the coupler design for the 650 Mhz PIP-II SRF cavities[108]. The coupler can deliver 500 kW CW power with 10% reflection. A water-cooled copper rod extends into the niobium cavity delivering the RF power. A ceramic window is used to isolate air from the vacuum. The coupler uses a copper electromagnetic shield (EMS) heat sink at the 50 K stage. The EMS has no physical contact with the 4 k SRF cavity. **Figure 57** demonstrates the components and the temperature map at stead-state.

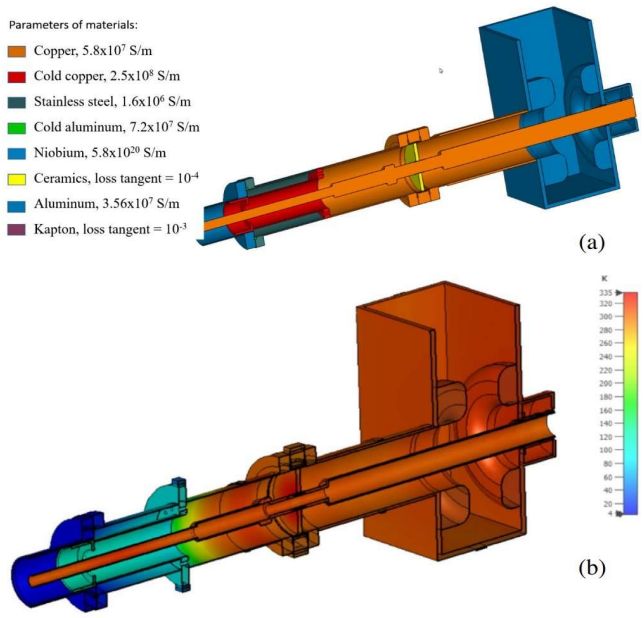

Figure 57. Thermal performance of the coupler at 500 kW. (a) Geometry and material properties and (b) steady state temperature map[96].

Based on the coupler design, the heat load of the 500-kW coupler is calculated. **Table 23** shows the calculated heat load. The conduction heat leak is calculated to be 0.6 W. There are additional heat leaks from the EMS and antenna tip to the 4 K SRF cavity. Based on the heat map from **Figure 57**, the leak is calculated to be 0.55 W. The coupler is expected to have a 1.2 W heat load at the 4K stage.

Table 23. Power loss for the coupler at 500 kW forward propagation and 10% reflection[96].

Component	Loss [W]	Cooling method
Outer Conductor and	0.6	4K stage
flange to cavity port AL gasket at the cavity port	1.5×10^{-3}	
EMS	31.5	50K stage
out conductor (vacuum side), upstream of 50 K stage	29.5	
Antenna	570	cooling water 300 K
Ceramic disk	43	
Kapton	5.5	
Outer conductor (air side)	44	
AL waveguide	255	

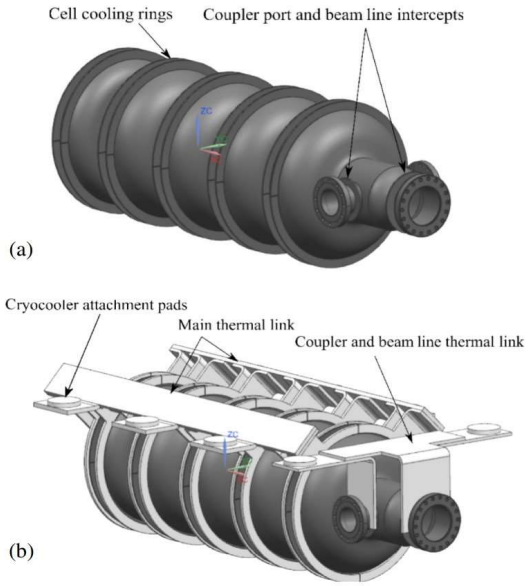

Figure 58. **The SRF cavity with the thermal link. (a) The five SRF cavities with the welded cooling ring. (b) Thermal link attached to the five cavities with bolts. For 1 MW operation, 14 W heat load is on the Main thermal Link and 6.3 W heat load is on the coupler and beam line thermal link.**

The cryomodule heat load is calculated with the RF coupler's heat load. **Figure 58** demonstrates the SRF cavities with the thermal links. **Figure 58 (b)** separates the cooling section into the cavity section and couple sections. The cavity section cools the SRF cavity. The coupler section cools the coupler and outlet beampipe.

The major heat loads for the main cooling section are from RF loss, beam loss, and conduction through the support and beam inlet. The major heat load is calculated in **Table 24**. A 20 *n*Ω surface resistance and 10 MeV beam energy are assumed for the RF loss. Based on the RF dissipated power equation and using values from Table 22, <12.5 W of the RF power is lost through the cavity. Based on an estimation from a previous study, 1W (1 ppm of average beam power) is assumed for beam loss. With heat load from conduction, there is a total of >14 W heat load on the main cooling section. The 6 PT420 cryocoolers provide 14.3 W of cooling power at 4.45 K for the main cooling section. The major heat loads for the coupler/beamline section are the heat load through the couplers and conduction and radiation through the outlet beam pipe. Rather than using the 1.2 W heat load at 4K for the coupler, we use a conservative 3 W heat load for the 500-kW coupler based on operations at Brookhaven National Laboratory. Therefore, the total heat load for the 1 MW operation is 6 W from the two couplers. With conduction and radiation through the outlet beampipe, there is a < 6.3 W heat load on the coupler/beamline section. The 2 PT425 cryocooler provides a 6.5 W cooling capacity at 4.6 K.

Table 24. Calculated heat load on the 5-cell cavity at cryostases for 1 MW operation.

Component	Heat load	Loss [W]	Cooling method
Cavity Body	RF dissipation @ 10 MeV and R_s = 20 nΩ	12.5	
	Radiation from thermal shield	0.05	
	Beam loss (taken as 1 ppm of average beam power [18])	1	
Cavity Inlet	Conduction through supports	0.1	
	Conduction through inlet beampipe	0.05	
	Radiation from inlet port [20]	0.24	
Cavity body + Inlet	**Heat load on main thermal link in figure 21b**	**14**	6x Cryomech PT420, cooling capacity 14.3 W @ 4.45 K
Cavity outlet	Couplers [21]	6	
	Conduction through outlet beampipe	0.05	
	Radiation through outlet beampipe [20]	0.04	
Cavity outlet	**Heat load on coupler and beamline thermal link in figure 21b**	**6.3**	2x Cryomech PT425 cryocoolers, cooling capacity 6.5 W @ 4.6 K

For lower powers, the 100 kW to 400 kW operation discussed herein, the RF dissipation will be the same, beam loss will scale linearly with beam power and one coupler could be removed. So, for 100 kW to 400 kW operation, the Cavity heat load will be reduced to 13 W and the couple heat lead will be reduced to 3.3 W.

SRF compact accelerator cost analysis

The cost breakdown of the full accelerator system is listed in **Table 25**. The cost analysis is largely based on past research at Fermilab. The 650 MHz. 1 MW SRF accelerator is designed to deliver 1 MW beam power. The cost analysis calculates the cost based on 100 kW and 400 kW operations. The major cost reduction from reducing 1 MW beam power to 100/400 kW is from the RF sources. The total cost of a 100-kW system is $5M. Increasing the accelerator power to 400 kW will cost $5.7m. The analysis assumed a functional magnetron. If Klystron or SSA powers the accelerator system, the cost will be closer to $7m.

Table 25. Capital cost of the 100 kW and 400 kW, 10 MeV SRF accelerator system [96,109].

Item	Cost [k$]
Electron injector	976.75
Beam delivery system	504.4
100 and 400 kW RF power source (magnetron)	230 / 920
Cryomodule	1554
Power coupler	282
Cryocoolers with HE compressors	492
650 Mhz Nb_3Sn SRF Cavity	402
BPM system	44.5
Vacuum vessel	100
Beamline (bellows, valves)	104
Auxillary hardware (Chillers, pumps)	93
Magnetic shield	65
Thermal Shield	16
Interlocks	175
Total (100/400 kW magnetron)	**5038.65 / 5728.65**

For the design of the SRF cavity both 1.3 GHz and 650 MHz were examined as these are both used at Fermi. The major difference between the two cavities is in physical size. The 1.3 GHz cavities is about 1/3 the size of the 650 MHz cavities. Though the compactness of the 1.3 GHz cavity will bring some advantages, it is harder to control and less efficient. Use of 650 MHz over 1.3 GHz brings 3 major advantages.

1) The 650 MHz cavity losses are 1.2-1.3 times lower than the 1.3 GHz cavity, which translates to 1-2 less cryocoolers for the application. The *R/Q* of the 650 MHz cavity is 634 Ω (**Table 22**) and the *R/Q* of the 1.3 GHz cavity is 1030 Ω. The loss is proportional to *R/Q*, thus the 1.3 GHz cavity will have 1.2-1.3 times more loss. The 1.2-1.3 times more RF power loss will lead to the 1-2 extra cryocoolers.

2) The larger aperture of the 650 MHz cavities leads to less fatal current intersection. The current intersection is caused by beam loss. In the heat load calculation, 1ppm beam loss is assumed and will cause 1 W extra heat load on the cryocoolers. Every watt of beam loss requires an extra cryocooler. The current intersection will be reduced by larger cavity aperture of the 650 MHz cavities.

3) The 650 MHz cavity will allow lower injection energy, which leads to less expensive and more reliable injectors. The first cavity of the SRF cavities must be designed for non-relativistic energy. The larger aperture of the 650 MHz cavity is easier to modify for this operation and can potentially handle lower injection energy.

Beam Delivery System

Once the beam is accelerated through the cavity it exits the vacuum of the accelerator through a window made from titanium or beryllium. The beam is shaped by magnets to a desired shape to hit the target, in this case

water. **Figure 59** below shows the penetration depth of the electron in water based on the energy of the electron. At 10 MeV energy, which is the case for all the accelerators discussed thus far, the variation in energy through the top 3 cm of water is 20 percent. Designing a delivery system that minimizes variation in dose seen by the water and utilizes all the incoming power is important.

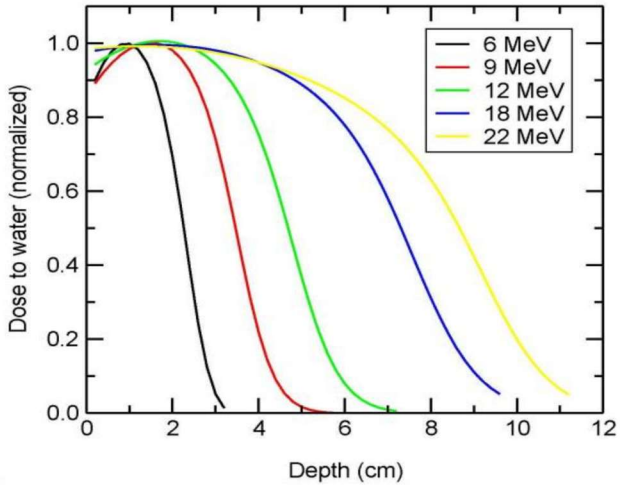

Figure 59. **Energy Deposition of Electrons in Water Based on the Energy of the Electron.**

An example of how an electron beam accelerator is used to treat water that has dye in it from a textile manufacturing facility is shown below in **Figure 60**. The electron beam comes down from the top of the picture into flowing water that has a controlled thickness to make sure a minimum dose is applied to all parts of the water.

Figure 60. Picture of the electron beam accelerator and water interaction area for an industrial accelerator.

While **Figure 60** shows an example of one type of beam delivery system, **Figure 61** shows five different contact schemes. Scheme 1 is the same as in **Figure 60.** Scheme 2 has an electron beam from both side of the water flow. This minimizes energy variation but has potential problems in implementation such as energy losses incurred from splitting the beam. Scheme 3 is in a closed square pipe which completely encloses the flow which prevents any flow from escaping but would incur energy loses in the electrons going through the wall of the pipe or a window in the pipe. Scheme 4 is water flowing out of a pipe and the electron beam directly going into the pipe. If the flow is low enough flow profile across the pipe is not too pronounced such as in laminar flow, this could be a viable option. Scheme 5 is where an electron beam goes into a continuously stirred tank reactor (CSTR) that

has a recycle line. This scheme has many advantages such as all the beam energy being utilized and the fact that CSTRs are well defined industrial tools.

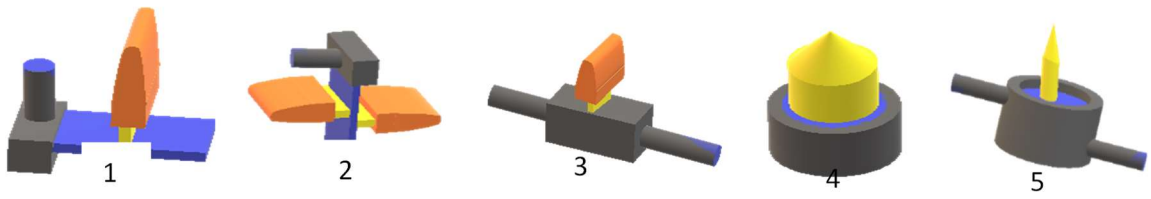

Figure 61. Possible alternate designs for beam delivery systems

Unfortunately, there was not sufficient time and resources to model these different flow schemes for EB treatment. For flow scheme 1 in **Figure 61**, the scan horn and sweeping magnets (shown in **Figure 62**) are viable for creating the proper electron field for contacting a flowing water stream beneath. Preliminary work on this was done at FNAL for a municipal water treatment system [110].

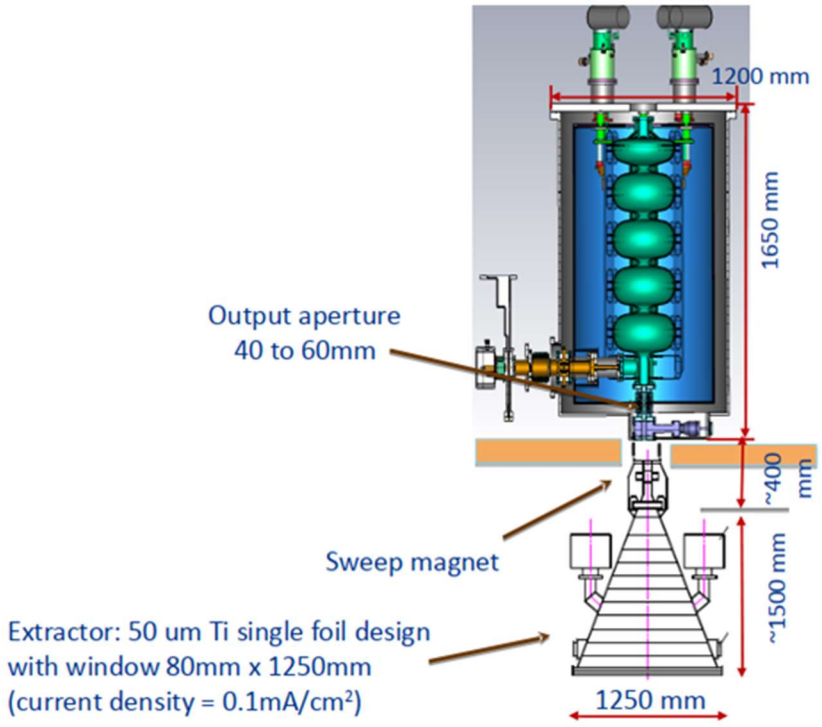

Figure 62. Example of a beam delivery system for the 650 MHz SRF accelerator.

Rhodotron Cost

Based on a quote from IBA, the 300 kW 10 MeV Rhodotron system costs 8.6 million dollars (7.89 euros from the quote). The Rhodotron delivered time is currently two years from ordering. The IBA quote includes the following components:

- The Rhodotron accelerator with 300 kW RF power supply.
- A generic beam delivery system.
- Safety system including radiation detectors for the Rhodotron Vault
- Two free PM and emergency service visits during the first year after installation

The Rhodotron accelerator system is the most viable commercially available high-power normal conducting e-beam accelerator system. It has the highest efficiency between of the normal conducting options.

Other General Information

Regulatory requirements for shielded electron beam accelerators depend on where operation takes place. It varies from state to state in the US and varies from country to country outside the US. In general, the regulatory process is uncomplicated and inexpensive. The regulatory requirements often require licensing and permitting, with prices seen in the 100s of dollars range. Permitting can involve radiation safety, environmental protection and occupational safety and health. Nothing was seen that would be considered too unreasonably expensive or difficult.

All the technologies discussed here are currently available in the market except what is mentioned here. SSA power supplies are currently available at high powers with efficiencies of 40-45% and that is what was used in the study. There is proof of principle of much higher efficiency at low powers. The timeline or possibility for delivering high power high efficiency SSA power is unknown as it is at an early stage. SRF technology is well developed and can be built today if liquid helium is used to cool the accelerator convectively. This is typically cost prohibitive though. The SRF compact accelerator technology that is presented herein which relies on conduction cooling has been demonstrated for a single cell cavity only. Prototypes are being built for the full power, multicell, 1.3 GHz and 650 MHZ compact SRF accelerators now. Time to market for these accelerators is money and demand specific and would require a dedicated study to give a realistic number, but on the current trajectory 5-10 years is plausible. High power, high duty factor magnetrons are assumed for SRF accelerator efficiency gains. 100 kW 1.3 GHz technology has already been demonstrated[111]. Getting these to market is a matter of money and demand as well but is much more straightforward and could possibly be done in 2-3 years.

Y2: Task 3 – Review Panel & Recommendations

Multiple subject matter experts from Fermilab with a combined experience of 7 to 8 decades on accelerator design, construction, commissioning, and operations reviewed the electron beam accelerator sections of the project. Technical expertise was heavy on RF power which is a major component of accelerator operating and capital costs. Beyond comments on writing style or some minor issues the following content was adjusted. To improve accuracy on content relating to Rhodotrons, IBA was contacted, a series of meetings held, and a quote acquired detailing costs and delivery times. There was a comment on the lifetime of klystrons, stating that they can last to over 100k hours while in the report a lifetime half of that was assumed. The

content was adjusted to acknowledge the fact that while Klystrons can last that long that under industrial operating conditions the lifetime is expected to be less. The final substantive comment that required additional modification of the report was about some assumptions regarding putting hardware in the radiation enclosure. The assumption was that there are no losses in the line from the source to the accelerator. This means that the source is close, but not necessarily in the accelerator enclosure. The source could be in the accelerator enclosure, but this would incur additional capital costs and maintenance issues. Comments were added to address this.

Y2: Task 4 – Final Report (White Paper)

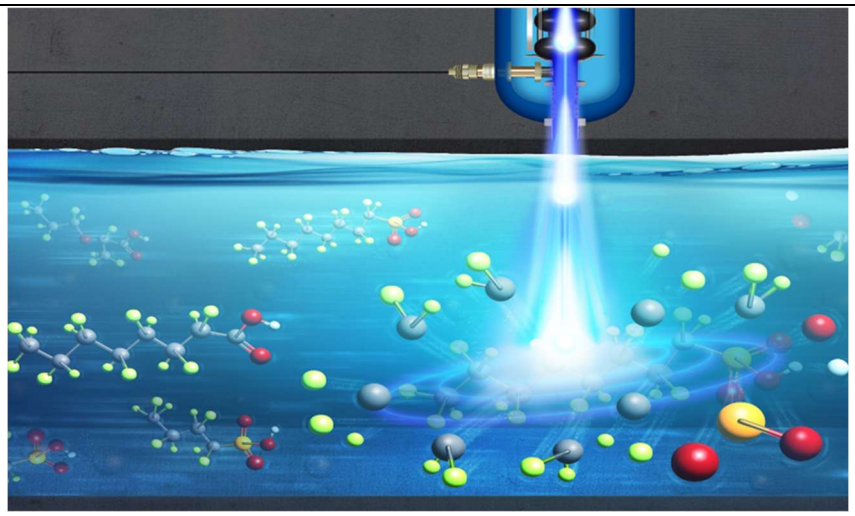

Figure 63. Schematic Representation of PFAS Being Destroyed by Electron Beam

Within the scope of the work of this project it was found that EB accelerators can completely destroy the PFAS compounds PFOA and PFOS. A simple representation of this is seen in the **Figure 63** above. While the exact degradation mechanism is not clear, it was apparent that the aqueous electrons created in the radiolysis of water played a major role since conditions that favor aqueous electron enhanced the PFAS breakdown. Degradation efficiency increased with increasing pH, decreased dissolved oxygen, and decreased dose rate. These conditions all increase aqueous electron availability. The rate limiting step of the degradation process is thought to be diffusion of the aqueous electron to the appropriate spot on the PFAS molecule. During the study it was found that increased temperature increases degradation efficiency, likely due to increased molecular motion, but this information was not used in energy efficiency and cost calculations. Degradation of PFOS appeared to initiate at the middle of the fluorocarbon chain and possibly near the head group with few short chain byproducts found. Degradation of PFOA molecule appeared to happen primarily by removal of the carboxylic acid head group as a first step. Under optimized conditions in the study, short chain byproducts of PFOA and PFOS were largely absent, but under suboptimal conditions there were trace amounts of the shorter chain byproducts formed.

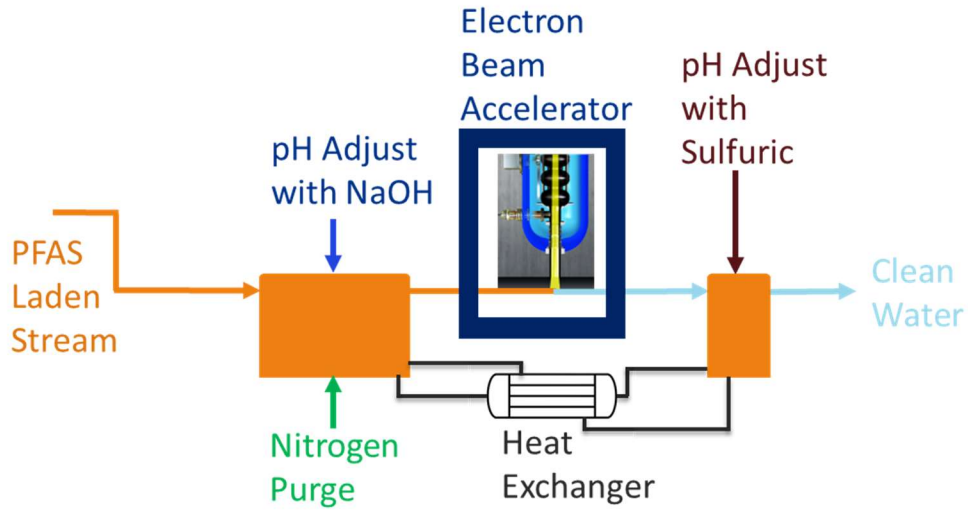

Figure 64. Simple schematic of the Electron Beam Accelerator in a Water Treatment System

Figure 64 above shows a simple schematic of the proposed electron beam water treatment skid. The nitrogen purge, pH adjustment and heat exchanger all boost degradation efficiency and reduce energy costs but do increase financial costs. Because of the relatively high number of aqueous electrons created, the process greatly favors destruction of concentrated PFA streams in the range of 1 ppm and higher. This concentration range is higher than most water contamination levels, so the application of electron beam would be greatly enhanced for most water treatment application using preconcentration steps like reverse osmosis or ion exchange. The cost of sequestering PFAS via granular activated carbon (GAC) and EB accelerators were compared. Two EB systems were examined closely and were a commercially available Rhodotron accelerator and an SRF accelerator under development at Fermilab. Direct comparison is very difficult, but the estimated 2022 capital cost was $3.3 M for GAC, $8.6 M for the Rhodotron, and $7.8 M and $5.5 M for two different versions of the Fermi accelerator. Capital cost was identified as a significant barrier to implementation of the EB technology. The Rhodotron EB systems currently are produced by the primary manufacturer, ABI, on the order of 20-30 per year. With economies of scale, it may be possible to manufacture greater numbers at some reduced cost. The manufacturer was unable to share specific information on this so an independent investigation of this would have to be done. Similarly, the costs estimated for the Fermilab accelerators are for prototypes and could be reduced substantially if manufactured at scale.

Operating cost comparison between EB and GAC is affected by PFAS concentration. At 10 ppm (removed to 4 ppt) the cost per mass of PFOA and PFOS destroyed ranges from $1,200 (Fermilab SRF) to $2,100 (Rhodotron) per kilogram for the accelerator technologies above. At 1 ppm PFOA or PFOS the cost increased to $11,900 (Fermi) to $21,600 (Rhodotron) per kilogram. The GAC system that was analyzed removed (not destroyed) PFAS for a cost of roughly $27,530 per kilogram. So, when operating costs are compared by mass of PFAS removed, the EB technology is advantageous at concentrations starting at 1 ppm. At 10 ppm PFOA and/or PFOS the cost per gallon of water treated ranged from 4.4 to 8.7 cents/gal (Fermilab SRF) to 7.9 to 15.4 cents/gal Rhodotron) for the accelerator technologies. At 1 ppm PFOA and/or PFOS (removed to 4 ppt) the cost ranged from 3.7 to 7.4 cents/gal (Fermilab SRF) to 6.8 to 13.5 cents/gal (Rhodotron) for the accelerator technologies. The operating cost to sequester PFAS from water was found to be 0.93 cents per gallon for the GAC system studied herein.

These combined results suggest that while e-beam can be used to treat low concentration PFAS in water it is more cost and energy efficient to treat PFAS at concentrations of 1 ppm and higher. The higher capital cost of EB systems is a barrier to the technology. This could be overcome by reduction in costs in manufacturing related to increasing quantities made. Fermilab's novel accelerator may also offer a more economically friendly option for capital and operating costs. In addition to the cost barrier a second barrier to electron beam technology adoption for PFAS destruction is lack of familiarity with the technology. Lack of sufficient data on pilot scale testing with a flowing waste stream is also a barrier to the technology. A proof of principle pilot scale demonstration would be paramount for any chance in adoption of the technology.

In terms of risks associated with EB destruction of PFAS, EB technology is proven, the Fermilab technology which is not fully proven would add benefits in terms of costs and flowrates that can be treated. Based on the results of the work herein there doesn't appear to be any major risk with the technology. With the application of the technology there is a potential risk with the exact composition of the water. Electron beams can treat water that is turbid, and biofouling is not an issue, both of which are problems with conventional water treatment technologies. However, some water may have other constituents that may consume some of the aqueous electrons that would otherwise go towards degradation of the PFAS thus making the process less energy efficient and more costly.

Electron beam treatment of water is a promising technology that not only can destroy PFAS but can also destroy a wide range of other recalcitrant chemicals of concern and provides a biocidal function that eliminates biofoulants and can kill microbial pathogens. Further development of the technology is important for addressing contaminants of emerging concern today and the future. An obvious next step in this work is to demonstrate the technology on a larger scale. Although EB technology has been implemented at industrial scale for other technologies and used to treat water outside the US for applications like removing dye in textile wastewater, none are currently used or available for testing in the US. Also, because diffusion was identified as a rate limiting step, some form of mixing technologies should be examined to help reduce the average diffusion path length needed for the aqueous electrons to travel to the dissolved PFAS molecules.

Conclusions and Recommendations

PFAS are a broad class of specialty chemicals used in a variety of applications [4]. PFAS are thermally and chemically stable due to the highly electronegative fluorine atom which induces a strong dipole moment in C-F bonds. The C-F bond is regarded as one of the strongest bonds in organic chemistry with a bond dissociation energy of up to 130 kcal/mol. Furthermore, the C-C bond in perfluorocarbon molecules becomes strengthened due to an electron inductive effect when multiple perfluorinated carbons are in series. Fluorine is also larger than a hydrogen atom but has an unusually short bond length which causes it to pack tightly around the carbon, thus shielding it from nucleophilic attack. As a result, PFAS have unique properties different from their hydrocarbon counterparts that allow them to be used in extreme thermal and chemical environments, or where combined oleophobic (oil resistant) and hydrophobic properties are desired. While the novel properties and unusual stability of PFAS provide for their many uses, the unintended consequence is that they can be resistant to normal degradation in the environment.

Some PFAS are classified as persistent organic pollutants and as emerging pollutants of concern. The two most frequently studied PFAS are perfluorooctanoic acid (PFOA) and perfluorooctane sulfonic acid (PFOS), and they serve as model compounds for evaluating PFAS. Accurate PFOS and PFOA measurements in biota and environmental media were made possible in the late 1990's due to the availability of commercial liquid chromatography with mass spectrometry (LC/MS) instruments at the time. Since then, improved instruments

and methods developed over the last 25 years, which have allowed for the measurement of several PFAS analytes in various environmental media such as water, air, soil, sediment, and biota.

Between 2000 and 2015 the manufacturers of PFAS in the US and EU ceased production of fluorochemicals that could lead to PFOS and PFOA. Today many of those substances are restricted for manufacture, use and import within the United States (US) and the European Union (EU)[112] . The USEPA began to require monitoring of PFOS and PFOA in municipal drinking water in 2012 as part of the third unregulated contaminants monitoring rule (UCMR3), and in 2016 established health-based advisory limits (HALs) for PFOA and PFOS at 70 ppt, combined concentration. Most recently in 2023, the EPA proposed a new PFAS National Primary Drinking Water Standard with limits for PFOS and PFOA at 4 ppt, which has been met with some criticism[113]. This has set the stage for an even greater need to reduce PFAS releases to the environment and to reduce PFAS in drinking water supplies.

Currently, physical treatment technologies are employed at large scale for removing PFAS from water. The most common technology is the use of granular activated carbon (GAC) sorption, although ion exchange (IE) sorption and reverse osmosis (RO) filtration treatment can also be effective. A pitfall to the use of physical removal processes like RO, IE and GAC is that each generates a secondary concentrated PFAS waste stream that requires further treatment or disposal. While thermal regeneration can augment GAC technology, it requires high temperatures to destroy all absorbed PFAS. Further, the re-use of regenerated GAC is limited to treatment of non-potable water. While high-temperature incineration may be effective at destroying PFAS in soils and other solid matrices, incineration of aqueous wastes is not practical. Furthermore, some uncertainty remains about the byproducts of PFAS incineration processes [114]. The pitfalls of physical removal methods have resulted in the need for development of reliable, realistic destructive technologies that can be applied directly to water to eliminate PFAS and that are scalable.

While confined largely to laboratory studies and some pilot scale testing, several novel destructive technologies have been developed and evaluated to treat PFAS in water, but with limited success. Those include sonolytic methods, electrochemical oxidation and reduction methods, surface plasma discharge, supercritical water oxidation, photolytic processes, and various advanced oxidation processes (AOPs) and/or advanced reductive processes (ARPs)[79]. However, few of those technologies have proven broadly successful to treat all types of PFAS. Further, some can require expensive additives with poor hazard profiles and may be more deleterious to the environment and biota than the PFAS they are intended to remove. Also, many utilize novel technologies that are not available commercially or have significant hurdles to scale up. Because of the high carbon-fluorine bond energy that needs to be broken, all destructive technologies for PFAS are typically energy intensive. They involve formation of highly reactive oxidizing species, such as hydroxyl radical ($^{\bullet}OH$), or strong reducing species such as hydrogen radical ($^{\bullet}H$) and solvated electron (e_{aq}^-) that can react with the PFAS to facilitate their decomposition. Most destructive technologies only produce either oxidative radicals or reductive radicals, but typically not both. Therefore, the technologies are often selective for only a specific class of PFAS. For example, oxidative processes can be somewhat effective with perfluoroalkyl carboxylates, but may not be effective against perfluoroalkyl sulfonates, which are typically more recalcitrant. In contrast, reductive processes involving e_{aq}^- can be effective in initiating breakdown of different types of PFAS[115], but still may require involvement of other radicals like $^{\bullet}OH$ in subsequent breakdown steps.

Irradiation of water with gamma ray (γ) or high-energy electron beam (EB) generates both oxidative and reductive radicals simultaneously during water radiolysis. The advantages of EB and γ-irradiation for water treatment of PFAS and other contaminants have been discussed[116]. It was shown as early as 2000 that PFOA and PFOS degradation occurred during EB pulsed radiolysis experiments[117], and later demonstrated that EB could result in as high as 95.7% removal for PFOA and 85.9% for PFOS under anoxic, alkaline conditions[118].

Further, the use of EB treatments to degrade PFOS in soil and aqueous samples was recently demonstrated in enclosed stainless-steel containers at high pressure and temperatures [119] .

Ionizing energy such as gamma is typically sourced from radioactive isotopes, often utilizing cobalt-60, and less frequently with cesium-137. While γ-irradiation has some advantages over EB such as increased penetration depth into water, there are significant downsides to using gamma. Cobalt-60 has a short 5.3-year half-life and requires replenishment at a frequency of about 10% annually and is produced by nuclear activation processes, making it expensive. Furthermore, the transport, storage and handling of γ-emitting radionuclides is inherently dangerous and storage at low security facilities presents a national security risk for its potential use in dirty bombs, and therefore is under consideration for phase-out of use[120]. In contrast, EB is electricity generated beta radiation and uses a mature technology commercially available at industrial scale since the late 1940's and used in a broad array of industrial, medical, and clinical applications. Although γ-processes and EB processes require shielding to protect from stray radiation exposure, EB is an on-off technology controlled by an electric switch, as opposed to γ-ray which is an always-on technology. Therefore, EB processes can be more easily engineered and maintained. Further, gamma from typical sources such as Cobalt-60 and Cesium-137 have fixed gamma energies below 1.5 MeV, while EB can generate electron energies as high as 10 MeV for water applications and can be more easily tailored for a specific application.

EB systems accelerate resting electrons to near the speed of light and can achieve electron energies up to 100s of MeV. Because electrons have mass, they require a high energy to penetrate at a practical depth in water. For example, a 10 MeV incident electron has a travel distance of about 5 cm in water with a bulk-water dose delivery at about 3.5 cm depth, while a lower energy 800 Kev electron can only penetrate a few millimeters into water and has a much lower dose delivery[121]. Water treatment applications of EB are practically limited to 10 MeV to prevent overheating of the accelerator and to avoid the occurrence of radionuclide formation by nuclear activation of high-Z elements that may be dissolved in the water or present in components of the EB system. Despite this limit, EB has been successfully used at industrial scale for treatment of SO_x and NO_x in flue gases[122], for removal of fecal coliforms in sewage sludge solids and wastewaters[81], and to remove textile dyes from high-volume wastewater at a large industrial textile dying complex [44].

The use of EB accelerator technology offers a viable and effective treatment technology for PFAS destruction in water. A recent evaluation of EB for PFAS treatment showed that the concept of energy-per-order (EEo) is a useful concept for comparing EB energy requirements with other destructive technologies. They showed that their estimated EEo for EB ranged from 31-176 kWh/m^3/order for PFAS treatment versus an EEo range for other destructive technologies at between 5–9595 kWh/m^3/order. Based on low EEo, EB has been promoted as a promising technology for PFAS treatment [116]. Before EB can be scaled up for use in PFAS treatment, a full evaluation and optimization of the technology is needed to identify the favorable conditions and parameters. Getoff discussed several important parameters to consider for optimizing radiation induced degradation of water pollutants, including absorbed dose, dose rate, depth-dose distribution, initial substrate concentration, synergistic effects of catalysts, as well as other parameters[123].

In the present work, we developed a simple test system with which to optimize EB for the destruction of both PFOA and PFOS in water under near-normal pressure and temperature conditions. This enabled us to better understand the EB parameters that are critical for use of a realistic EB treatment system to remove PFOS and PFOA from water. In our test system we evaluated the effects of EB dose, EB dose rate, pH, dissolved oxygen concentration (DO), temperature, and initial PFAS concentration over five orders of magnitude. All these parameters effect the amount and ratio of the species created from water radiolysis that are available for PFAS destruction. We also evaluated the effects of adding known PFAS-degrading photocatalysts titanium dioxide (TiO2) and hexagonal boron nitride (hBN). We determined kinetics of removal of PFOS and PFOA, and

other related PFAS, and measured for anticipated soluble and volatile fluorinated intermediate products, as well as for fluoride ion and sulfate ion, with near 100% mass balance. We also screened select samples for unknown PFAS intermediate products by sensitive high-resolution mass spectrometric analysis but did not observe any. In the end we defined the optimal EB parameters for complete destruction of PFOA and PFOS, which was able to achieve some of the fastest removal rates for PFOA and PFOS for all published destruction techniques of PFAS in water. We further conducted a cost and energy analysis of EB technology versus a conventional GAC system operated by 3M for PFAS treatment of contaminated groundwater at a former landfill site. On a cost per mass PFAS ($/kg) removed, EB was very competitive with GAC removal, however on a cost per gallon ($/gal) of treatment, GAC was significantly cheaper, as expected. Our experimental results and cost analysis enabled us to perform a comprehensive evaluation for best fit of the technology for PFAS removal from water. The best fit for EB technology identified involved treating higher concentration waste streams between 1-20 ppm of PFAS, or higher. Such waste streams are typical of reverse osmosis (RO) reject water or ion exchange (IE) regenerant solutions, however, other waste streams such as landfill leachates, or highly contaminated groundwater at AFFF sites may be a consideration as well. Experimentally, we showed that EB can be applied successfully to RO reject water and IE regenerant solutions from a treatment system at a fluorochemical manufacturing facility, and successfully applied to PFAS contaminated groundwater.

The accelerator efficiency (% of the incoming power that is used in water treatment) is the dominating factor in accelerator choice. The radio frequency (RF) power supply and the accelerator design (superconducting versus warm technology) drive the accelerator efficiency. The IBA Rhodotron was the best option of industrially available accelerators but operates at 43% efficiency at the conditions of the study. The Fermilab designed accelerator can operate at 55% efficiency under similar conditions, or 77% efficiency when powered by a magnetron which would have to be built for that frequency and amount of power. As power consumption is the primary driving factor in the operating cost of the EB accelerator, increasing efficiency by over 30% will drive costs further down to cost parity with GAC for treating concentrations in the 100s of ppb range.

Overall, the study showed that electron beam can be very effective at destruction of PFAS, with 100% destruction of PFOA and PFOS, in water compared to conventional water treatment technologies that separate the PFAS into a different phase. The usefulness for EB from this study was limited to higher concentrations of PFAS in water. This was attributed to the fact that while there is an abundance of active species from radiolysis, like aqueous electrons, there is a diffusion limiting step of the active species getting to the PFAS molecule. An obvious next step for this work is to demonstrate the technology on a pilot scale. Part of this larger scale demonstration would involve investigating ways of overcoming the diffusion limited step to further increase the efficiency of the process. Another part of a pilot scale study would be incorporating the EB system in an overall water treatment system with a preconcentrating step, as EB works better with more concentrated PFAS solutions. Funding and site location of the pilot system are critical next steps.

Challenges & Lessons Learned

Several procedural and bureaucratic challenges were encountered during this project. Shortly after the initiation of this project in Q4 of 2019, the U.S and World became engrossed in the nearly 2-year COVID-19 pandemic crisis. By March of 2020, President Trump issued a COVID-19 National Emergency and a travel ban for non-US citizens traveling from Europe, and California issued a statewide stay-at-home order which shortly thereafter expanded nationwide. By April of 2020 the requirement to wear masks, social distancing, lockdowns, and business/government closures, except for essential personnel, was the norm. Fortunately, the primary personnel of the present project were deemed essential and allowed to have access to facilities during the project timeframe. However, the COVID-19 pandemic had a substantial impact on this project for most of the

project timeline, increasing the difficulties of nearly every aspect, including accessing facilities, delays in shipping of materials and ordering supplies, obtaining professional services for repair work, and the increased risks associated with potential exposures at work. This goes without saying we also largely served as our own IT support and facilities/laboratory support at times. Additionally, while the project had a substantial travel budget for planned visits between 3M and Fermilab, those funds largely could not be used in a timely manner due to COVID-19 related travel restrictions. The COVID-19 impacts also affected the interviewing and hiring of a postdoctoral associate for the project in early 2020. While nothing could be done to avert a pandemic, one lesson learned was that the request for a 6-month extension, granted by DOE for this project, aided significantly in completion of project objectives. However, this essentially changed the timeline dynamics, from an approximately 2-year project to essentially a 3-year project without the benefit of additional funding. Also, during this time it was frequently encountered that the DOE SharePoint-based budgeting system for FNAL budget submissions did not work well. Other challenges encountered during the research project were the losses of project personnel to other projects, due largely to personnel commitments to a 2-year project that ran for nearly 3 years without additional funding, and some retirements that occurred.

In additional to the bureaucratic and procedural challenges, technical challenges were also encountered. This included significant downtime on the experimental e-beam system A2D2 at Fermilab, which required external repair technician (delayed by COVID-19 restrictions) and internal Fermilab support to order parts and repairs. Another technical challenge was the observation from testing results that showed e-beam parameters optimized for PFOA and PFOS, did not work well for short chain perfluoroalkyl sulfonates and will require significant further effort to evaluate and address for use of e-beam to treat PFAS contaminated water, which can often contain a variety of PFAS of different fluorocarbon chain lengths.

U.S Provisional Patents

A U.S. provisional patent entitled Electron Beam Application to the Treatment of PFAS Water Streams was filed by Fermi National Laboratory during the performance of this agreement. The patent application number is 63/530,219 (DOE S# 179,679).

Works Cited

[1] World Water Assessment Programme. Water in a Changing World. The United Nations World Water Development Report 3 (UNESCO, 2009).

[2] C. J. Vörösmarty et al., "Global threats to human water security and river biodiversity", Nature 467, 7315, p555-561 (2010).

[3] S.B. Grant et al., "Taking the "Waste" Out of "Wastewater" for Human Water Security and Ecosystem Sustainability", Science 337, p681-686 (2012).

[4] J. Glűge, M. Scheringer, I.T. Cousins, J.C. DeWitt, G. Goldenman, D. Herzke, R. Lohmann, C.A. Ng, X. Trier, and Z. Wang. 2020. An overview of the uses of per- and polyfluoroalkyl substances (PFAS). *Environ. Sci.: Process Impacts.* 22:2345-2373; DOI 10.1039/D0EM00291G

[5] Ojha, S., Thompson, P.T., Powell, C.D. *et al.* Identifying and sharing per-and polyfluoroalkyl substances hot-spot areas and exposures in drinking water. *Sci Data* **10**, 388 (2023). https://doi.org/10.1038/s41597-023-02277-x

[6] Hu, X. C. *et al*. Detection of poly-and perfluoroalkyl substances (PFAS) in US drinking water linked to industrial sites, military fire training areas, and wastewater treatment plants. *Environ. Sci. Tech. Let.* **3**, 344–350 (2016). https://pubs.acs.org/doi/full/10.1021/acs.estlett.6b00260

[7] EPA and 3M ANNOUNCE PHASE OUT OF PFOS. News Release May 16, 2000. https://www.epa.gov/archive/epapages/newsroom_archive/newsreleases/33aa946e6cb11f35852568e1005246b4.html

[8] USEPA Fact Sheet: 2010/2015 PFOA Stewardship Program. https://www.epa.gov/assessing-and-managing-chemicals-under-tsca/fact-sheet-20102015-pfoa-stewardship-program#what

[9] Brendel et al. Environ Sci Eur. (2018) 30:9 https://doi.org/10.1186/s12302-018-0134-4

[10] UCMR-5. USEPA Fifth Unregulated Contaminant Monitoring Rule. 2021. https://www.epa.gov/dwucmr/fifth-unregulated-contaminant-monitoring-rule

[11] J. P. Giesy and K. Kannan, "Peer Reviewed: Perfluorochemical Surfactants in the Environment," Environ. Sci. Technol., vol. 36, no. 7, pp. 146A-152A, Apr. 2002.

[12] Du Z, S Deng, Y Bei, Q Huang, B Wang, J Huang, G Yu. 2014. Adsorption behavior and mechanism of perfluorinated compounds on various adsorbents-A review. J. Haz. Mat. 274:443-454

[13] Zaggia A, L Conte, L Falletti, M Fant, A Chiorboli. 2015. Use of strong anion exchange resins for removal of perfluoroalkylted subtances from contaminated drinking water in batch and continuous pilot plants. *Water Res.* 91: 137-146.

[14] "Drinking Water Health Advisories for PFOA and PFOS," FACT SHEET, p. 5, Nov. 2016.

[15] I. Ross et al., "A review of emerging technologies for remediation of PFAS," Remediat. J., vol. 28, no. 2, pp. 101–126, Mar. 2018.

[16] Rahman MF, S Peldszus, WB Anderson. 2014. Behavior and fate of perfluoroalkyl and polyfluoroalkyl lsubstances (PFAS) in drinking water treatment: a review. *Water Research* 50:318-340

[17] Glover CM, O Quinones, ERV Dickenson. 2018. Removal of perfluoroalkyl and polyfluoroalkyl substances in potable reuse systems. *Water Res.* 144:454-461

[18] Meegoda JN, Bezerra de Souza B, Casarini MM, Kewalramani JA. A Review of PFAS Destruction Technologies. Int J Environ Res Public Health. 2022 Dec 7;19(24):16397. doi: 10.3390/ijerph192416397. PMID: 36554276; PMCID: PMC9778349.

[19] C. D. Vecitis, H. Park, J. Cheng, B. T. Mader, and M. R. Hoffmann, "Treatment technologies for aqueous perfluorooctanesulfonate (PFOS) and perfluorooctanoate (PFOA)," Front. Environ. Sci. Eng. China, vol. 3, no. 2, pp. 129–151, Jun. 2009.

[20] Vecitis CD, H Park, J Chaeng , BT Mader and MR Hoffman. 2008. Kinetics and Mechanism of the Sonolytic Conversion of the Aqueous Perfluorinated Surfactants, Perfluorooctanoate (PFOA), and Perfluorooctane Sulfonate (PFOS) into Inorganic Products. *J. Phys. Chem. A* 112:4261-4270

[21] Vecitis CD, H Park, J Cheng, BT Mader and MR Hoffman. 2008. Enhancement of perfluorooctanoate and perfluorooctanesulfonate activity at acoustic cavitation bubble interfaces. *J. Phys. Chem. C* 112:16850-16857.

[22] Cheng J, CD Vecitis, H Park, BT Mader, MR Hoffman. 2008. Sonochemical degradation of perfluorooctane sulfonate (PFOS) and perfluorooctanoate (PFOA) in landfill groundwater: Environmental matrix effects. *Environ. Sci. Technol.* 42:857-8063

[23] Campbell TY, CD Vecitis, BT Mader and MR Hoffman. 2009. Perfluorinated surfactant chain-length effects on sonochemical kinetics. *J. Phys Chem. A*. 113:9834-9842.

[24] Cheng J, CD Vecitis, H Park, **BT Mader**, MR Hoffman. 2010. Sonochemical degradation of perfluorooctane sulfonate (PFOS) and perfluorooctanoate (PFOA) in groundwater: Kinetic effect of matrix inorganics. *Environ. Sci. Technol.* 44:445-450.

[25] Park H, CD Vecitis, J Cheng, NF Dalleska, **BT Mader** and MR Hoffman. 2011. Reductive degradation of perfluoroalkyl compounds with aquated electrons generated by iodide photolysis at 254 nm. *Photochem. Photobiol. Sci.* 10:1945-1953

[26] Park H, CD Vecitis, J Cheng, W Choi, BT Mader and MR Hoffman. 2009. Reductive defluorination of aqueous perfluorinated alky surfactants: Effects of ionic headgroup and chain length. *J. Phys Chem. A*. 113:690-696.

[27] Ma, S, M Wu, L Tang, R Sun, C Zang, J Xiang, X Yang, X Li and G Xu. 2017. EB degradation of perfluorooctanoic acid and perfluorooctane sulfonate in aqueous solution. *Nucl. Sci. Technol.* 28:137.

[28] C. N. Kurucz, T. D. Waite, and W. J. Cooper, "The Miami Electron Beam Research Facility: a large-scale wastewater treatment application," Radiat. Phys. Chem., vol. 45, no. 2, pp. 299–308, Feb. 1995.

[29] A. Lazarine, "Development of an electron beam irradiation design for use in the treatment of municipal biosolids and wastewater effluent," 2008.

[30] B. Han, J. Kyu Kim, Y. Kim, J. Seung Choi, and K. Young Jeong, "Operation of industrial-scale electron beam wastewater treatment plant," Radiat. Phys. Chem., vol. 81, no. 9, pp. 1475–1478, Sep. 2012.

[31] J. W. T. Spinks and R. J. Woods, An introduction to radiation chemistry. Wiley, 1990.

[32] Z. Zhang, J.-J. Chen, X.-J. Lyu, H. Yin, and G.-P. Sheng, "Complete mineralization of perfluorooctanoic acid (PFOA) by γ-irradiation in aqueous solution," Sci. Rep., vol. 4, Dec. 2014.

[33] Cooper, W. J., Meacham, D. E., Nickelsen, M. G., Lin, K., Ford, D. B., Kuruczand, C. N. & Waite, T. D. The Removal of Tri- (TCE) and Tetrachloroethylene (PCE) from Aqueous Solution using High Energy Electrons. Air Waste 43, 1358–1366 (1993).

[34] Cooper - 2002 - MTBE and priority contaminant treatment with high energy electron beam injection. https://reader.elsevier.com/reader/sd/pii/S0969806X02003444?token=A5BAF2E26FE4A5BFA366B04E8C4A974FEDDB5E5008E578713965DFF93C122E1A8E5F3E1E6A281E7F77B8A97D70D2DB92&originRegion=us-east-1&originCreation=20220911014051 doi:10.1016/S0969-806X(02)00344-

[35] Nickelsen, M. G., Cooper, W. J., Lin, K., Kurucz, C. N. & Waite, T. D. High energy electron beam generation of oxidants for the treatment of benzene and toluene in the presence of radical scavengers. Water Res. 28, 1227–1237 (1994).

[36] Wu, M., Shi, W., Wang, Y., Jiao, Z., Wang, J., Ding, G. & Fu, J. Degradation of halogenated benzenes in solution by electron beam irradiation method. Environ. Technol. 30, 191–197 (2009).

[37] Thihara Rodrigues, F., Marchioni, E., Lordel-Madeleine, S., Kuntz, F., Casañas Haasis Villavicencio, A. L. & Julien-David, D. Degradation of profenofos in aqueous solution and in vegetable sample by electron beam radiation. Radiat. Phys. Chem. 166, 108441 (2020).

[38] Xu, G., Yao, J., Tang, L., Yang, X., Zheng, M., Wang, H. & Wu, M. Electron beam induced degradation of atrazine in aqueous solution. Chem. Eng. J. 275, 374–380 (2015).

[39] Weihua, S., Zheng, Z., Rami, A.-S., Tao, Z. & Desheng, H. Degradation and detoxification of aqueous nitrophenol solutions by electron beam irradiation. Radiat. Phys. Chem. 65, 559–563 (2002).

[40] Silva, V. H. O., dos Santos Batista, A. P., Silva Costa Teixeira, A. C. & Borrely, S. I. Degradation and acute toxicity removal of the antidepressant Fluoxetine (Prozac®) in aqueous systems by electron beam irradiation. Environ. Sci. Pollut. Res. 23, 11927–11936 (2016).

[41] Van Lancker, M., Herer, A., Cleland, M., Jongen, Y., Abs, M., The IBA Rhodotron: an industrial high-voltage high-powered electron beam accelerator for polymers radiation processing, Nuc. Inst. Meth. Phys. Res. Sec. B: Beam Interactions with Materials and Atoms, Volume 151, Issues 1–4, 242-246 (1999).

[42] https://www.iba-industrial.com/the-rhodotron/

[43] Kurucz, C. N., Waite, T. D. & Cooper, W. J. The Miami Electron Beam Research Facility: a large scale wastewater treatment application. Radiat. Phys. Chem. 45, 299–308 (1995).

[44] Zimek, Z. and Kaluska, I. Economical Aspects of Radiation Sterilization with Electron Beam. https://www.osti.gov/etdeweb/servlets/purl/644045

[45] Dainton, F. S. The Radiation Chemistry of Water and Aqueous Solutions. https://pubs.acs.org/doi/pdf/10.1021/ja00871a055 (2002) doi:10.1021/ja00871a055.

[46] The Radiation Chemistry of Water - 1st Edition. https://www.elsevier.com/books/the-radiation-chemistry-of-water/draganic/978-0-12-221650-3.

[47] Pikaev, A. K. & Ershov, B. G. PRIMARY PRODUCTS OF THE RADIOLYSIS OF WATER AND THEIR REACTIVITY. *Russ. Chem. Rev.* 36, 602 (1967)

[48] Le Caër, S. Water Radiolysis: Influence of Oxide Surfaces on H2 Production under Ionizing Radiation. *Water* 3, 235–253 (2011).

[49] Woods, R. J. & Pikaev, A. K. *Applied Radiation Chemistry: Radiation Processing*. (John Wiley & Sons, 1994).

[50] Pikaev, A. K. & Ershov, B. G. PRIMARY PRODUCTS OF THE RADIOLYSIS OF WATER AND THEIR REACTIVITY. *Russ. Chem. Rev.* 36, 602 (1967)

[51] Draganic, I. G. & Draganic, Z. D. THE RADIATION CHEMISTRY OF WATER. 239.

[52] Lousada, C., Soroka, I., Yagodzinskyy, Y., Tarakina, N., Todoshchenko, O., Hänninen, H., Korzhavyi, P. & Jonsson, M. Gamma radiation induces hydrogen absorption by copper in water OPEN. *Sci. Rep.* 6, 1–8 (2016).

[53] Song, Z., Tang, H., Wang, N. & Zhu, L. Reductive defluorination of perfluorooctanoic acid by hydrated electrons in a sulfite-mediated UV photochemical system. *J. Hazard. Mater.* 262, 332–338 (2013).

[54] Bentel, M. J., Yu, Y., Xu, L., Li, Z., Wong, B. M., Men, Y. & Liu, J. Defluorination of Per- and Polyfluoroalkyl Substances (PFAS) with Hydrated Electrons: Structural Dependence and Implications to PFAS Remediation and Management. *Environ. Sci. Technol.* 53, 3718–3728 (2019).

[55] Stratton, G. R., Dai, F., Bellona, C. L., Holsen, T. M., Dickenson, E. R. V. & Mededovic Thagard, S. Plasma-Based Water Treatment: Efficient Transformation of Perfluoroalkyl Substances in Prepared Solutions and Contaminated Groundwater. *Environ. Sci. Technol.* 51, 1643–1648 (2017).

[56] CN Kurucz et al., "The Miami electron beam research facility: a large scale waste water treatment application", Radiat. Phys. Chem. Vol. 45, pp299-308 (1995).

[57] B Han et al., "Operation of industrial-scale electron beam wastewater treatment plant", Rad. Phy. Chem. 81, p1475-1478 (2012).

[58] 3M 2023 Global Impact Report. https://multimedia.3m.com/mws/media/2292786O/3m-2023-global-impact-report.pdf (last accessed 9/1/2023)

[59] 3M to Exit PFAS Manufacturing by the End of 2025. Press Release, Dec.20, 2022. https://news.3m.com/2022-12-20-3M-to-Exit-PFAS-Manufacturing-by-the-End-of-2025

[60] C. D. Vecitis, H. Park, J. Cheng, B. T. Mader, and M. R. Hoffmann, "Treatment technologies for aqueous perfluorooctanesulfonate (PFOS) and perfluorooctanoate (PFOA)," Front. Environ. Sci. Eng. China, vol. 3, no. 2, pp. 129–151, Jun. 2009.

[61] Vecitis CD, H Park, J Chaeng , BT Mader and MR Hoffman. 2008. Kinetics and Mechanism of the Sonolytic Conversion of the Aqueous Perfluorinated Surfactants, Perfluorooctanoate (PFOA), and Perfluorooctane Sulfonate (PFOS) into Inorganic Products. *J. Phys. Chem. A* 112:4261-4270

[62] Cheng J, CD Vecitis, H Park, BT Mader, MR Hoffman. 2008. Sonochemical degradation of perfluorooctane sulfonate (PFOS) and perfluorooctanoate (PFOA) in landfill groundwater: Environmental matrix effects. *Environ. Sci. Technol.* 42:857-8063

[63] Campbell TY, CD Vecitis, BT Mader and MR Hoffman. 2009. Perfluorinated surfactant chain-length effects on sonochemical kinetics. *J. Phys Chem. A*. 113:9834-9842.

[64] Park H, CD Vecitis, J Cheng, W Choi, BT Mader and MR Hoffman. 2009. Reductive defluorination of aqueous perfluorinated alky surfactants: Effects of ionic headgroup and chain length. *J. Phys Chem. A*. 113:690-696.

[65] S Biswas, SSRKC Yamijala and BM Wong. Degradation of per- and polyfluoroalkyl substances with dydrated electrons: A new mechanism from first-principles calculations. Env. Sci. Technol. 56,12, 8167-8175. 2022. https://doi.org/10.1021/acs.est.2c01469

[66] De Silva AO, Muir DC, Mabury SA. Distribution of perfluorocarboxylate isomers in select samples from the North American environment. Environ Toxicol Chem. 2009 Sep;28(9):1801-14. doi: 10.1897/08-500.1. PMID: 19358623.

[67] M.S. Ross, C.S. Wong, J.W. Martin. 2012. Isomer-specific biotransformation of perfluorooctane sulfonamide in Sprague-Dawley rats *Environ Sci Technol*. 46(6):3196-203. https://doi: 10.1021/es204028v

[68] A. Kärrman, K. Elgh-Dalgren , C. Lafossas and T. Møskeland. 2011. Environmental levels and distribution of structural isomers of perfluoroalkyl acids after aqueous fire-fighting foam (AFFF) contamination *Environmental Chemistry* 8(4): 372-380.

[69] L. Jinxia Liu, G. Zhong, W. Li, S.Mejia Avendaño. 2019. Isomer-specific biotransformation of perfluoroalkyl sulfonamide compounds in aerobic soil. *Science of The Total Environment* 651(1) 766-774

[70] J.P. Benskin JP, A. O. De Silva, L. J. Martin, G. Arsenault, R. McCrindle, N. Riddell, S.A. Mabury, J.W. Martin. 2009. Disposition of perfluorinated acid isomers in sprague-dawley rats; Part 1: Single dose *Env. Toxicol. Chem.* 28(3):542-554. https://doi-org.mmm.idm.oclc.org/10.1897/08-239.1

[71] K Londhe, C Lee, CA McDonough, AK Venkatesan. The Need for Testing Isomer Profiles of Perfluoroalkyl Substances to Evaluate Treatment Processes. *Environmental Science & Technology* 2022, *56* (22) , 15207-15219. https://doi.org/10.1021/acs.est.2c05518

[72] 3M Battery Electrolyte HQ-115 Technical Data Sheet. October 2012

[73] 3M Ionic Liquid Antistat FC-4400 Product Information Sheet. June 2009.

[74] Trajanowics, M, A Bojanowska-Czajka, I Bartosiewicz, and K Kulisa. Advanced oxidation/reduction processes treatment for aqueous PFOA and PFOS-a review of recent advances. *Chem. Eng. J.* 2018. 336:170-199. https://doi.org/10.1016/j.cej.2017.10.153

[75] BR Miller, M Rigby, LJM Kuijpers, PB Krummel, LP Steele, M Leist, PJ Fraser, A McCulloch, C Harth, P Salameh, J Mühle, RF Weiss, RG Prinn, RHJ Wang, S O'Doherty, BR Greally, and PG Simmonds. HFC-23 (CHF_3) emission trend response to HCFC-22 ($CHClF_2$) production and recent HFC-23 emission abatement measures. Atmos. Chem. Phys., 10, 7875–7890, 2010. https://doi.org/10.5194/acp-10-7875-2010

[76]https://www.dcceew.gov.au/environment/protection/ozone/rac/global-warming-potential-values-hfc-refrigerants

[77] Gu Y, Liu T, Wang H, Han H, Dong W. Hydrated electron-based decomposition of perfluorooctane sulfonate (PFOS) in the VUV/sulfite system. Sci Total Environ. 2017 Dec 31;607-608:541-548. doi: 10.1016/j.scitotenv.2017.06.197. Epub 2017 Jul 27. PMID: 28704677.

[78] Song, Z., Tang, H., Wang, N., & Zhu, L. (2013). Reductive defluorination of perfluorooctanoic acid by hydrated electrons in a sulfite-mediated UV photochemical system. *Journal of Hazardous Materials, 262*, 332–338.

[79] Meegoda, J.N.; Bezerra de Souza, B.; Casarini, M.M.; Kewalramani, J.A. A Review of PFAS Destruction Technologies. *Int. J. Environ. Res. Public Health* **2022**, *19*, 16397. https://doi.org/10.3390/ijerph192416397

[80] Kaushik Londhe, Cheng-Shiuan Lee, Yi Zhang, Slavica Grdanovska, Thomas Kroc, Charlie A. Cooper, and Arjun K. Venkatesan. 2021. *ACS ES&T Engineering 1* (5), 827-841. DOI: 10.1021/acsestengg.0c00222

[81] Siwek, M., Edgecock, T. Application of electron beam water radiolysis for sewage sludge treatment—a review. *Environ Sci Pollut Res* **27**, 42424–42448 (2020). https://doi.org/10.1007/s11356-020-10643-0

[82] L Duan, B Wang, K Heck, S Guo, CA Clark, J Arredondo, M Wang, TP Senftle, P Westerhoff, X Wen, Y Song and MS Wong. Efficient photocatalytic PFOA degradation over boron nitride. Env. Sci. Technol. 2020. 7:613-619. https://dx.doi.org/10.1021/acs.estlett.0c00434?ref=pdf

[83] Xu, B., Ahmed, M. B., Zhou, J. L., & Altaee, A. (2020a). Visible and UV photocatalysis of aqueous perfluorooctanoic acid by TiO2 and peroxymonosulfate: Process kinetics and mechanistic insights. *Chemosphere, 243*, 125366.

[84] https://www.calgoncarbon.com/app/uploads/DS-DSRRXPH15-EIN-E1.pdf

[85] https://www.calgoncarbon.com/products/dsrc/

[86] SB Busra, Y Zhang Y, JF Reuther, NB Saleh, AK Venkatesan, OG Apul, 2021. "Thermal Regeneration of Spent Granular Activated Carbon Presents an Opportunity to Break the Forever PFAS Cycle". *Environ. Sci. Technol.* 55:5608-5619.

[87] JQ Adams and RM Clark. Cost Estimated for GAC Treatment Systems. J. Am. Water Works Assoc. 81:35-42. 1989

https://doi.org/10.1002/j.1551-8833.1989.tb03320.x

[88]https://www.epa.gov/newsreleases/epa-announces-new-drinking-water-health-advisories-pfas-chemicals-1-billion-bipartisan

[89]https://www.epa.gov/newsreleases/biden-harris-administration-proposes-first-ever-national-standard-protect-communities

[90]ECT2 website: https://www.ect2.com/

[91] J. Ungrin, N.H. Drewell, N.A. Ebrahim, J-P. Labrie, C.B. Lawrence, V.A. Mason, and B.F. White, "IMPELA: AN INDUSTRIAL ACCELERATOR FAMILY," EPAC 1988, pp. 1515-1517.

[92] V. Bezuglov, A. Bryazgin, K. Chernov, B. Faktorovich V. Gorbunov, E. Kokin, M. Korobeynikov, A. Lukin, I. Makarov, S. Maximov, A. Panfilov, V. Radchenko, E. Shtarklev, A. Sidorov, V. Tarnetsky, M. Tiunov, V. Tkachenko, A. Vlasov, L. Voronin, "HIGH-POWER INDUSTRIAL ACCELERATOR ILU-14 FOR E-BEAM AND X-RAY PROCESSING," Proceedings of LINAC2014, Geneva, Switzerland, TUIOA05

[93] [4] A. A. Bryazgin, V. I. Bezuglov, E. N. Kokin, M. V. Korobeinikov, G. I. Kuznetsov,I. G. Makarov, G. N. Ostreiko, A. D. Panfilov, V. M. Radchenko, G. V. Serdobintsev, A. V. Sidorov, V. V. Tarnetsky, M. A. Tiunov, B. L. Faktorovich,

K. N. Chernov, and V. G. Cheskidov, "ILU_14 Industrial Electron Linear Accelerator with a Modular Structure, " Instruments and Experimental Techniques, 2011, Vol. 54, No. 3, pp. 295–311.

[94] Marc Van Lancker, Arnold Herer, Marshall R. Cleland, Yves Jongen, Michel Abs, "The IBA Rhodotron: an industrial high-voltage high-powered electron beam accelerator for polymers radiation processing," Nuclear Instruments and Methods in Physics Research B 151 (1999) 242-246.

[95] E. Zaplatin, et all, "Euclid Modified SRF Conical Half-Wave Resonator Design", IPAC14, Dresden, Germany, 2014.

[96] R. C. Dhuley, I. Gonin, S. Kazakov, T. Khabiboulline, A. Sukhanov, V. Yakovlev, A. Saini, N. Solyak, A. Sauers, J. C. T. Thangaraj, K. Zeller, B. Coriton, R. Kostin, "Design of a 10 MeV, 1000 kW average power electron-beam accelerator for wastewater treatment applications," Phys. Rev. Accel. Beams 25, 041601 (2022).

[97] T. Khabiboulline, V. Yakovlev, T. Kroc, "Analysis of RF high power sources for 1MW – range, 10 MeV CW industrial accelerator," FERMILAB-PUB-20-369-DI-TD, May 29, 2020.

[98] VKL7796 klystron, Communication and Power Industries (CPI), https://www.cpii.com/product.cfm/1/20/107

[99] F.H. Raab, "High-Efficiency Power Amplifiers for Particle Accelerators," https://science.osti.gov/-/media/np/pdf/sbir-sttr/SBIR_STTR_2014/Day2/Raab_High-Efficiency-Amplifiers.pdf?la=en&hash=AF0FC930B514EB88481BE39435A33D5FEDB61C6D

[100] Lenci, S., Balkcum, A., Bohlen, H., Mizuhara, A., Wright, E., Li, Y., & Tornoe, R. (2004). RF sources for 3rd & 4th generation light sources. In Proceedings of the 2004 FEL Conference, Trieste, Italy. August 29-September 3. Accessed at http://www. elettra. trieste. it/fel2004/proceedings/on April (Vol. 3, No. 2008, pp. 566-569).

[101] Choroba, Stefan. "The High Power RF System for the European XFEL." Proc. 29th Linear Accelerator Conference (LINAC'18), Beijing, China, 16-21 September 2018.

[102] Akimov, A., et al. Pulse Power Supply System for the 10 MW Tesla Klystron. No. BUDKER-INP-2002-59. SIS-2003-149, 2002.

[103] R&K Company Limited – Solid State Amplifier Supplier (https://rk-microwave.com/)

[104] Gatesair – Solids State Amplifier Supplier (https://www.gatesair.com/)

[105] G. Kazakevich, R.P. Johnson, Ya. Derbenev, V. Yakovlev, "Utilization of the CW magnetrons as coherent RF sources for superconducting RF accelerators," Nuclear Inst. and Methods in Physics Research A, Volume 1039, 11 September 2022, 167086.

[106] Magnetron prices from Mega Industries https://www.megaind.com/product/100kw-l-band-magnetron-tube/

[107] D. Oepts, A. Van der Meer, and P. Van Amersfoort, "The free-electron-laser user facility felix," Infrared physics & technology, vol. 36, no. 1, pp. 297–308, 1995.

[108] Pronitchev, O., and S. Kazakov. "Design of main coupler for 650 MHz SC cavities of PIP-II project." Proceedings of NAPAC2016, Chicago, IL, USA (2016).

[109] J. C. T. Thangaraj, A. Saini, V. Yakovlev, I. Gonin, N. Solyak, R. Dhuley, T. Kroc, M. Geelhoed, I. Tropin, N. Mokhov, et al., "Conceptual design of a 10-megawatt electron beam irradiation facility for bio-solid waste treatment," tech. rep., Fermi National Accelerator Lab.(FNAL), Batavia, IL (United States), 2018.

[110] Final Report Conceptual Design of an Electron Accelerator for Bio-Solid Waste Treatment. Fermi National Accelerator Lab, Aug.4, 2017

[111] M. Read et al., "A 100 kW 1.3 GHz phase locked magnetron for accelerators," 2018 IEEE International Vacuum Electronics Conference (IVEC), Monterey, CA, USA, 2018, pp. 249-250, doi: 10.1109/IVEC.2018.8391496.

[112] U.N. Environment Program, Stockholm Convention on POPs. http://chm.pops.int/Implementation/IndustrialPOPs/PFAS/Overview/tabid/5221/Default.aspx. last accessed Feb 22, 2023.

[113] https://www.epa.gov/sdwa/and-polyfluoroalkyl-substances-pfas

[114] https://www.eenews.net/articles/defense-department-hits-the-brakes-on-pfas-incineration/.

[115] Tenorio, R, J Liu, X Xiao, A Maizel, CP Higgins, CE Schaefer and TJ Strathmann. Destruction of per- and polyfluoralkyl substances in aqueous film-forming foam (AFFF) with UV-sulfite photoreductive treatment. Env.Sci. Technol. 2020. 54:6957-6967

[116] Trajanowics, M, A Bojanowska-Czajka, I Bartosiewicz, and K Kulisa. Advanced oxidation/reduction processes treatment for aqueous PFOA and PFOS-a review of recent advances. *Chem. Eng. J.* 2018. 336:170-199. https://doi.org/10.1016/j.cej.2017.10.153

[117] Szajdzinska-Pietek E, and JL Gebicki. Pulse radiolysis investigation of perfluoriante dsurfactatns in aqueous solutions. *Res. Chem Intermed.* 2000. 26:897-912.

[118] Ma, S, M Wu, L Tang, R Sun, C Zang, J Xiang, X Yang, X Li and G Xu. EB degradation of perfluorooctanoic acid and perfluorooctane sulfonate in aqueous solution. 2017. Nucl. Sci. Tech. 2*:137 https://doi.org/10.1007/s41365-017-0278-8

[119] LaSsalle, J, R. Gao, R Rodi, C Kowald, M Feng, VK Sharma, T Hoelen, P Bireta, EF Houtz, D Staack, SD Pillai. 2021. *Radiation Physics Chemistry*. 189:109705 https://doi.org/10.1016/j.radphyschem.2021.109705

[120] Chou JW, M. Skornicki and JT Cohen. 2018. *F1000Res.* 7:348. https://doi.org/10.12688/f1000research.14090.1

[121] Gryczka, U, Z Zimek, M Walo, D Chmielewska-Smietanko and S Bulka. Advanced electron beam (EB) wastewater treatment system with low background x-ray intensity generation. 2021. Appl Sci. 11-11194. https://doi.org/10.3390/app112311194

[122] Jun-Hyeong P, J Ahn, K Kim, Y Son. Historic and futuristic review of electron beam technology for the treatment of SO2 and NOx in flue gas. 2019. Chem. Eng. J. 355:351-366.

[123] Getoff, N. Factors influencing the efficiency of radiation-induced degradation of water pollutants. 2002. Rad. Phsy. Chem. 65:437-446. https://doi.org/10.1016/0969-806X(95)00059-7